January 2009

Improving the Cathode Conditions by Pressurizing and Carbon Dioxide Addition to Enhance the Practicality of MFC Treatment of Wastewater

Jeffrey Fornero
Washington University in St. Louis

Washington University in St. Louis

Department of Energy, Environmental, and Chemical Engineering

Dissertation Examination Committee:

Largus Angenent, Chair

Milorad Dudukovic, Co-Chair
Danial Giammar
Petra Levin
Shelley Minteer
Palghat Ramachandran
Yinjie Tang

IMPROVING THE CATHODE CONDITIONS BY PRESSURIZING AND CARBON DIOXIDE ADDITION TO ENHANCE THE PRACTICALITY OF MFC TREATMENT OF WASTEWATER

By

Jeffrey Joseph Fornero

A dissertation presented to the
Graduate School of Arts and Sciences
of Washington University in
partial fulfillment of the
requirements for the degree
of Doctor of Philosophy

August, 2009

Saint Louis, Missouri

Abstract

An increasing global energy demand coupled with a more rigorous governmental regulatory environment (including identifying carbon dioxide as a pollutant) is becoming more and more incompatible with engineering practices that were developed in an era of lower energy costs and less regulation. It is, therefore, not a surprise that researchers are looking towards bioelectrochemical systems (BESs) as a potential superior technology to produce environmentally-benign and sustainable energy, replace energy intensive processes, and/or produce chemical products.

The overall tenet of my thesis-based research was to understand the important mechanisms that limit the power output for BESs during wastewater treatment and to use this understanding to enhance power output and add practicality. Chapter 1 of my thesis is an introduction and shares the individual aims and organization of the thesis. In chapter 2, I evaluated the quantity of stored chemical energy in wastewater and the microbial metabolic processes, which are used to metabolize organic substrates into electricity. In addition, wastewater pre-acidification was identified as necessary to initiate waste hydrolysis into soluble substrates, which are more easily consumed by the BES anodic microbial community. In chapter 3, I developed an engineering evaluation of a laboratory-scale BES, which developed a better understanding of BES rate limitations by the ion fluxes. This work resulted in several realizations on how the BESs performance could be improved. In chapter 4, I performed a laboratory study to demonstrate that a pressurized BES cathode improved oxygen reduction reaction kinetics and increased power densities. The study also highlighted the influence of importance of transmembrane ion gradients and electroosmotic drag on the BES ion flux. In chapter 5,

I used a CO_2/bicarbonate buffered water process to maintain a stable acidic BES catholyte pH without adding any other buffer. This also increased the anolyte pH, alkalinity, and conductivity, which aided in a superior performance. By including the CO_2/bicarbonate buffering, the study coupled BES wastewater treatment with a potential CO_2 remediation technology. Finally, in chapter 6, I summarized my findings and discussed which future activities should be performed to fasten the technology transfer of BESs from the bench to the real world.

Acknowledgements

My sincere appreciation is extended to Dr. Lars Angenent for offering me an opportunity to work and learn in the Angenent Lab. He has consistently challenged me to do my best and patiently persevere in all my work. I also want to thank Dr. Miriam Rosenbaum for her scientific rigor and experimental support, particular after the Angenent Lab moved to Cornell. Dr. Zhen He took me under his wing when I began working in the lab and I am grateful for his patience while introducing me to microbial fuel cells. My thanks also goes out to my lab friends; Sarah Dryden Perkins, Matthew Agler, Marcelo Garcia, Ben Bocher, and Arvind Venkataraman. Your help and support was always eagerly given and greatly appreciated.

Additionally, I want to thank Dr. Daniel Giammar for his challenge to take an engineering fundamentals approach to my research because it has given me great insight into microbial fuel cell performance. A special thank you is also in order for Dr. Milorad Dudukovic's help and guidance after Dr. Angenent moved to Cornell, especially his willingness to co-chair my dissertation committee. Furthermore, I appreciate Dr. Petra Levin, Dr. Palghat Ramachandran, Dr. Shelley Minteer, and Dr. Yinjie Tang for their willingness to help guide me in my research by participating on my dissertation committee.

Thank you's are also in order for Kim Coleman, who helped me navigate my way into the graduate school program; Rose Baxter, who assisted me in meeting the myriad requirements and details necessary to reach this point in my thesis; and Beth Mehringer who helped answer every question imaginable to keep my work moving forward.

The financial support for this work was provided through a specific collaborative agreement between Largus T. Angenent and the Fermentation Biotechnology Research Unit, USDA, Agricultural Research Service, Peoria, Illinois and the National Science Foundation through grant no. 0645021.

On a personal level, thank you to my friend and colleague, Abhas Singh, a most excellent roommate, teacher, and conversationalist. To my parents, thank you for raising me and stressing the value of a good education. My greatest appreciation, however, is to my wife Becky and my children Michael and Hannah for their love, patience, sacrifices, and support while I pursued this degree. I am truly a blessed man and am in awe of the grace extended to me. And most importantly, I want to thank my Lord and Savior, Jesus Christ, through whom all of this was made possible.

Trust in the Lord with all your heart,

And lean not on your own understanding;

In all your ways acknowledge Him,

And He shall direct your paths.

Soli Deo Gloria!

Jeff Fornero

Department of Energy, Environmental, and Chemical Engineering

Washington University

Saint Louis, MO.

August, 2009

Table of Contents

Table of Figures

Table of Tables

Chapter 1

Thesis Proposal

Abstract

In this chapter, I provide an introduction describing how microbial fuel cells operate. In addition, I present my four thesis aims, which directed the course of my exploration.

Introduction:

The attractiveness of bioelectrochemical system technology resides in the ability to treat wastewater while concurrently producing electricity. There are two fundamental types of bioelectrochemical systems (BES), microbial fuel cells (MFC) and microbial electrolysis cells (MECs). Both rely on the anode as the sole electron provider for the bioelectrochemical systems, whereas MFCs generate a potential autonomously, the cathode voltage of an MEC is supplemented with an external power supply, which causes a higher current flow. MFC technology has been proposed as a possible sustainable technology to extract electricity from wastewater streams. This is in stark contrast to current wastewater treatment that requires a net input of energy.

MFCs, like all fuel cells, exploit the electron transfer that occurs between two independent yet related oxidation-reduction half reactions. In the MFC anaerobic anode chamber, bacteria oxidize organic substrates in wastewater to attain energy for cell maintenance and growth with either fermentation or anaerobic respiration reactions. With fermentation reactions, bacteria use the oxidized substrate, the initial electron donor, as the terminal electron acceptor to reoxidize reducing equivalents through substrate level phosphorylation reactions. These reactions produce a relatively small amount of energy for the cell (e.g., adenosine triphosphate [ATP]) because of the high chemical energy remaining in the reaction products. In contrast, some bacteria are able to use anaerobic respiration reactions to reoxidize reducing equivalents. With anaerobic respiration, reducing equivalent (e.g., nicotinamide adenosine dinucleotide [NADH]) transfer electrons through a cell membrane electron transport chain, which simultaneously 1. oxidizes the reducing equivalents (e.g., NAD^+); 2. generates a proton gradient; and 3. transfers electrons to the terminal electron acceptor. The re-oxidation of reducing equivalents is necessary for the cell to continue to gain energy through the oxidation of organic substrates. Oxidative phosphorylation reactions that produce cellular energy (ATP) are driven by a proton gradient. The MFC anode electrode is the terminal electron acceptor for bacteria that are able to deposit electrons on the electrode. Lastly, after electron deposition on the anode, the electrons flow via an external electrical circuit to the cathode, where they participate in a reduction reaction with the fuel cell terminal electron acceptor [1].

Bacteria with the ability to oxidize organic compounds completely to CO_2 and use the anode electrode as the terminal electron acceptor are identified “electricigens” [2].

Electricigens transfer their electrons to the anode electrode via direct contact, electron mediators, or electrically conductive pili [3]. Thus, the anode electrode potential is determined by the chemistry in the anode; by the reducing components (electron mediators and redox-proteins) that will be oxidized at the anode electrode. Electricigens that use anaerobic respiration reactions to transfer electrons to the anode electrode exploit a higher electrochemical potential difference (between the reduced organic substrate and the terminal electron acceptor) than fermenting bacteria that use the fermentation product as the terminal electron acceptor. With the exploitation of the higher energy electrochemical potential difference, the electricigens have an energy advantage over anodic fermenting bacteria that utilize fermentation products as terminal electron acceptors. Therefore, electricigens obtain more usable energy (ATP) than the fermenting bacteria. With a distinct energy advantage, the electricigens could theoretically be the dominant anode bacteria. This, however, is not the case because 1. electricigens need to be close to the anode electrode for the electron transfer to occur, 2. growth rates differ between respiring and fermenting bacteria, and 3. most electricigens can only take up acids, thus complex organic substrates (sugars) must be fermented first. Thus, to obtain an electric current, the anode microbial community needs a good balance of electricigens and fermenting bacteria. Further, if a biofilm develops on the anode electrode, mass transport limitations are created for nutrients and waste products to and from the electricigens, respectively [4]. When a biofilm thickens, the outer sections furthest away from the electrode, may host fermenting bacteria, while the sections closer to the anode electrode may host more electricigens. [5]

In a MFC, the electrons move from the anode electrode, through an external circuit, to the cathode electrode because of the potential difference between the anode and cathode, with the cathode having the higher electrochemical potential (oxidation state). Placing a resistor or other electrical load in the external circuit allows the MFC to generate electrical power. MFC cathode configurations and catholyte fluid options vary [6-12], however, the most common design includes a platinum (Pt) coated carbon electrode submersed in an oxygenated phosphate buffered solution. The Pt catalyzes an oxygen reduction reaction and creates an electron acceptor site for the electrons arriving from the anode (Fig. 1-1). Thus, oxygen is the terminal electron acceptor for the MFC, whereas the anode electrode is the terminal electron acceptor for the bacteria. The oxygen reduction reaction is accompanied by the consumption of protons and generation of hydroxide ions in the catholyte, which leads to increases in the catholyte pH as wastewater is treated. Some researchers have used phosphate buffered catholytes to mitigate catholyte pH increases [13] because pH differences between the acidic anode and basic cathode account for 59 mV/pH MFC voltage losses according to the Nernst equation [14]. Others, however, use air cathodes to improve the oxygen reduction reaction kinetics, because of the limited solubility of oxygen in the phosphate buffered catholyte. While air cathodes have shown improved oxygen reduction capabilities, the increased voltage losses from the pH gradient become more prominent. The pH gradient develops because of the relatively small amount of anolyte that permeates across the ion exchange membrane with an air cathode; therefore, the proton consumption/hydroxide ion generation occurs in a relatively small fluid volume, resulting in a higher catholyte pH.

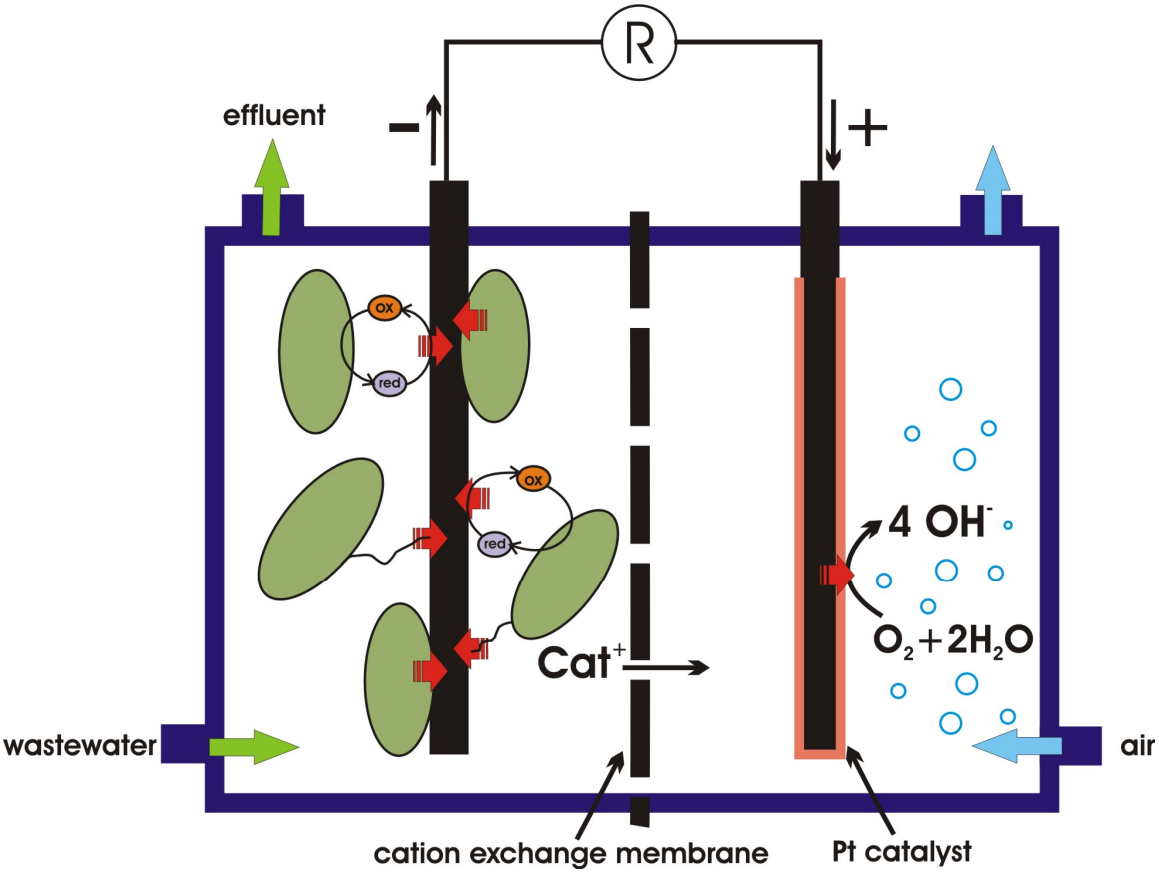

Figure 1-1. The working principle of a microbial fuel cell: substrate (in wastewater) is metabolized by bacteria, which transfer the gained electrons to the anode electrode through three mechanisms: direct cell contact, shuttling via electron mediators (red/ox), or shuttling via nanowires. Electrons flow from the anode (negative pole) to the cathode (positive pole) via an electric circuit and power is generated because of an external resistor (R). Cation transfer from the anolyte to the catholyte ensures electroneutrality when a cation-exchange membrane is installed. On the cathode surface of MFCs, oxygen is reduced by taking up electrons ($O_2 + 4\ e^- \rightarrow 2\ O^{2-}$) and then combines with protons to yield hydroxide ions ($4O^{2-} + 4H^+ \rightarrow 4\ OH^-$).

As discussed, MFCs take advantage of the electron transfer between two independent yet related oxidation-reduction half reactions. To maintain independent reactions in the anode and cathode chambers, semi-permeable ion-selective membranes are used to segregate the anolyte and catholyte fluids. In addition to the electron transfer, an ion exchange between the anode and cathode is necessary to maintain MFC electroneutrality. The ion transfer is mediated by an ion exchange membrane, which

depending upon whether an anion or cation exchange membrane is selected, allows the passage of anions/hydroxide ions or cations/protons, respectively. At neutral pH levels, MFC researchers have found that the transfer of ions other than protons or hydroxide ions, enable fuel cell electroneutrality because these ions are in much higher concentration than the proton or hydroxide ion concentration (~10^{-6} M) [14]. This is in contrast to hydrogen fuel cells in which protons are moving through an electrolyte. My research has also provided evidence that ion and pressure gradients influence the MFC power densities (chapters 4 and 5) and monovalent ions are more readily transferred than divalent ions because of their smaller hydration radius and lower membrane resistance (chapter 4).

For MFC wastewater treatment to be practically applied, significant technical challenges remain to be solved, including 1. Low coulombic efficiencies (recovery of electrical energy versus stored chemical energy) while treating complex organic waste substrates; 2. Low power densities associated with dilute wastewater streams; 3. Managing a high cathode and low anode pH; and 4. Reducing the cathode to anode oxygen crossover across the membrane because oxygen in the anode decreases power densities. My thesis work addressed these fundamental challenges.

Aim 1 – Conduct a comprehensive literature review comparing microbial fuel cell with activated sludge technologies with an emphasis on microbiology.

The literature review explores whether MFC technology can replace activated sludge processes for secondary wastewater treatment with an emphasis on the

microbiology and reactor configuration for full-scale treatment. It also addresses the *present* limitations and problems of electric current generation when a complex wastewater is treated with a diverse and nondefined community of microbes in large-scale systems. These challenges include low coulombic efficiencies, slow kinetic rates, and nonlinear power density increases during scale-up efforts.

Wastewater Characteristics: We discuss the diversity of wastewater physical and chemical properties and their influence on MFC treatment. In particular, we compare the coulombic efficiencies of MFCs treating soluble versus particulate organic substrates. Because particulate organic matter is mainly composed of proteins, polysaccharides, and lipids, the polymeric compounds must first be converted to low molecular-weight organic substrates, such as sugars, amino acids, and volatile fatty acids before they are able to be used by bacteria. And since particle conversion is slow, the hydrolysis of organic particulates to lower molecular weight substrates can be regarded as the rate-limiting step in bacterial processing.[15] Thus, bacterial particle hydrolysis rates have an implication for MFC wastewater treatment, which is discussed in chapter 2.

Bacteria and Energy Management: Anodic bacteria oxidize organic substrates to gain energy for cell maintenance and growth with either fermentation or anaerobic respiration reactions, which have different terminal electron acceptors. The theoretical electrochemical potential difference (maximum energy gain) between the metabolic electron donor (NADH) and the MFC terminal electron acceptor oxygen is 1.16 V [16].

Bacteria that are able to exploit the relatively higher potential of the anode electrode compared to other electron acceptors, such as carbon dioxide for autotrophic methanogens, will transfer electrons to the electrode to gain more energy, therefore, deriving a competitive advantage. Thus, MFC designs and operations need to promote the use of anode respiring bacteria to maximize the current generation from the organic substrate transformations.

Wastewater Treatment with MFCs: To further develop MFC systems as full-scale wastewater treatment systems, Researchers in the field anticipate a requirement for modular reactor configurations with multiple MFC cells in series and parallel to boost the potential and current, respectively. Multiple MFC cells will be necessary to maintain the anode microbial consortia and cathode reduction catalyst in close association across an ion exchange membrane, which separates the anode and cathode chambers. Finally, I predict that the main economic gain from treating wastewater with MFCs will be biological oxygen demand (BOD) removal without nonrenewable energy consumption rather than electric power generation per se, and that the choice of MFC technology over activated sludge technology may be driven by social and environmental considerations rather than by purely economical considerations.

Aim 2 – Investigate the effect of an air pressurized cathode on microbial fuel cell performance

This laboratory study evaluated the impact of increasing the air pressure to an MFC cathode. In addition to the cathode pressurization, MFC performance differences between anion and cation exchange membranes (AEM and CEM, respectively) were evaluated. Lastly, routing the MFC anolyte to the cathode as a method of reducing the pH imbalance was studied.

Pressurized Cathode Chamber and MFC Power Densities: MFC power densities are often constrained by the oxygen reduction reaction rate on the cathode electrode. One important factor for this is the normally low solubility of oxygen in the aqueous cathode solution, which creates mass transport limitation and hinders oxygen reduction at the electrocatalyst (platinum, Pt). In this investigation, I increased the air pressure in the cathode chamber to increase the solubility and consequently the availability of oxygen, which is a function of the partial pressure. With an increase in the cathode air pressure, the oxygen diffusion from the cathode to anode was considered.

Ion Gradients Influence Internal Resistance and Power Densities: By comparing power densities with an AEM versus a CEM under the same operating conditions, the influence of ion gradients on power densities was explored. With ion transport being imperative to maintain electroneutrality, ohmic losses become important because they contribute to MFC total system losses. The differences in the ion gradients, potential losses, and power densities are discussed in chapter 4.

Monovalent versus Divalent Ion Charge Transfer Resistance: A comparison of catholyte trends for both the AEM and CEM with a nonreplenished phosphate buffered catholyte resulted in different cell potential profiles. The reason for the difference was attributed to whether monovalent or divalent ions were crossing the ion exchange membrane to maintain electroneutrality. Since only phosphate ions were maintaining the charge balance, the presence of monovalent or divalent phosphate ions depended on the phosphate ion protonation, which is a function of the catholyte pH. Thus, the influence of the catholyte pH relative to the equilibrium of monovalent and divalent phosphate ions is presented in chapter 4.

Aim 3 – Compare the performance of liquid cathode and air cathode MFCs with and without the addition of carbon dioxide to the cathodes

This study compared the performance differences between two identical MFCs with AEMs, with one operated as a liquid cathode and the other as an air cathode. With the liquid cathode MFC, carbon dioxide was added to the cathode to understand the impact on the cathode pH and ion migration. Subsequent to this, a phosphate buffered catholyte was used to compare the differences the pH, ionic composition, and ionic concentration had on the power density. The air cathode was operated in an air-only and an air/carbon dioxide mixture configuration. MFC performance with the different liquid and air cathode configurations were compared and contrasted.

Carbon dioxide addition to the liquid cathode: Carbon dioxide was added to a reverse osmosis (RO) water catholyte to determine the effect bicarbonate ion buffering had on the cathode pH, MFC pH gradient, and electroneutrality ion migration. The ability to maintain a small MFC pH gradient with carbon dioxide buffering was a significant accomplishment because the development of large pH gradients is common with prolonged MFC operations. The use of the RO water catholyte also provided an opportunity to understand the influence cation transport on the cathode pH and power densities.

Cathode to anode ion migration and anolyte properties: Adding carbon dioxide to the cathode not only influenced the catholyte ionic composition, but also influenced anolyte properties as a result of ion electromigration. Chapter 5 describes the effects the cathode ion migration had on anolyte properties, MFC performance, and wastewater treatment. The study also links MFC anodic wastewater treatment with cathodic carbon dioxide utilization.

Liquid and air cathode comparisons: Comparisons between liquid and air cathode configurations were performed to understand how the different configurations affected MFC power densities and ion fluxes. The influence the different configurations had on electroneutrality maintenance ion fluxes was significant in that it led to an understanding of the MFC power density rate limitations.

References:

(1) Madigan, M. T.; Martinko, J. M.; Parker, J., *Brock Biology of Microorganisms*; 9th ed.; Prentice Hall, Inc.: Englewood Cliffs, NJ, 2000.

(2) Lovley, D. R., Microbial Energizers: Fuel cells that keep on going. *Microbe.* 2006, *1*, 323-329.

(3) Gorby, Y. A.; Yanina, S.; McLean, J. S.; Rosso, K. M.; Moyles, D.; Dohnalkova, A.; Beveridge, T. J.; Chang, I. S.; Kim, B. H.; Kim, K. S.; Culley, D. E.; Reed, S. B.; Romine, M. F.; Saffarini, D. A.; Hill, E. A.; Shi L.; Elias, D. A.; Kennedy, D. W.; Pinchuk, G.; Watanabe, K.; Ishii, S.; Logan, B. E.; Nealson, K. H.; Fredrickson, J. K., Electrically conductive bacterial nanowires produced by *Shewanella oneidensis* strain MR-1 and other microorganisms. *Proc. Nat. Acad. Sci. U.S.A.* 2006, *103*, 11358-11363.

(4) Menicucci, J.; Beyenal, H.; Marsili, E.; Veluchamy, R. A.; Demir, G.; Lewandowski, Z., Procedure for determining maximum sustainable power generated by microbial fuel cells. *Environ. Sci. Technol.* 2006, *40*, 1062-1068.

(5) Liu, H.; Cheng, S. A.; Logan, B. E., Production of electricity from acetate or butyrate using a single-chamber microbial fuel cell. *Environ. Sci. Technol.* 2005, *39*, 658-662.

(6) He, Z.; Minteer, S. D.; Angenent, L. T., Electricity generation from artificial wastewater using an upflow microbial fuel cell. *Environ. Sci. Technol.* 2005, *39*, 5262-5267.

(7) He, Z.; Shao, H. B.; Angenent, L. T., Increased power production from a sediment microbial fuel cell with a rotating cathode. *Biosens. Bioelectron.* 2007, *22*, 3252-3255.

(8) Liu, H.; Logan, B. E., Electricity generation using an air-cathode single chamber microbial fuel cell (MFC) in the absence of a proton exchange membrane. *Environ. Sci. Technol.* 2004, 38, 4040-4046.

(9) Min, B.; Logan, B. E., Continuous electricity generation from domestic wastewater and organic substrates in a flat plate microbial fuel cell. *Environ. Sci. Technol.* 2004, *38*, 5809-5814.

(10) Park, D. H.; Zeikus, J. G., Impact of electrode composition on electricity generation in a single-compartment fuel cell using *Shewanella putrefaciens*. *Appl. Microbiol. Biotechnol.* 2002, *59*, 58-61.

(11) Rabaey, K.; Clauwaert, P.; Aelterman, P.; Verstraete, W., Tubular microbial fuel cells for efficient electricity generation. *Environ. Sci. Technol.* 2005, *39*, 8077-8082.

(12) Rabaey, K.; Lissens, G.; Siciliano, S. D.; Verstraete, W., A microbial fuel cell capable of converting glucose to electricity at high rate and efficiency. *Biotechnol. Lett.* 2003, *25*, 1531-1535.

(13) Rozendal, R. A.; Hamelers, H. V. M.; Buisman, C. J. N., Effects of membrane cation transport on pH and microbial fuel cell performance. *Environ. Sci. Technol.* 2006, *40*, 5206-5211.

(14) Harnisch, F.; Schröder, U.; Scholz, F., The suitability of monopolar and bipolar ion exchange membranes as separators for biological fuel cells. *Environ. Sci. Technol.* 2008, *42*, 1740-1746.

(15) Ubukata, Y., Fundamental mechanisms of phosphate removal by anaerobic/aerobic activated sludge in treating municipal wastewater. *Eng. Life Sci.* 2006, *6*, 51-56.

(16) Schröder, U., Anodic electron transfer mechanisms in microbial fuel cells and their energy efficiency. *Phys. Chem. Chem. Phys.* 2007, *9*, 2619-2629.

Chapter 2

Electric power generation from municipal, food, and animal wastewaters using microbial fuel cells

Fornero J. J., Rosenbaum M., and Angenent L. T., Electric power generation from municipal, food, and animal wastewaters using microbial fuel cells. Submitted as a review paper to *Electroanalysis*, to be published in January, 2010.

Abstract

Researchers in the fields of Biological and Environmental Engineering have shown a real potential to apply microbial fuel cell (MFC) technology to wastewater treatment. Motivations of their work are based on the economic, environmental, and social needs for sustainable wastewater treatment systems and renewable energy. In this chapter, we explore if MFC technology can replace activated sludge processes for secondary wastewater treatment with an emphasis on the microbiology and reactor configuration for full-scale treatment. We will also discuss the *present* limitations and problems of electric current generation when a complex wastewater is treated with a diverse and nondefined community of microbes in large-scale systems. These challenges include low coulombic efficiencies, slow kinetic rates, and nonlinear power density increases during scale-up efforts. To further develop MFC systems as full-scale

wastewater treatment systems, we anticipate a requirement for intricate reactor configurations with multiple MFC cells in series and parallel to boost the potential and current, respectively. Finally, we predict that the main economic gain from treating wastewater with MFCs will be biological oxygen demand (BOD) removal without nonrenewable energy consumption rather than electric power generation per se, and that the choice of MFC technology over activated sludge technology may be driven by social and environmental considerations rather than by purely economical considerations.

Wastewater Characteristics

We project the treatment of municipal and industrial wastewater with MFC technology to reduce or eliminate energy usage in wastewater treatment facilities. Municipal wastewater is included here as a source of organic compounds, despite a low concentration of biochemical oxygen demand (BOD) (~ < 300 mg/L), and thus a low energy density. Initially, however, MFC technology will be explored with high-strength industrial wastewater with concentrations exceeding 2,000 mg (BOD)/L because of the higher energy densities that can be achieved. Many of these wastewaters are generated in the food industry and are rich in easily degradable carbohydrates and organic acids with relatively low concentrations of organic nitrogen (e.g., proteins).[10,12,25,37] Animal wastewaters from the livestock-related industry are often particularly high in organic material content (~ 100,000 mg chemical oxygen demand [COD]/L for animal wastes) and may contain high levels of nitrogen-containing components, such as proteins, and harder to degrade organic materials, such as cellulose. [21] In addition, slaughterhouse wastewaters from the livestock-related industry may also include lipids besides

carbohydrates, organic acids, and proteins. Despite considerable variability in the characteristics of wastewater depending on their sources, the following general characterization parameters were defined:[11]

- "Soluble" wastewater, which is characterized as nonsettleable and noncoagulable, is composed of readily biodegradable COD, readily hydrolysable COD, and inert substrates.
- "Colloidal" wastewater, which is characterized as nonsettleable, is composed of heterotrophic biomass, inert substrates, and slowly-biodegradable COD substrate.
- "Particulate" wastewater, which is characterized as settleable, is composed of biomass, slowly-biodegradable COD, and inert substrates.

The primary organic compound in wastewater is particulate organic matter. Particulate organic matter is 100 to 300 μm in size and is mainly composed of proteins, polysaccharides, and lipids.[11] To be utilized by bacteria, the polymeric compounds must first be converted to low molecular-weight organic substrates, such as sugars, amino acids, and volatile fatty acids. Particle conversion, which is accomplished through particle degradation and/or hydrolysis, is slow. Hydrolysis of entrapped organic particulates to lower molecular weight substrates can be regarded as the rate-limiting step in bacterial processing because the rate of breakdown of soluble and colloidal wastewater components is much faster.[52] To convert the particulate fraction of wastewater into electricity without the requirements of a very large MFC volume, engineers can design a two-step process in which particulate compounds are first hydrolyzed and pre-acidified in a mixed tank. Then, the pre-acidified solution with mainly carboxylic acids is fed to a MFC to treat mainly soluble wastewater. The addition of a pre-acidification tank before

a high-rate anaerobic digester system is already standard for the treatment and bioconversion of high-strength wastewater, such as brewery wastewater, into methane gas.

MFC Technology

History. In 1912, Michael Potter, a botany professor at the University of Durham, United Kingdom, demonstrated that microbes created a voltage potential and conveyed a current.[50] This technology is now known as the microbial fuel cell (MFC). During the last five years, increasing energy costs and the desire for environmentally sustainable energy sources have stimulated research on how to use MFCs for simultaneous wastewater treatment and energy generation. This surge in activity resulted in considerable improvements in power densities and power output, showing a real potential to scale up.[4,30,45]

How It Works. The MFC for wastewater treatment is an engineered system designed to support a nondefined mixed culture of microbes in the anode chamber. These MFCs transform (treat) organic substrates (in wastewater) through oxidation-reduction reactions and transport electrons through an electric circuit for the generation of electric power. The oxidation reactions occur in the anode compartment where bacteria metabolize organic substrates to generate energy for cell maintenance and biomass synthesis. As energy and electrons are liberated by the oxidation reactions, the electricigens and other electron-transferring bacteria in the anaerobic foodweb are able to deposit electrons to the anode electrode, which acts as the anode compartment's electron

acceptor (Fig. 1-1). Electricigens are bacteria that can respire with the solid electrode, while conserving energy by oxidizing organic molecules, such as acetate, completely to carbon dioxide.[31]

The electrons transfer from the anode electrode via an external circuit to the cathode electrode because of a potential difference. MFC cathodes have a number of different configuration and catholyte fluid options[17,18,29,36,38,42,43,45] – the conventional design includes a platinum (Pt) coated carbon electrode submersed in a phosphate buffered solution. The Pt catalyzes the reduction of oxygen and creates a donor site for the electron transfer from the anode. In such fuel cell systems, oxygen is the terminal electron acceptor and the anode, therefore, is an intermediate electron acceptor (Fig. 1-1). With the electron transfer from the anode to the cathode, it is necessary to maintain electroneutrality in the fuel cell. Charge balance maintenance is mediated by an ion exchange membrane that allows the passage of cations/protons or anions/hydroxide ions, depending on the pH and membrane selected between the anode and cathode chambers. For cation exchange membranes at neutral pH levels, researchers have found a movement of cations, such as sodium and potassium, from synthetic wastewater to the catholyte.[47,53] This is in contrast to hydrogen fuel cells in which protons are moving through an electrolyte.[24] The membranes also function to separate the environmental conditions with the goal to maximize the potential difference between anode and cathode electrodes. The latter is important to optimize the electric power generation.

Bacteria and Energy Management. Microorganisms gain energy for their function by transferring electrons from an electron donor to a terminal electron acceptor.

One of the key metabolic mediators in microbial energy generation is the coenzyme nicotinamide adenine dinucleotide (NAD^+/NADH), which as an intermediate electron acceptor is reduced from NAD^+ to NADH. For cellular respiration to proceed, reduced NADH must then be reoxidized to NAD^+ via a redox reaction ($NADH \rightarrow NAD^+ + H^+ + 2e^-$).[32] Aerobic heterotrophic bacteria gain energy by transferring electrons from a reduced organic substrate through metabolic and respiratory pathways to their terminal electron acceptor oxygen. Under anaerobic conditions (no oxygen present) the reoxidation of NADH can still be accomplished through respiration when alternative electron acceptors, such as nitrate[48], soluble or insoluble iron (Fe^{3+}), or solid electrodes[31], are present. An alternative pathway for heterotrophic bacteria under anaerobic conditions is fermentation. During fermentation, the reoxidation of NADH (transfer of electrons to a terminal electron acceptor) occurs with electron acceptors formed by the same metabolic pathway that donated the electrons to the NADH.[14]

In the anaerobic environment of a MFC anode, the solid anode electrode can, thus, also act as an electron acceptor facilitating anaerobic respiration and the reoxidation of NADH to NAD^+ (even though oxygen remains the terminal electron acceptor in the cathode of a conventional MFC; Fig. 1-1). The electron transfer from the intracellular NADH can be accomplished through direct cell contact with the anode electrode[6], shuttling via electron mediators[34,40,41], or shuttling via nanowires or other filamentous appendages[13,22] (Fig. 1-1). Other terminal electron acceptors in the cathode of the MFC, such as nitrate in biological cathodes, were also proposed or proven to facilitate electron transfer.[9.16] This may be important for wastewater treatment because nitrate removal is critical in regards to nutrient removal.

The theoretical potential difference (maximum gain) between the biological standard potential (E'_0 [V]) (pH = 7.0) of the terminal metabolic electron donor NADH and the terminal electron acceptor oxygen is 1.16 V (+ 0.840 V - (- 0.320 V)).[49]

$NAD^+ + H^+ + 2e^- \rightarrow NADH$ $\quad E'_0 = - 0.320$ V

$O_2 + 4H^+ + 4e^- \rightarrow 2H_2O$ $\quad E'_0 = + 0.840$ V

If the electron acceptor is changed to nitrate ($E'_0 = + 0.421$ V), the potential difference to NADH decreases to 0.741 V and the amount of energy available for the transforming bacteria decreases accordingly.[16]

$NO_3^- + 2H^+ + 2e^- \rightarrow NO_2^- + H_2O$ $\quad E'_0 = + 0.421$ V

The cathode oxygen reduction reaction will not yield the theoretical + 0.84 V potential because the potential is reduced by activation polarization losses. Further, as resistances are lowered and the current increases, ohmic losses and concentration polarization losses become more prominent. A more achievable potential for the MFC cathode when considering losses is + 0.51 V.[49] Bacteria that are able to exploit the relatively higher potential of the anode electrode compared to other electron acceptors, such as carbon dioxide for autotrophic methanogens, will transfer electrons to the electrode to gain more energy, therefore, deriving a competitive advantage. Besides generating a high power output, the measured potential difference between anode and cathode must, therefore, also be maximized to select for a microbial community with enhanced electrochemical activity.[44]

Angenent Lab data (unpublished) compared the MFC microbial communities of the inoculum with the anode biofilm after three months of operation. The inoculum was

a mixture of bacteria and archaea (granular sludge) from an anaerobic bioreactor treating brewery wastewater. The MFC treated an artificial wastewater with sucrose as the electron donor. Results show (Fig. 2-1) the phyla Proteobacteria increased from 27% to 69% for the inoculum and MFC biofilm, respectively. Within the Proteobacteria, members of the genera *Rhodoferax* (Beta subgroup), *Geobacter*, *Desulfovibrio* (Delta subgroup), *Shewanella*, *Psuedomonas*, and *Aeromonas* (Gamma subgroup) have been shown to generate electric current in pure culture studies. The enrichment of electrochemically active microbes and the number of phyla represented within the biofilm reflect the MFC microbial diversity and complexity of the anodic food web.

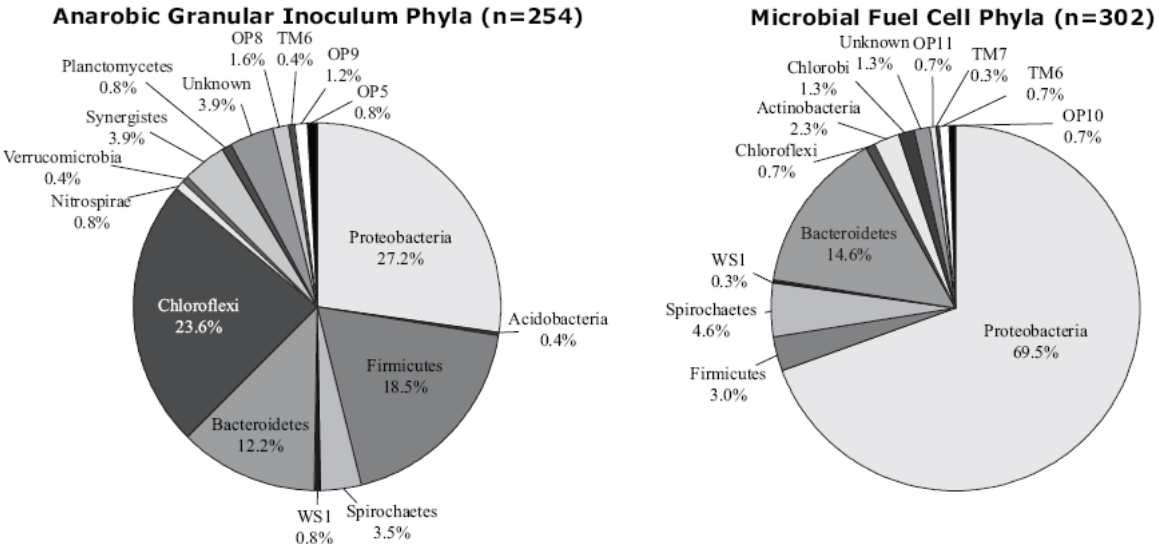

Figure 2-1. Distribution of observed phyla from the anaerobic granular inoculum and the UMFC. (Angenent Lab – Unpublished)

Wastewater Treatment with MFCs. Lab-scale MFCs have been operated on synthetic (e.g., sucrose, glucose, acetate) and real wastewater (e.g., municipal, hospital, brewery, animal wastewater)[17,19,20,28,35,36,41-43]. Hexose, butyrate, and acetate were chosen

here as model components for a complex wastewater with a diverse composition of organic compounds. The half reactions in a MFC with these substrates are:

$$C_6H_{12}O_6 + 6H_2O \rightarrow 6CO_2 + 24H^+ + 24e^-$$

$$CH_3CH_2CH_2COOH + 2H_2O \rightarrow 2CH_3COOH + 4H^+ + 4e^-$$

$$CH_3COOH + 2H_2O \rightarrow 2CO_2 + 8H^+ + 8e^-$$

The removal of reducing equivalents (electrons) from the anode chamber is basically similar to decreasing the chemical oxygen demand (COD) concentration from the wastewater. Therefore, the calculation of the coulombic efficiency for the oxidation in the anode chamber is performed based on the amount of BOD or COD removed by the mixed culture in the anode chamber and the electric current generated (equation 1 shows that the Faraday constant is used to convert the removed BOD [or COD] to the equivalent amount of electrons).

In the following paragraphs A-I, we give an overview of different MFC research studies that used either synthetic or real wastewater as the electron donor. We discuss the operation parameters and the specific performance data. Table 2-1 summarizes all performance data and lists the compared studies ordered from highest to lowest coulombic efficiency.

§[1]	Anode volume (mL)	Synthetic or real wastewater substrate type[2]	Concentration (mg/L)[3]	Maximum power[4]	External resistor (Ω)[5]	Coulombic efficiency (%)[6]	Reference
F	560	Acetate	458	48 W/m^3	20	98	(42)
D	40	Glucose	2,000	3,600 mW/m^2	< 100	89	(43)
D	240	Glucose	NP[7]	4,310 mW/m^2	< 100	81	(41)
F	390	Glucose	467	35 W/m^3	20	74	(42)
B	22	Acetate	1,000	286 mW/m^2	33	65	(36)
B	22	Butyrate	1,000	220 mW/m^2	33	50	(36)
F	**390**	**Hospital wastewater**	**332**	**25 W/m^3**	**NP[7]**	**36**	**(42)**
C	28	Acetate	800	506 mW/m^2	218	29	(28)
B	22	Starch	1,000	242 mW/m^2	33	21	(36)
H	28	BSA	1,100	354 mW/m^2	> 50	20.6	(20)
F	**390**	**Municipal wastewater**	**429**	**10 W/m^3**	**75**	**20**	**(42)**
B	22	Dextran	1,000	150 mW/m^2	33	17	(36)
E	440	Sucrose	800	29 W/m^3	20	14.2	(19)
B	22	Glucose	1,000	212 mW/m^2	33	14	(36)
E	520	Sucrose	1,000	170 mW/m^2	66	8.1	(17)
I	**28**	**Swine waste (soluble fraction)**	**8,320**	**261 mW/m^2**	**200**	**8**	**(35)**
C	28	Butyrate	1,000	305 mW/m^2	1,000	7.8	(28)
A	**22**	**Municipal wastewater**	**379**	**72 mW/m^2**	**470**	**6**	**(36)**
H	28	Peptone	500	269 mW/m^2	> 50	6.0	(20)
H	**28**	**Slaughterhouse wastewater**	**1,420**	**80 mW/m^2**	**> 50**	**5.2**	**(20)**
G	**5,400**	**Brewery wastewater**	**1,168**	**5 W/m^3**	**10**	**3.6**	**This chapter**

[1] Described in the paragraphs A-I.
[2] Real wastewater substrate in bold, these wastewaters were not pre-acidified.
[3] COD concentration was used for the real wastewater substrates
[4] Maximum power density in mW per m^2 anodic electrode surface area and maximum power output in W per M^3 of total anodic volume.
[5] Used to obtain the maximum power except for the Min et al.[36] for which we reported the average values.
[6] Data from maximum power density of output was used the calculate the coulombic efficiency except for the Min et al.[36]
[7] NP: information not provided by authors

Table 2-1. Coulombic efficiencies and maximum power densities or output achieved in MFCs with nondefined mixed cultures in the anode chamber using various anode volumes, substrates, and external resistances. The data are ordered based on coulombic efficiency with the highest percentages on the top. Real wastewater substrate solutions (without pre-acidification) are given in bold.

A. Min and Logan[36] reported that a lab-scale MFC with an anode volume of 22 mL was able to continually generate electricity from wastewater while at the same time reducing the COD concentration of the waste stream. The experiment was conducted by batch feeding municipal wastewater with an influent COD concentration that varied between 246 and 379 mg/L. The MFC was able to produce a maximum power density of 72 mW/m^2 (per anode electrode surface area) with a hydraulic retention time (HRT) of

1.1 h and a COD removal efficiency of 42%. The coulombic efficiency for domestic wastewater was ~ 6% at an average power density of 56 mW/m^2 and a 1.4-h HRT.

B. The power densities and coulombic efficiencies for various chemical compounds that were introduced into the same acclimated MFC at a concentration of 1,000 mg/L were higher. For example, adding acetate increased the power density to 286 mW/m^2 and the coulombic efficiency to 65% at a 0.68-h HRT and an external resistor of 33 Ω. The COD removal efficiencies for acetate and all the other introduced compounds (i.e., starch, glucose, dextran, and butyrate) were lower than the COD removal efficiencies for the municipal wastewater due to a shorter HRT. In addition, the COD removal efficiencies were greater for the fermentable substrates (i.e., starch and glucose) than the nonfermentable substrates (i.e., acetate and butyrate) while the coulombic efficiencies showed an opposite trend (Table 1-1). The difference in COD removal efficiency was explained by the selection of higher energy substrates as a fuel source, lower bacterial conversion rates of the nonfermentable substrates, and the significant presence of fermentative bacteria within the MFC bacterial consortia.[36]

C. In another MFC study from the Logan laboratory with a 28-mL anode volume, Liu et al.[28] generated electricity from butyrate and acetate. The substrate was processed in batch until the MFC voltage decreased to < 0.030 V, an indication that the electricity production from the waste was near exhaustion. The individual batch periods lasted ~ 20 h with substrate removal efficiencies of 98 and 99% for butyrate and acetate, respectively. For acetate at a concentration of 800 mg/L the power density was 506

mW/m^2 with a coulombic efficiency of 29%, while butyrate (1,000 mg/L) showed a lower power density of 305 mW/m^2 and coulombic efficiency of 7.8%.

D. Rabaey et al.[43] in the Verstraete laboratory obtained a maximum power density of 3,600 mW/m^2 and coulombic efficiency of 89% in a batch-operated MFC fed with glucose at a concentration of 2,000 mg/L. The anode volume for their MFC was 40 mL and the optimum external resister was 100 Ω. In a follow-up study in the same lab with a similar MFC with an anode volume of 240 mL, a maximum power density of 4,310 mW/m^2 (external resistor < 100 Ω) and an 81% coulombic efficiency was reported when fed glucose.[41] The very low volatile fatty acid levels in the anolyte and hydrogen concentrations in the headspace (below detection) explain the relatively high coulombic efficiency for glucose, while methane generation in the well functioning MFC was suppressed.[41] This is important because it shows that MFCs can be efficient energy conversion devices in regards to yields if the internal losses (e.g., ohmic and polarization losses) are minimized. However, even at these efficient operating conditions, the maximum volumetric loading rate before extinction (i.e., the power density or output decreases even though the loading rate increases) was only 2.5 g COD/L/d.[43] In the second paper from the Verstraete lab, the loading rate was 1 g COD/L/d.[41] Such loading rates are much lower compared to high-rate anaerobic digestion systems, such as the upflow anaerobic sludge blanket (UASB) or the anaerobic migrating blanket reactor (AMBR) for which volumetric loading rates > 20 g COD/L/d have been reported.[5,26,51]

E. Rather than using a batch-fed MFC, He et al.[17] in our laboratory fed a sucrose solution at a concentration of 1,000 mg/L continuously to an upflow microbial fuel cell (UMFC) with a cation-exchange membrane and an anode volume of 520 mL (Fig. 2-2). We obtained a maximum power density of 170 mW/m^2 and a coulombic efficiency of 8.1% at an external resistor of 66 Ω. In a follow-up study with a second-generation UMFC (440 mL anode volume – Fig. 2-2), we lowered the internal resistance compared to the first-generation UMFC by decreasing the distance between the electrodes and increasing the membrane surface area, resulting in a higher power output (a maximum volumetric power of 29.2 W/m^3 and a coulombic efficiency of 14.2% was achieved at a lower external resistance of 20 Ω). A sucrose solution was fed continuously at a concentration of 800 mg/L to the anode. The volumetric loading rate with the highest power output in this study was 3.4 g COD/L/d.[19]

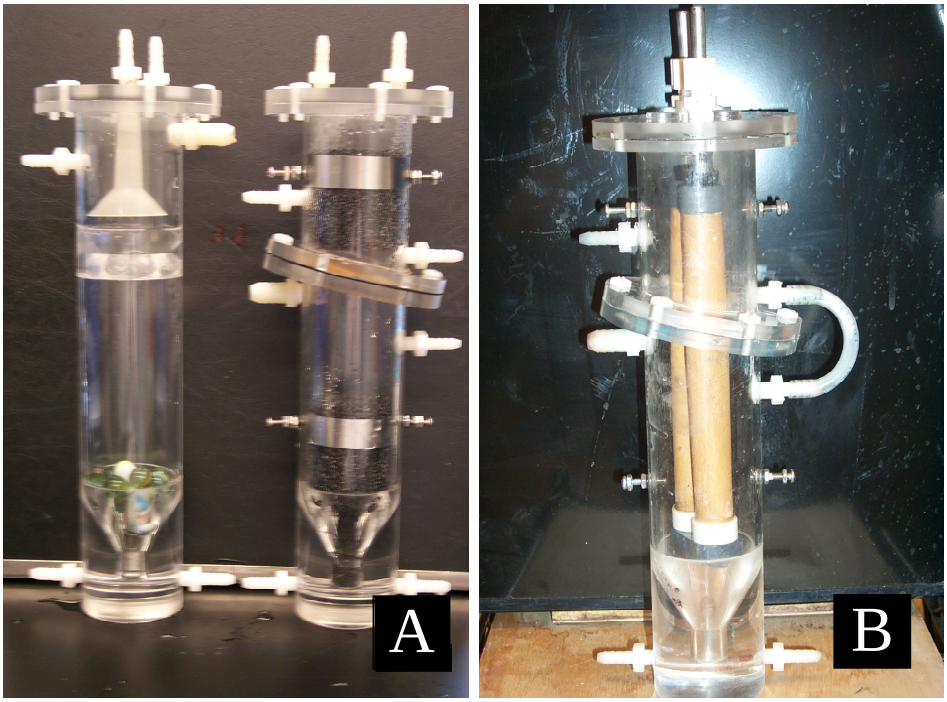

Figure 2-2. Pictures of lab-scale bioreactors: A. UASB reactor (left) and first-generation UMFC reactor (right) ; and B. second-generation UMFC reactor with an interior cathode configuration. The anodic electrode that consisted of granular activated carbon was omitted for the second-generation UMFC to show the cathode configuration.

F. A continuously-fed tubular MFC (total anode compartment volume of 560 mL for acetate and 390 mL for the other substrates) with an outside cathode was tested for four different wastewater solutions: synthetic acetate, synthetic glucose, pre-filtered municipal wastewater, and pre-filtered hospital wastewater. The maximum power outputs for these wastewaters were 48 (20-Ω external resistor), 35 (20 Ω), 10 (75 Ω), and 25 (Ω not reported) W/m^3 at COD concentrations of 458, 467, 429, and 332 mg/L and coulombic efficiencies of 98, 74, 20, and 36%, respectively. The MFC power output increased when acetate, peptone, or digester effluent (with a high acetate concentration) was augmented to municipal wastewater influent to show that power was limited by the absence of

readily degradable organics. In other words, slow degradation kinetics of complex organics in real wastewater was restricting power output in W/m^3. In addition, the authors described the accumulation of recalcitrant materials and active biomass, which accounted for 70% of the fed COD from municipal wastewater over a period of 60 days, explaining partly why a lower coulombic efficiency was achieved for real municipal wastewater compared to synthetic wastewater.[42]

G. A low coulombic efficiency during treatment of a complex wastewater was also shown in our lab with a high-strength waste stream from the brewery industry (no pre-acidification was performed for this clarified spent grain liquor). We choose this wastewater with a COD concentration of 533 – 2,800 mg/L (after dilution with make-up water) because of its high energy density. The COD and BOD removal efficiencies in a MFC with a 5.4-L anode volume were relatively low and varied from 28.8 - 32.9% and 47 - 85%, respectively, because of the predominance of slowly degradable organic material. Treatment with this MFC resulted in a maximum power output of 5.0 W/m^3 (external resistance of 10 Ω and a pH of 7.3) and a sustainable coulombic efficiency of 1.5 – 3.6% with an external resistor of 100 Ω (total current of 6.6 – 6.8 mA). The cell potential with the latter external resistor was between 0.66 and 0.68 V. After an operating period of five months, a thick biofilm developed on the anodic electrode, and entrapment of organic particles from the wastewater may explain the low coulombic efficiency during removal of BOD. In addition, we observed an increase in methane generation over time due to the development of pockets in the thick anodic biofilm where electricigens could not compete with methanogens due to insulating effects of the biofilm

on the electrode material. We had already published that methane generation was an important factor that will reduce the coulombic efficiency in MFCs.[17] Unexpectedly, however, the internal resistance (measured by the steady discharging method) remained at 3.83 Ω before and after a thick biofilm developed during an operating period of five months while the coulombic efficiency decreased from 1.5 - 3.6% to 0.6%. Upon cleaning the MFC after the operating period, it became clear that organic particles and biomass had, indeed, accumulated in the anode chamber, similarly as what was seen by Rabaey et al..[42]

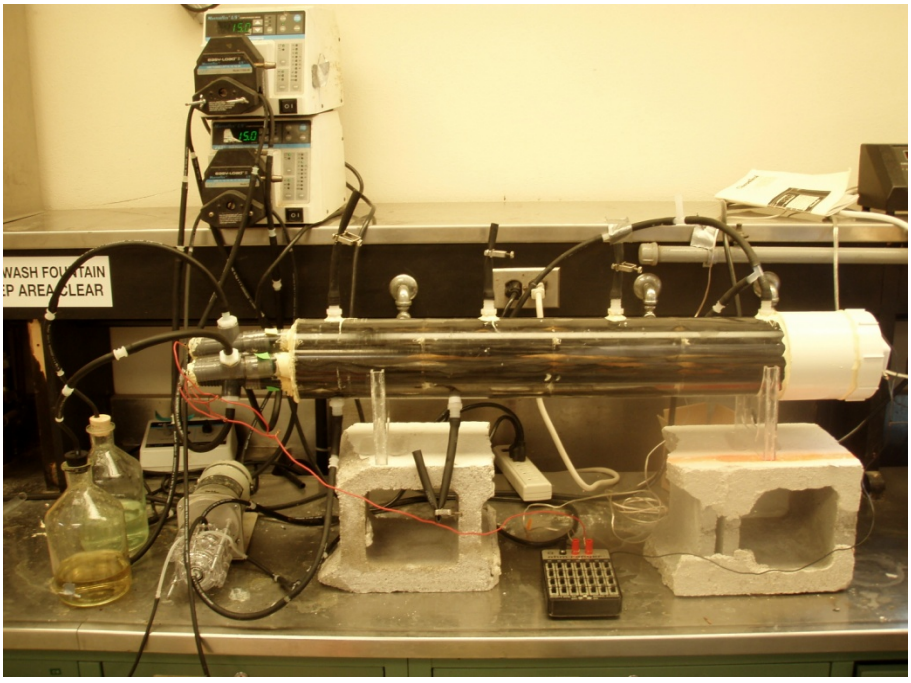

Figure 2-3. A 6-liter MFC setup before the treatment of real brewery wastewater. The anodic and cathodic electrode material consisted of 2-m strings of carbon fiber (Panex 30 - unsized, Zoltek, St. Louis, MO) and the four internal cathode chambers (two cathode loops) were fabricated by rolled up cation exchange membrane material (CMI-7000, Membrane International, Glen Rock, NJ). Ferricyanide solution was recirculated through the cathode tubes. Real wastewater from a brewery was pumped into the anode chamber at a flow rate of 1.4 L/d with 7.2 L/d of make-up water for dilution (the overall hydraulic retention time was 15 h), which resulted in a volumetric loading rate of 0.9 – 1.9 g COD/L/d. Effluent from the 5.4-liter anode chamber was recirculated and mixed with the diluted brewery wastewater.

H. Protein mixtures make up a large fraction of the organic material in municipal wastewater and wastewater from livestock-related industries. Heilmann and Logan[20] performed a study on the electricity generation from protein-rich wastewaters using a MFC with a 28-mL anode. In this study, three different protein containing waste streams (bovine serum albumin [BSA] added to municipal wastewater [1,100 mg/L], peptone added to municipal wastewater [500 mg/L], and a high protein content slaughterhouse wastewater [1,420 mg BOD/L]) were evaluated. The maximum power densities were 354, 269, and 80 mW/m^2 for the BSA, peptone, and slaughterhouse wastewater, respectively (external resistance > 50 Ω). In addition, BOD removal efficiencies were 90, 86, and 93% with maximum coulombic efficiencies of 20.6, 6.0, and 5.2%, respectively. While this experiment involved batch rather than continuously operating MFCs, the high removal efficiencies indicate the ability of bacteria to convert protein into low molecular-weight substrates. The duration of the batch tests lasted ~ 30 h, with the maximum power achieved in ~ 7 h. The highest power was achieved with BSA, which is a less complex protein than either peptone or proteins in slaughterhouse wastewater.[20]

I. Swine waste with a complex substrate composition, consisting of proteins, celluloses, and lipids, was also tested as a substrate for a MFC with an anode volume of 28 mL.[35] However, the swine waste in this study also contained a high concentration of soluble organic material (soluble COD concentration of 8,320 mg/L), and therefore the complex substrate constituents were likely not converted to electricity, but instead to low-molecular weight compounds, such as acetate. The authors obtained a maximum power density of 261 mW/m^2 with an external resistor of 200 Ω. The soluble COD removal

efficiency was 27% and the coulombic efficiency was 8%.[35] One likely reason for the relatively low coulombic efficiency was the diffusion of oxygen into the anodic chamber, which would be the terminal electron acceptor during the removal of COD. Such oxygen diffusion was apparent because of ammonia oxidation that was observed in the anodic compartment.[35]

We have compared these MFC studies to verify that complex wastewater substrates result in lower coulombic efficiencies compared to easily degradable synthetic substrates, such as glucose and acetate (Table 2-1 is ordered based on coulombic efficiency). Comparisons between studies are difficult because anode sizes, electrode and membrane materials, inocula, reactor configurations, anolyte and catholyte conductivity, oxygen influx to the anode, cathode electron transfer mechanisms, temperatures, pH levels, etc. are different, resulting in variable internal resistances. Despite this problem, a trend emerged with hospital wastewater, municipal wastewater, slaughterhouse wastewater, swine waste, and brewery wastewater (in bold) showing lower coulombic efficiencies with a highest level of 36% compared to synthetic wastewaters with a highest level of 98%. The lower coulombic efficiencies are attributed to increased energy expenditures for the microbes to hydrolyze particulate organic substrates, slower kinetic rates to convert organic macromolecules into more easily metabolized simple sugars and carboxylic acids, and a more complex anodic food web. The complex food web is the main reason for the low coulombic efficiencies because organic substrates are consumed by a diversity of bacteria and archaea, so only relatively small amounts or organics can be converted to current by electricigens.

Anodic foodweb. One reason for the trend of higher coulombic efficiencies for glucose and carboxylic acids compared to the lower values for higher-molecular weight substrates or more complex wastewaters, is the loss in efficiency of electron transfer for the anodic foodweb. For a complex substrate, fermenters must first convert polymers, such as (poly)saccharides and proteins, to acetate and hydrogen, which can then be converted to electrons (to the anodic electrode), protons, and CO_2 by electricigens. During the study of Rabaey et al.[42] with a continuous-fed tubular MFC, the highest coulombic efficiency was achieved with acetate (vs. glucose) because the electricigens, such as *Geobacter* sp., convert acetate to CO_2, protons, and electrons directly without having to sustain a fermentative population. Indeed, we have observed a microscopic non-visible biofilm when feeding solely acetate to the anode compartment while a thick biofilm was visible with the naked eye when feeding glucose or sucrose. Liu et al.[28] found a higher coulombic efficiency of 13.2% with acetate compared to 7.7% with butyrate. This lower efficiency for butyrate as a substrate can likely be explained by the need for acetogenic bacteria to first generate acetate and hydrogen as their end product without generating any electric current. Subsequently, the produced acetate may then be further oxidized to CO_2 and the produced hydrogen oxidized by electricigens, who are using the electrode as the electron acceptor. In other words, a loss in efficiency is apparent when a two-step process of biological oxidation of butyrate occurs rather than direct acetate oxidation with the anodic electrode. For the metabolic processes and biosynthesis to sustain the anodic foodweb, energy (electrons) is required from the organic compounds in wastewater.

The anodic foodweb of nondefined mixed cultures has not been studied in detail and the question remains if complex compounds in wastewater are first converted to acetate and hydrogen by fermenters after which electricigens convert acetate and hydrogen into current, or if some of the fermentable compounds are directly converted into current by fermenters or other anaerobic respirers? Workers have shown that nondefined mixed cultures acquired electrochemical activity over the operating period of the fuel cell.[17,41] For instance, Rabaey et al.[41] showed increased electrochemical activity with cyclic voltammetry and an enriched community of diverse bacteria from the phyla Firmicutes (e.g., *Lactococcus* sp., *Enterococcus* sp., *Clostridium* sp.), Alphaproteobacteria, Betaproteobacteria, and Gammaproteobacteria (*Pseudomonas* sp.). The DNA finger-printing technique that was used to characterize the community did not detect typical electricigens, such as *Geobacter* spp.. However, they may have been important in the foodweb albeit at a relatively low level of 1-5% of the bacterial community, and therefore remained not detected due to the nonsensitive nature of this molecular biology technique. *Pseudomonas* sp., which can oxidize acetate in the anaerobic anode compartment in the presence of a working electrode, was detected, isolated, and able to excrete metabolites that can mediate electron transfer (when propagated in a rich nutrient medium).[41] Indeed, under anaerobic conditions when no alternative electron accepters were present, the activity of *Pseudomonas* sp. was enhanced when an anodic electrode was present in a MFC compared to a serum bottle without an electrode (this organism does not ferment and needs a terminal electron acceptor to respire with), which may indicate a role in electron transfer for *Pseudomonas* sp. in the nondefined mixed culture.[41] In a follow-up study, these workers showed that

production of electron mediators by *Pseudomonas* sp. benefited the electron transport for other microbes, such as *Enterococcus faecium*, possibly explaining why a mixed culture of microbes can generate a higher current density compared to a pure culture.[40] Kim et al.[23] isolated various bacteria from an anodic biofilm and found additional phylogenetic bacterial groups, including fermenters and anaerobic respirers, which were electrochemically active. For instance, two enriched cultures of species of Bacteroidetes (a prevalent phylum in their biofilm) showed electrochemical activity with cyclic voltammetry.[23] However, we do not know the relative importance of each of these electrochemically active bacteria in a dense and diverse anodic biofilm. Therefore, measuring electrochemical activity for a bacterium isolated from the anode may not necessarily identify an electron transferring bacterium of importance to the overall electric current generation. Besides fermenters and anaerobic respirers, Kim et al.[23] found 16S rRNA gene sequences from electricigens in the genera *Geobacter* and *Shewanella*. In addition, the two isolated *Pseudomonas* sp. strains were not electrochemically active.

Present Challenges

Low coulombic efficiency. Thus far, we have discussed that the: 1. entrapment and accumulation of organic particles from wastewater in the anodic biofilm[42]; 2. production of methane[17]; 3. losses in efficiency due to the energetic requirements to sustain fermentative and acetogenic communities in the anodic foodweb[36]; and 4. diffusion of the terminal electron acceptor oxygen into the anode[35] are all responsible for low coulombic efficiencies, especially during the treatment of real wastewater. Other

factors that could also contribute to lowering the coulombic efficiency are the: 1. presence of other terminal acceptors, such as nitrate, soluble Fe(III), and sulfate, in the wastewater; 2. energetic requirements for electricigens to sustain bacterial metabolism and biosynthesis; and 3. escape of gaseous products, such as hydrogen, with the off gas. In this chapter we have highlighted that the coulombic efficiency for real wastewater treatment with MFC systems must be improved by, for example, placing pre-acidification tanks in front of MFC systems. Pre-acidifying wastewater would reduce the biofilm thickness of the anodic electrode by shifting the anodic foodweb from predominant activity by fast-growing fermenters towards predominant activity by slow-growing electricigens, similarly as found in anaerobic digesters.[3] A thin biofilm would reduce the likelihood of harboring methanogens, and thus methane generation.

Recent biofilm modeling papers, have also suggested that increasing biofilm thickness and biomass accumulation would reduce the current density due to a decrease in biofilm conductivity.[33] With similar biomass compositions, however, these authors found with their model that biofilm thickness by itself did not have an effect on current density. We have found empirically in our 6-L MFC that the internal resistance and power output did not change during the increase in biofilm thickness (at a pH of 7.3 and a temperature of ~ 22°C), but that the coulombic efficiency had decreased considerably. Marcus et al.[33], suggested that a higher shear and turbulence is advantageous to maintain a thin, dense biofilm with the goal to reduce entrapment of biomass and to sustain a high current density.

Slow kinetic rates. A low coulombic efficiency limits power density or power output, however, the slow kinetic rate of electron transfer from anodic microbes to electrodes in MFCs may be more crucial. As mentioned above, beyond a volumetric loading rate of 2.5 and 3.4 g COD/L/d, an extinction effect of the power density was observed.[17,41] Such volumetric loading rates are competitive with high-rate-aerated activated sludge systems but not with high-rate anaerobic digestion systems.[41,51] One way of increasing the rates is to increase the activity of the biomass by changing operating conditions. Indeed, an optimum anode electrode potential has increased the biofilm activity (per biomas concentration) of electron transfer to the anode electrode.[1]

Another way of increasing the rates may be by optimizing biofilm thickness. A modeling paper by Picioreanu et al.[39] showed that the resistance to substrate diffusion increases with biofilm thickness. This would slow microbial conversion rates, and thus reduce the current output and volumetric loading rate. Thus, maintaining thin anodic biofilms is imperative to improve the volumetric loading rates, which has a direct effect on the required MFC volume. However, this creates a problem that was observed in a study by Aelterman et al..[1] The thin biofilm requirement dictated by substrate diffusion resistances, resulted in low levels of active biomass in their MFC (~ 30 times lower than anaerobic digestion), which explained the lower kinetic rates of substrate removal for MFCs compared to anaerobic digesters despite similar biomass activities of ~ 3.4 g COD/g volatile suspended solids/d. They described the unique nature of anodic biofilms: "Biofilms growing on electrodes are subject to a duality that is rarely observed in natural conditions: the substrate concentrations are the highest at the outer layers of the biofilm while the electrode is only available at the inner layer of the biofilm. This feature

requires the development of thin and open biofilm structure, which allows for a sufficient migration of substrate without hampering the transfer of electrons to the electrode".[1] Development of an electrode material with a vast surface area may resolve this problem, but it should, at the same time, assure high shear forces to slough off biofilm layers and remove entrapped organic particles from wastewater.

Reactor scale up. Electrochemical techniques, such as impedance spectroscopy, have shown that high internal resistance in MFCs is influenced by the slow movement of ions between the electrodes due to a high electrolyte resistance of the anode and cathode solutions or the ion exchange membrane (i.e., ohmic limitations). Researchers have, therefore, often miniaturized MFCs, because this inherently increases the membrane surface area to volume ratio and reduces the distance between electrodes, resulting in decreased electrolyte resistances (and thus increased power output).[8,27,36,43,46] For example, Liu et al.[27] increased the power density from 720 to 1210 mW/m^2 in a 28-mL MFC by shortening the distances between the electrodes. Such a miniaturization approach is helpful for research purposes to circumvent internal resistances due to reactor configuration limitations, however, this approach is not practical for wastewater treatment systems that require large reactor volumes.

Knowledge that was gained from hydrogen or methanol fuel cell fields cannot automatically be translated into MFC optimizations, especially when it comes to scale up. The energy density per unit volume of hydrogen gas or methanol is much higher than for wastewater (hydrogen gas [300 bar]: 119.9 MJ/kg, methanol: 19.9 MJ/kg[24], and wastewater: 0.58 J/kg). In accordance, the volumes of fuel streams are much higher for

MFCs than for hydrogen and methanol fuel cells. With large treatment volumes, scale up is of the highest importance, but we cannot use a single MFC volume because of the requirements of high potential and current levels. To reach these high potential and current levels, we have to place individual MFCs in an electrical array (as explained in the outlook section below), and thus the scale up needs to be only from the mL scale to the L scale. This three orders of magnitude scale up without performance losses, however, is still a great challenge. Here, we discuss three tasks/challenges that are important/must be overcome during scale up, to: 1. maintain low internal resistance while increasing the level of electrochemically-active biomass; 2. optimize reactor designs; and 3. develop new ways of separating the anode from the cathode:

Maintain low internal resistance while increasing the levels of electrochemically-active biomass. For a low internal resistance, a close proximity of anode to exchange membrane to cathode, as well as a sufficiently large exchange membrane surface area is crucial. On the other hand, we need high surface, porous anode materials to offer enough surface area for the desired thin biofilm of electricigens. A high power density cell would, thus, call for a more or less two-dimensional thin layer assembly of anode/exchange membrane/cathode to minimize the internal resistance, while an optimized coulombic efficiency cell would call for a three-dimensional, porous anode that allows for optimized biotransformation. Achieving close proximity, and, still, an efficient three-dimensional anode design has been accomplished for a mL-scale MFC but will be a challenge for a L-scale MFC. In addition, clogging by accumulating biomass and particles from wastewater must be prevented.

Optimize reactor designs. One way to realize this could be with a tubular MFC design (shell and tube design). However, this raises another challenge - with our present knowledge, the electrical connection of one individual L-scale MFC to another MFC (in series) would happen at one site of the long tubular cell, which means that electrons must flow to this specific connection site. This problem has been circumvented for hydrogen and methanol fuel cells by using bipolar plates to directly connect the anode from one cell to the cathode of the next cell, without electrical wiring, which allows a direct transfer of electrons through the chain of individual cells in a fuel cell stack without major resistance losses.[24] Such bipolar plates, which are placed between two individual cells, are made of highly conductive material, where almost the entire surface of one site of an individual anode is touching a bipolar plate that is then touching almost the entire surface of one site of an individual cathode from the neighboring cell. For a L-scale MFC this would only work in a large flat panel design, which is not practical due to its size and complexity. Another challenge for a scaled-up MFC design is the distribution of the performance within one individual fuel cell and between fuel cells. If anywhere, a low biotransformation activity zone exists this will consume energy from the system, reducing the overall power output. This phenomenon is well known to occur in hydrogen and methanol fuel cells.[24]

Develop new ways of separating the anode and cathode. The selection of an ion exchange membrane will also become more and more crucial during scale up. Researchers from the Schröder laboratory and the Hamelers laboratory showed that the highly-selective (and expensive) proton exchange membrane for hydrogen fuel cells (Nafion) is not ideal for MFCs because at neutral pHs cations are moving from the anode

to the cathode rather than protons.[47,53] Another study from the Schröder laboratory showed that the performance of an anion exchange membrane is better than a cation exchange membrane, but even then the membrane resistance is too high.[15] One approach to reduce the internal resistance is to remove the ion exchange membrane and work without any membrane or an ultrafiltration membrane. This may be useful for mL-scale MFCs, however, in a L-scale MFC a considerable liquid pressure gradient would cause massive mixing of anolyte and catholyte. We anticipate a low coulombic efficiency as a result due to the intrusion of oxygen into the anode.

Outlook: Economic Evaluation

The treatment of high organic content wastewater represents the most promising application of MFC technology at a large scale because of the higher energy density of the solution compared to, for example, municipal wastewater. This can be further illustrated with an overview of MFC wastewater treatment economics for a theoretical and relatively small 100,000 L/d wastewater stream with an organic concentration of 2,000 mg BOD/L. We assume here that our MFC has an 8-h HRT (and thus an anode volume of 33,333 L), an 85% BOD removal efficiency, and a 20% coulombic efficiency (Table 2-1 shows a maximum coulombic efficiency of 22% for real wastewater). With these assumptions the current generation is:

$$Coulombic\ efficiency = \frac{(molecular\ weight\ O_2)(current)}{(Faraday\ const.)(e^- / mole\ O_2)(flow\ rate)(BOD\ removal)}\ 100\% \qquad \text{(equation 1)}$$

$$20\% = \frac{(32\ g\ O_2 / mole\ O_2)(current)}{(96,485\ Coulombs / mole\ e^-)(4\ moles\ e^- / mole\ O_2)(1.157\ L / s)(1.7\ g\ O_2 / L)} \Rightarrow Current = 4,744\ A$$

The above current calculation is insufficient to calculate the total power generation - power generation is calculated as the potential multiplied by the current (Ohms law) - and therefore the potential for the MFC needs to be determined. We achieved a sustainable potential of ~ 0.67 V at an external resistor of 100 Ω for our 6-liter MFC described in this chapter, and here we assume a potential of 0.6 V. In addition, using the MFC potential requires some further assumptions for this theoretical wastewater treatment scenario (based on current understanding of MFC technology):

1. A single 33,333 L anode chamber is not feasible. To achieve high MFC power densities, it is essential to maintain the anode and cathode reactions in close proximity while separated by an ion exchange membrane. The close spacing requirements result in the necessity of MFC designs with numerous smaller MFC cells. For this economic evaluation, we assume individual MFCs with anode volumes of 20 L. Then, the total MFC array will consist of 1,667 MFC cells (33,333 L of total anode volume / 20 L of anode volume per one MFC cell).
2. The 1,667 fuel cells need to be placed into an electrical array with both series and parallel connections to add potential and current, respectively (similarly to fuel cells and photovoltaic cells).[2,24] The series connections will add potential - generating a 12-V potential will be desirable to charge batteries or to convert the current from a DC to AC. To achieve a 12-V potential, we assume that twenty 0.6-V MFCs must be placed in series. The parallel connections will add current - the 83 groups of 20 MFC cells in series will be connected in

parallel.

The current generation from the 83 MFC groups in parallel is determined with the assumption that the current generation from each MFC is proportional to the total current generation from the 33,333 L of total anode volume, or 2.85 A per 20-L of anode volume (equivalent to a power output of 85 W/m^3). This is according to a best-possible scenario because in series the cell with the lowest potential and in parallel the group of MFCs with the lowest current will dictate the total potential and current, respectively (similar to fuel cells).[2] In addition, the 85 W/m^3 is much higher than the 5 W/m^3 we achieved with the 6-L MFC, but we anticipate that the higher power output can be achieved by further improving the MFC configuration and by pre-acidifying the wastewater (the latter to improve the coulombic efficiency). The current generation for 83 MFCs in parallel will equal 236.2 A (83 multiplied with 2.85 A). Thus, the power generation will be 2,834 W according to Ohms law (The system coulombic efficiency = ~1.0% based on 236.2A). On an annual basis, this represents an electrical power generation of 24,758 kWh. Thus, the total value of the power generated from this wastewater treatment is $2,971 per year when we assume an electricity value of $0.12 / kWh (a representative value in the USA).

Such a value of electricity generation will not recover the investment costs. Even if the anticipated 20% MFC coulombic efficiency could be tripled to 60% (which has not been achieved with real wastewater, but could be a reality when, for example, a pre-acidification tank is installed before the MFC), the resulting $8,937 value of annual generated electricity is also unlikely to recover the investment. With the more dilute municipal wastewater (~ 300 - 500 mg BOD/L), the economics based on just electricity

generation are even more unfavorable. The economic evaluation of our theoretical wastewater-to-electricity conversion, however, remains incomplete. A ~ 2,000 mg BOD/L waste stream requires treatment, which presently is costly and energetically unfavorable due the requirement of aeration (i.e., adding a terminal electron acceptor) to the mixed liquor in activated sludge treatment tanks. Currently, if our wastewater stream was discharged to a municipal wastewater treatment facility, the municipality would impose a waste treatment fee of ~ $0.53 / kg BOD to cover municipal costs (for a BOD concentration > 300 mg/L and based on data from municipalities in Chicago, IL and St. Louis, MO), which includes the electricity cost for aeration. Thus, the cost to treat our wastewater stream at a municipal wastewater treatment plant with activated sludge tanks (secondary treatment) is $32,760 per year.

Combined, the total MFC cost justification will be $35,731 per year. The present value of a MFC system can then be calculated with engineering economics and the following assumptions: inflation - 3%; electricity inflation – 6%; wastewater treatment inflation – 5%; and MFC service life – 10 years. For a 100,000 L wastewater with a 2,000 mg BOD/L and a coulombic efficiency of 20%, the net present value equals $380,528 or $228 / 20-L MFC. These MFC economic justifications are driven by electricity revenue generation and municipal waste treatment cost. However, the latter economic driver is more important regardless of energy costs. Even if future electricity costs will rise considerably (beyond 6% annually), the treatment costs will likely still be more important than electricity generation per se, because electricity consumption is a relatively high cost factor for activated sludge treatment at a municipal wastewater treatment plant. Currently, ~ 50% of the costs for municipal secondary wastewater

treatment is to cover electricity consumption to run aeration blowers (or $8,624 per year for our wastewater example at an electricity cost of $0.12 /kWh)[7], and this percentage would increase when the cost of electricity rises. It is also clear from this economic evaluation that the capital costs of MFC construction must be relatively low to make this intricate system economically viable. Lastly, our example does not reflect any MFC operating costs, which will likely include surveillance and chemical costs.

Even though the return of investment may never be high, social and environmental considerations may make MFC technology feasible. Instead of consuming electricity for aeration (~ 71,867 kWh per year for our 100,000 L/d wastewater stream example - based on information from Burton)[7], the combined annual electricity savings and generation by replacing activated sludge with MFCs would mount to 96,693 kWh. This could reduce the need for new electrical power plants, especially since ~ 35 billion kWh is consumed by the 15,000 wastewater treatment plants in the U.S. (~ 1.5% of the total annual U.S. electricity consumption)[7], and would lower the carbon dioxide emissions from nonrenewable energy sources. In addition, the economics of MFC treatment would improve if carbon trading becomes institutionalized. The estimation of energy savings does show, however, that since 50% of energy use at the municipal wastewater treatment is for aeration[7], generating 24,826 kWh of electricity per year by MFCs would not completely replace the other 71,867 kWh per year needed for treating our wastewater, which is used for pumps, biosolids treatment, and disinfection. Thus, further optimization efforts are necessary to create a sustainable, zero carbon wastewater treatment plant.

To promote a successful scale up effort, we must now focus on the development of more efficient MFC configurations with low cost, sustainable materials. To further improve the coulombic efficiency of wastewater-to-electricity conversion, pretreatment of real wastewater (e.g., pre-acidification) is necessary while oxygen diffusion from the cathode into the anode must be circumvented. In addition, and maybe more importantly, the microbial kinetics must be improved to decrease the necessary volume (i.e., shortening the HRT by increasing the volumetric loading rates) compared to activated sludge systems and to make MFC technology competitive to commercial high-rate anaerobic digestion systems.

Acknowledgement

J.J.F. was supported through a collaborative agreement with the Fermentation Biotechnology Research Unit, USDA, Agricultural Research Service, Peoria, IL. M.R. is working in the Angenent group as a postdoctoral research scientist of the Fermentation Biotechnology Research Unit, USDA, Agricultural Research Service, Peoria, IL L.T.A. was supported by the U.S. National Science Foundation via a NSF CAREER grant, award number 0645021. We thank Ryan Mackin (Washington University) for the fabrication of the 6.0-liter MFC, Adam Webb (Washington University) for assistance during the 6-liter MFC operating period, Al Beers (Anheuser-Busch, Inc.) for providing real brewery wastewater, and Ray Ehrhard (Washington University) for helpful discussions regarding the economic evaluation of wastewater treatment.

References:

(1) Aelterman, P.; Freguia, S.; Keller, J.; Verstraete, W.; Rabaey, K., The anode potential regulates bacterial activity in microbial fuel cells. *Appl. Microbiol. Biotechnol.* 2008, *78*, 409-418.

(2) Aelterman, P.; Rabaey, K.; Pham, H. T.; Boon, N.; Verstraete, W., Continuous electricity generation at high voltages and currents using stacked microbial fuel cells. *Environ. Sci. Technol.* 2006, *40*, 3388-3394.

(3) Alphenaar, A., Anaerobic granular sludge: characterization, and factors affecting its functioning, in environmental technology; Wageningen Agricultural University, Wageningen, The Netherlands, 1994.

(4) Angenent, L. T.; Karim, K.; Al-Dahhan, M. H.; Wrenn, B. A.; Domínguez-Espinosa, R., Production of bioenergy and biochemicals from industrial and agricultural wastewater. *Trends Biotechnol*. 2004, *22*, 477-485.

(5) Angenent, L. T.; Zheng, D.; Sung S.; Raskin, L., Microbial community structure and activity in a compartmentalized, anaerobic bioreactor. *Water Environ. Res.* 2002, *74*, 450-461.

(6) Bond, D. R.; Lovley, D. R., Electricity production by *Geobacter sulfurreducens* attached to electrodes. *Appl. Environ. Microbiol.* 2003, *69*, 1548-1555.

(7) Burton, F. L., Water and wastewater industries: Characteristics and energy management opportunities 1996, Electric Power Research Institute, Inc. (EPRI), Community Environmental Center, 1996.

(8) Chiao, M.; Lam, K. B.; Lin, L., Micromachined microbial fuel cell. *IEEE*. 2003, 383-386.

(9) Clauwaert, P.; Rabaey, K.; Aelterman, P.; de Schamphelaire, L.; Pham, T. H.; Boeckx, P.; Boon, N.; Verstraete, W., Biological denitrification in microbial fuel cells. *Environ. Sci. Technol*. 2007, *41*, 3354-3360.

(10) Fuchs, W.; Binder, H.; Mavrias, G.; Braun, R., Anaerobic treatment of wastewater with high organic content using a stirred tank reactor coupled with a membrane filtration unit. *Water Res*. 2003, *37*, 902-908.

(11) Ginestet, P.; Maisonnier, A.; Sperandio, M., Wastewater COD characterization: Biodegradability of physico-chemical fractions. *Water Sci. Technol.* 2002, *45*, 89-97.

(12) Gohil, A; Nakhla, G., Treatment of food industry waste by bench-scale upflow anaerobic sludge blanket-anoxic-aerobic system. *Water Environ. Res*. 2006, *78*, 974-985.

(13) Gorby, Y. A.; Yanina, S.; McLean, J. S.; Rosso, K. M.; Moyles, D.; Dohnalkova, A.; Beveridge, T. J.; Chang, I. S.; Kim, B. H.; Kim, K. S.; Culley, D. E.; Reed, S. B.; Romine, M. F.; Saffarini, D. A., ; Hill, E. A.; Shi, L.; Elias, D. A.; Kennedy, D. W.; Pinchuk, G.; Watanabe, K.; Ishii, S.; Logan, B. E.; Nealson, K. H.; Fredrickson, J. K., Electrically conductive bacterial nanowires produced by *Shewanella oneidensis* strain MR-1 and other microorganisms. *Proc. Nat. Acad. Sci. U.S.A.* 2006, *103*, 11358-11363.

(14) Gottschalk, G., *Bacterial Metabolism*; 2nd ed.; Springer-Verlag: New York, NY, 1986.

(15) Harnisch, F.; Schröder, U.; Scholz, F., The Suitability of monopolar and bipolar ion exchange membranes as separators for biological fuel cells. *Environ. Sci. Technol.* 2008, *42*, 1740-1746.

(16) He, Z.; Angenent, L. T., Application of bacterial biocathodes in microbial fuel cells. *Electroanalysis*. 2006, *18*, 2009-2015.

(17) He, Z.; Minteer, S. D.; Angenent, L. T., Electricity generation from artificial wastewater with an upflow microbial fuel cell. *Environ. Sci. Technol.* 2005, *39*, 5262-5267.

(18) He, Z.; Shao, H.; Angenent, L. T., Increased power production from a sediment microbial fuel cell with a rotating cathode. *Biosens. Bioelectron.* 2007, *22*, 3253-3255.

(19) He, Z.; Wagner, N.; Minteer, S. D.; Angenent, L. T., The upflow microbial fuel cell with an interior cathode: Assessment of the internal resistance by impedance spectroscopy. *Environ. Sci. Technol.* 2006, *40*, 5212-5217.

(20) Heilmann, J.; Logan, B. E., Production of electricity from proteins using a microbial fuel cell. *Water Environ. Res*. 2006, *78*, 531-537.

(21) Hoffmann, R.; Garcia, M. L.; Veskivar, M.; Karim, K.; Al-Dahhan, M. H.; Angenent, L. T., Effect of shear on performance and microbial ecology of completely-stirred anaerobic digesters treating animal manure. *Biotechnol. Bioeng*. 2008, *100*, 38-48.

(22) Ishii, S. I.; Shimoyama, T.; Hotta, Y.; Watanabe, K., Characterization of a filamentous biofilm community established in a cellulose-fed microbial fuel cell. *BMC Microbiology*. 2008, *8*, 6.

(23) Kim, G. T.; Webster, G.; Wimpenny, J. W. T.; Kim, B. H.; Kim, H. J.; Weightman, A. J., Bacterial community structure, compartmentalization and activity in a microbial fuel cell. *J. Appl. Microbiol.* 2006, *101*, 698-710.

(24) Larminie, J.; Dicks, A., *Fuel Cell Systems Explained*; 2nd ed.; John Wiley & Sons, Ltd.: Chichester, West Sussex, England, 2003.

(25) Lepisto, S. S.; Rintala, J. A., Start-up and operation of laboratory-scale thermophilic upflow anaerobic sludge blanket reactors treating vegetable processing wastewaters. *J. Chem. Technol. Biotechnol*. 1997, *68*, 331-339.

(26) Lettinga, G., Anaerobic digestion and wastewater treatment systems. Antonie Van Leeuwenhoek. 1995, *67*, 3-28.

(27) Liu, H.; Cheng, S.; Logan, B. E., Power generation in fed-batch microbial fuel cells as a function of ionic strength, temperature, and reactor configuration. *Environ. Sci. Technol.* 2005, *39*, 5488-5493.

(28) Liu, H.; Cheng, S.; Logan, B. E., Production of electricity from acetate or butyrate using a single-chamber microbial fuel cell. *Environ. Sci. Technol.* 2005, *39*, 658-62.

(29) Liu, H.; Logan, B. E., Electricity generation using an air-cathode single chamber microbial fuel cell in the presence and absence of a proton exchange membrane. *Environ. Sci. Technol*. 2004, *38*, 4040-4046.

(30) Logan, B. E.; Hamelers, B.; Rozendal, R.; Schröder, U.; Keller, J.; Freguia, S.; Aelterman, P.; Verstraete, W.; Rabaey, K., Microbial fuel cells: Methodology and technology. *Environ. Sci. Technol.* 2006, *40*, 5181-5192.

(31) Lovley, D. R., Bug juice: Harvesting electricity with microorganisms. *Nat. Rev. Microbiol.* 2006, *4*, 497-508.

(32) Madigan, M. T.; Martinko, J. M., *Brock Biology of Microorganisms*; Eleventh ed.; Pearson/Prentice Hall, Upper Saddle River, NJ, 2006.

(33) Marcus, A. K.; Torres, C. I.; Rittmann, B. E., Conduction-based modeling of the biofilm anode of a microbial fuel cell. *Biotechnol. Bioeng.* 2007, *98*, 1171-1182.

(34) Marsili, E.; Baron, D. B.; Shikhare, I. D.; Coursolle, D.; Gralnick, J. A.; Bond, D. R., *Shewanella* secretes flavins that mediate extracellular electron transfer. *Proc. Nat. Acad. Sci. U.S.A.* 2008, *105*, 3968-3973.

(35) Min, B.; Kim, J.; Oh, S.; Regan, J. M.; Logan, B. E., Electricity generation from swine wastewater using microbial fuel cells. *Water Res.* 2005, *39*, 4961-4968.

(36) Min, B.; Logan, B. E., Continuous electricity generation from domestic wastewater and organic substrates in a flat plate microbial fuel cell. *Environ. Sci. Technol.* 2004, *38*, 5809-5814.

(37) Mulkerrins, D.; O'Connor, E.; Lawlee, B.; Barton, P.; Dobson, A., Assessing the feasibility of achieving biological nutrient removal from wastewater at an Irish food processing factory. *Bioresour. Technol*. 2004, *91*, 207-214.

(38) Park, D. H.; Zeikus, J. G., Impact of electrode composition on electricity generation in a single-compartment fuel cell using *Shewanella putrefaciens*. Appl. *Microbiol. Biotechnol*. 2002, *59*, 58-61.

(39) Picioreanu, C.; Head, I. M.; Katuri, K. P.; van Loosdrecht, M. C. M.; Scott, K., A computational model for biofilm-based microbial fuel cells. *Water Res*. 2007, *41*, 2921-2940.

(40) Rabaey, K.; Boon, N.; Hofte, M.; Verstraete, W., Microbial phenazine production enhances electron transfer in biofuel cells. *Environ. Sci. Technol.* 2005, *39*, 3401-3408.

(41) Rabaey, K.; Boon, N.; Siciliano, S. D.; Verhaege, M.; Verstraete W., Biofuel cells select for microbial consortia that self-mediate electron transfer. *Appl. Environ. Microbiol*. 2004, *70*, 5373-5382.

(42) Rabaey, K.; Clauwaert, P.; Aelterman, P.; Verstraete, W., Tubular microbial fuel cells for efficient electricity generation. *Environ. Sci. Technol.* 2005, *39*, 8077-8082.

(43) Rabaey, K.; Lissens, G.; Siciliano, S.D.; Verstraete, W., A microbial fuel cell capable of converting glucose to electricity at high rate and efficiency. *Biotechnol. Lett.* 2003, *25*, 1531-1535.

(44) Rabaey, K.; Rodriguez, J.; Blackall L. L.; Keller J.; Gross, P.; Batstone, D.; Verstraete, W.; Nealson, K. H., Microbial ecology meets electrochemistry: Electricity-driven and driving communities. *ISME J*. 2007, *1*, 9-18.

(45) Rabaey, K; Verstraete, W., Microbial fuel cells: Novel biotechnology for energy generation. *Trends Biotechnol*. 2005, *23*, 291-298.

(46) Ringeisen, B. R.; Henderson, E.; Wu, P. K.; Peietron, J.; Ray, R.; Little, B.; Biffinger, J. C.; Jones-Meehan, J. M., High power density from a miniature microbial fuel cell using *Shewanella oneidensis* DSP10. *Environ. Sci. Technol*. 2006, *40*, 2629-2634.

(47) Rozendal, R. A.; Hamelers, H. V. M.; Buisman, C. J. N., Effects of membrane cation transport on pH and microbial fuel cell performance. *Environ. Sci. Technol*. 2006, *40*, 5206-5211.

(48) Schlegel, H. G., *General Microbiology*; Cambridge University Press: Cambridge, UK, 1992.

(49) Schröder, U., Anodic electron transfer mechanisms in microbial fuel cells and their energy efficiency. *Phys. Chem. Chem. Phys*., 2007, *9*, 2619-2629.

(50) Shukla, A. K.; Suresh, P.; Berchmans, S.; Rajendran, A., Biological fuel cells and their applications. *Curr. Sci*., 2004, *87*, 455-468.

(51) Tchobanoglous, G.; Burton, F. L.; Stensel, H. D., *Wastewater Engineering, Treatment and Reuse*; 4th ed.; Metcalf & Eddy, McGraw Hill: New York, NY, 2003.

(52) Ubukata, Y., Fundamental mechanisms of phosphate removal by anaerobic/aerobic activated sludge in treating municipal wastewater. *Eng. Life Sci.* 2006, *6*, 51-56.

(53) Zhao, F.; Harnisch, F.; Schröder, U.; Scholz F.; Bogdanoff P.; Hermann, I., Challenges and constraints of using oxygen cathodes in microbial fuel cells. *Environ. Sci. Technol*. 2006, *40*, 5193-5199.

Chapter 3

BES Engineering Evaluation

Abstract

In this chapter, I developed an engineering evaluation of a laboratory-scale BES in response to questions asked by my dissertation committee during my thesis proposal. The questions centered around seven different aspects of BES performance. Section 1 covers the derivation of the Nernst equation and its application to the BES half-reactions. By calculating the anode and cathode potentials with the Nernst equation, the theoretical performance boundaries of the MFC were established. Section 2 addresses coulombic efficiency calculations. Coulombic efficiencies measure the percentage of electrons captured as electric current compared to the total electrons produced from the oxidation of organic substrates. These calculations determined the actual versus possible electricity production from the BES wastewater being treated. Coulombic efficiency calculations also help account for the fate of electrons not captured as current in the BES. In section 3, the BES solution chemistry is evaluated. Emphasis was placed on understanding CO_2 absorption, hydration, and dissociation and the influence of the CO_2 partial pressure on pH and BES bicarbonate ion concentrations. Development of the chemistry was critical to explaining chapter 5 results, where BES electroneutrality maintenance with bicarbonate ions increased the BES anolyte pH, total alkalinity, and conductivity.

Section 4 identifies the governing equations that best describe BES performance. These equations describe the ion flux, charge transfer, material balance, and charge balance. Working with these equations increased my understanding of BES rate limitations by the ion fluxes. Additionally, rate constants were developed for the anode oxidation, oxygen reduction rate, and carbon dioxide uptake rate. Overall, this work resulted in several realizations on how the BES performance could be improved. Membrane processes were considered and quantified in section 5. This work focused on the importance of the Nernst-Planck equation and applying the equation to understand physical processes that affect the ion flux, which in turn affect BES power densities. Membrane ion concentration gradients, ion diffusion, ion electromigration, and pH and alkalinity considerations were developed. Section 6 included energy comparisons between the laboratory-scale BES and commercial wastewater treatment systems. Lastly, in section 7, the BES microbiology was presented to define biochemical pathways to electricity and biogas production, and the overall carbon fate. Table 3-1 (located at the end of the chapter) contains the experimental data used for the engineering evaluation.

1) Derive and develop the Nernst Equation for the MFC half reactions

1a) Nernst Equation derivation

Consider a fuel cell with the following reaction and mole fractions y_A, y_B, y_C, and y_D present in the anode and cathode streams. (α, β, γ, and δ are the stoichiometric coefficients of the reaction)

$$\alpha A_{\text{anode reactant}} + \beta B_{\text{cathode reactant}} \rightarrow \gamma C_{\text{anode product}} + \delta D_{\text{cathode product}} \quad (1)$$

The work (W) the fuel cell can produce is related to the enthalpy (H), temperature (T), and entropy (S) of the system products and reactants.

$$W = \Delta H - T\Delta S \quad (2)$$

Assuming the work is reversible at an infinitesimal level, equation (2) can be rewritten considering an infinitesimal consumption of reactants, generation of products, and transfer of electrons. With an infinitesimal change of reactants and products, the illustration will assume the mole fractions remain constant. Thus,

$$dW = dH - TdS \quad (3)$$

Expanding equation (3) with dn_i representing the infinitesimal change in reaction reactants, products, and electrons yields the following:

$$dW = H_A dn_A + H_B dn_B + H_C dn_C + H_D dn_D - T\left(S_A dn_A + S_B dn_B + S_C dn_C + S_D dn_D\right) \quad (4)$$

From the reaction stoichiometry (1), the dn_i's are related by the following relationships:

$$\frac{dn_A}{\alpha} = \frac{dn_B}{\beta} = -\frac{dn_C}{\gamma} = -\frac{dn_D}{\delta} = dn \quad (5)$$

Substituting dn for each of the dn_i's in equation (4) yields:

$$dW = \alpha H_A dn + \beta H_B dn - \gamma H_C dn - \delta H_D dn - T\left(\alpha S_A dn + \beta S_B dn - \gamma S_C dn - \delta S_D dn\right) \quad (6)$$

Moving the dn's to the left side of equation (6) gives:

$$dW = \alpha H_A dn + \beta H_B dn - \gamma H_C dn - \delta H_D dn - T\left(\alpha S_A dn + \beta S_B dn - \gamma S_C dn - \delta S_D dn\right) \quad (7)$$

The enthalpy and entropy terms can be further defined as follows:

$$H_i = H_{fi}^o + \left(H_T - H_{298}\right)_I \quad (8)$$

$$S_i = S_i^o - R\ln\{i\}, \text{ where } \{i\} = \text{chemical activity of species i} \quad (9)$$

To simplify the enthalpy term (8), the remainder of the derivation will assume the standard temperature of 25°C, which is a reasonable assumption for MFCs, thus $H_i = H^o_{fi}$. Now, substituting the simplified enthalpy (8) and entropy (9) terms into equation (7) and grouping the chemical activity terms produces the following equation.

$$\frac{dW}{dn} = \frac{\alpha H_A^o + \beta H_B^o - \gamma H_C^o - \delta H_D^o - T\left[\alpha S_A^o + \beta S_B^o - \gamma S_C^o - \delta S_D^o\right]}{-RT\ln\left[\frac{\{C\}^\gamma \{D\}^\delta}{\{A\}^\alpha \{B\}^\beta}\right]} \quad (10)$$

As previously noted in equation (3), dW = dH – T dS. This equation is also equal to the Gibbs free energy (G), thus:

$$dG = dW = dH - TdS \quad (11)$$

Substituting the Gibb's free energy equation (11) into equation (10) yields:

$$\frac{dG}{dn} = \alpha G_A^o + \beta G_B^o - \gamma G_C^o - \delta G_D^o - RT\ln\left[\frac{\{C\}^\gamma \{D\}^\delta}{\{A\}^\alpha \{B\}^\beta}\right] \quad (12)$$

Since $dn = dn_A/\alpha = dn_B/\beta = -dn_C/\gamma = -dn_D/\delta$, the equation can be transformed to:

$$dG = G_A^o dn_A + G_B^o dn_B - G_C^o dn_C - G_D^o dn_D - RT\ln\left[\frac{\{C\}^\gamma \{D\}^\delta}{\{A\}^\alpha \{B\}^\beta}\right] \quad (13)$$

Equation (11) noted that the differential work of a fuel cell (dW) could be related to the differential change in the Gibbs free energy (dG). The work of the fuel cell can be

further defined as the charge (Q) in coulombs multiplied by the electrical potential in volts (E).

$$dW = dG = EQ \tag{14}$$

Since the charge (Q) is carried out by electrons, the total charge is calculated by multiplying the number of electrons transferred (n) multiplied by the charge per electron (F), where F is Faraday's constant (96,485 coulombs/mole e^-)

$$Q = nF \tag{15}$$

The fuel cell work (14) can be related to the electron transfer (15) by the following equation, where dn represents an infinitesimal transfer of electrons:

$$dW = dG = FEdn \tag{16}$$

Because work can only be performed when the reaction generates a negative change in the Gibb's free energy (-dG), the above equation can be rewritten as

$$dG = -FEdn, \text{ or } E = -\frac{dG}{Fdn} \tag{17}$$

Therefore, equation (13) can be simplified by substituting equation (17) to yield:

$$E = E^o + \frac{RT}{Fdn}\ln\left[\frac{\{C\}^\gamma\{D\}^\delta}{\{A\}^\alpha\{B\}^\beta}\right] \tag{18}$$

To reflect the stoichiometry of the original reaction (1) and the transfer of entire electrons (n) as opposed to differential electrons (dn), the final equation can be written as:

$$E = E^o + \frac{RT}{nF}\ln\left[\frac{\{C\}^\gamma\{D\}^\delta}{\{A\}^\alpha\{B\}^\beta}\right] \tag{19}$$

The above equation is the Nernst equation.

1b) Nernst Equation for the MFC half reactions:

General:

- Standard environmental conditions (pH = 7) will be used.
- The standard electrode potential will be defined as a reduction potential (cathode positive potential, anode negative potential).
- Unless otherwise noted, all MFC performance data will come from Table 3-1, located at the end of Chapter.
- Molar concentrations have been used to represent chemical activities since dilute solutions (< 0.1 M) were used during the experiment.

1b1) Anode acetate oxidation reaction:

In the MFC anode, acetate (CH_3COO^-) is oxidized to bicarbonate and protons.[1]

$$CH_3COO^- + 4H_2O \rightarrow 2HCO_3^- + 9H^+ + 8e^- \qquad \Delta G^{o'} = +104.6\,kJ/mol \quad (20)$$

The acetate oxidation potential at standard environmental conditions can be found with the following equation.

$$\Delta G^{o'} = -nF\Delta E_H{}^{o'} \quad (21)$$

$$\Delta G^{o'} = +104.6\,kJ/mol = -nF\Delta E_H{}^{o'} \quad (22)$$

$$\Delta E_H{}^{o'} = -\frac{+104.6\,kJ/mol \times 1000\,J/kJ}{(8e^-/mol)\,(96{,}485\,Coulombs/mol))}$$

$$\Delta E_H{}^{o'} = -0.136\ V = -136\,mV$$

1b2) Cathode oxygen reduction reaction:

In the acidic catholyte, the oxygen reduction reaction can be represented with two reaction pathways, a direct four-electron pathway and two electron peroxide pathway.[2]

Direct four-electron pathway:

$$O_2(aq) + 2H_2O + 4e^- \rightarrow 4OH^- \qquad E_o^{'} = 840\,mV \qquad (23)$$

Peroxide pathway:

$$O_2 + 2H^+ + 2e^- \rightarrow H_2O_2 \qquad E_o^{'} = 670\,mV \qquad (24)$$

Hydrogen peroxide can be further reduced to water:

$$H_2O_2 + 2H^+ + 2e^- \rightarrow 2H_2O \qquad E_o^{'} = 1770\,mV \qquad (25)$$

or,

$$2H_2O_2 \rightarrow 2H_2O + O_2 \qquad (26)$$

The direct four-electron pathway will be used for the remainder of this illustration.

To determine the Gibb's free energy from the oxygen reduction reaction standard environmental potential (23), the following equation is used.

$$\Delta G^{o'} = -nF\Delta E_H{}^{o'} \qquad (21)$$

$$\Delta G^{o'} = -(4)\,(96{,}485\,Coulombs/mol)\,(0.84\,V) \qquad (27)$$

$$\Delta G^{o'} = -324{,}189.6\,J/mol = -324.2\,kJ/mol$$

1c) Net anode and cathode reaction:

The anode and cathode half reactions can be added to arrive at the net MFC reaction.

$$CH_3COO^- + 4H_2O \rightarrow 2HCO_3^- + 9H^+ + 8e^- \qquad \Delta G^{o'} = -104.6\,kJ/mol \qquad (20)$$

$$+(2\times) \qquad O_2 + 2H_2O + 4e^- \rightarrow 4OH^- \qquad \Delta G^{o'} = -648.4 kJ/mol \qquad (23)$$

$$CH_3COO^- + 8H_2O + 2O_2 \rightarrow 2HCO_3^- + 9H^+ + 8OH^- \qquad \Delta G^{o'} = -753\,kJ/mol \qquad (28)$$

The MFC net reaction potential (28) at standard environmental conditions can be calculated as follows,

$$\Delta G^{o'} = -753\,kJ/mol = -nF\Delta E_o^{'} \qquad (29)$$

$$\Delta E_H{}^{o'} = \frac{-753\,kJ/mol \times 1000\ J/kJ}{(8e^-/mol)\,(96{,}485\,Coulombs/mol))}$$

$$\Delta E_H{}^{o'} = 0.976\,V = 976\,mV$$

The theoretical cell potential calculated from adding the actual half reaction potentials equals:

$$E_{cell} = E_{cathode} - E_{anode} \qquad (30)$$

$$E_{cell} = 0.840\,V - (-0.136\,V)$$

$$E_{cell} = 0.976\,V = 976\,mV$$

1d) Calculate the voltages for each half reaction:

MFC half-reaction potentials at standard conditions were determined in sections 1b1 and 1b2. Half reaction and net reaction potentials for actual conditions can be determined using the Nernst Equation (19), which was derived in section 1a.

$$E = E^o + \frac{RT}{nF}\ln\left[\frac{\{C\}^\gamma\{D\}^\delta}{\{A\}^\alpha\{B\}^\beta}\right] \qquad (19)$$

E^o values for the acetate oxidation (-0.602 V) and oxygen reduction (1.253 V) reactions were calculated with the Nernst equation by substituting $E_H^{o'}$ values for the acetate oxidation (-0.136 V) and oxygen reduction (0.976 V) reactions, $[H^+] = 1.0 \times 10^{-7}$, and [products] = [reactants] = 1.0 M and then solving for E^o.

Anode acetate oxidation half reaction actual potential at pH = 6.83:

$$E = -0.602\,V - \frac{(8.314\,J/mol-K)(298\,K)}{(8e^-)(96{,}485\,C/mol)} \ln \frac{\left[HCO_3^-\right]^2\left[H^+\right]^9}{\left[CH_3COO^-\right]} \qquad (31)$$

$$E = -0.602\,V - (3.21\times10^{-3}\ \text{V}) \ln \frac{\left[4.35\times10^{-3}\right]^2\left[1.48\times10^{-7}\right]^9}{\left[5.8\times10^{-3}\right]}$$

$$E = -0.602\ V - (-0.473\ V)$$

$$E = -0.129\ V = -129\ mV$$

Note: Equation 31 was also solved using chemical activities in lieu of molar concentrations and the same -129 mV result was obtained.

Cathode oxygen reduction half reaction actual potential at pH = 5.25:

$$E = 1.253V - \frac{(8.314\,J/mol-K)\,(298\,K)}{(4e^-)\,(96{,}485\,C/mol)} \ln \frac{\left[\text{OH}^-\right]^4}{\left[O_2\right]} \qquad (32)$$

$$E = 1.253V - (6.42\,\text{x}\,10^{-3}\ \text{V}) \ln \frac{\left[1.78\,\text{x}\,10^{-9}\right]^4}{\left[2.65\,\text{x}\,10^{-4}\right]}$$

$$E = 1.253\ V - 0.465\ V$$

$$E = 0.788\ V = 788\ mV$$

Net MFC reaction actual potential:

$$E_{cell} = E_{cathode} - E_{anode} \tag{30}$$

$$E_{cell} = 788\ mV - (-129\ mV) \tag{33}$$

$$E_{cell} = 917\ mV$$

In reality, the MFC does not realize the 917 mV theoretical potential from the oxidation of acetate and concurrent reduction of oxygen. Potential losses occur in at least seven different areas and are illustrated in Fig. 3-1.[3]

Sources of MFC Potential Loses

1) Bacterial anabolism and catabolism
2) Anode overpotential losses
3) Anolyte ohmic resistance losses
4) Membrane losses
5) Catholyte ohmic resistance losses
6) Oxygen reduction reaction activation energy losses

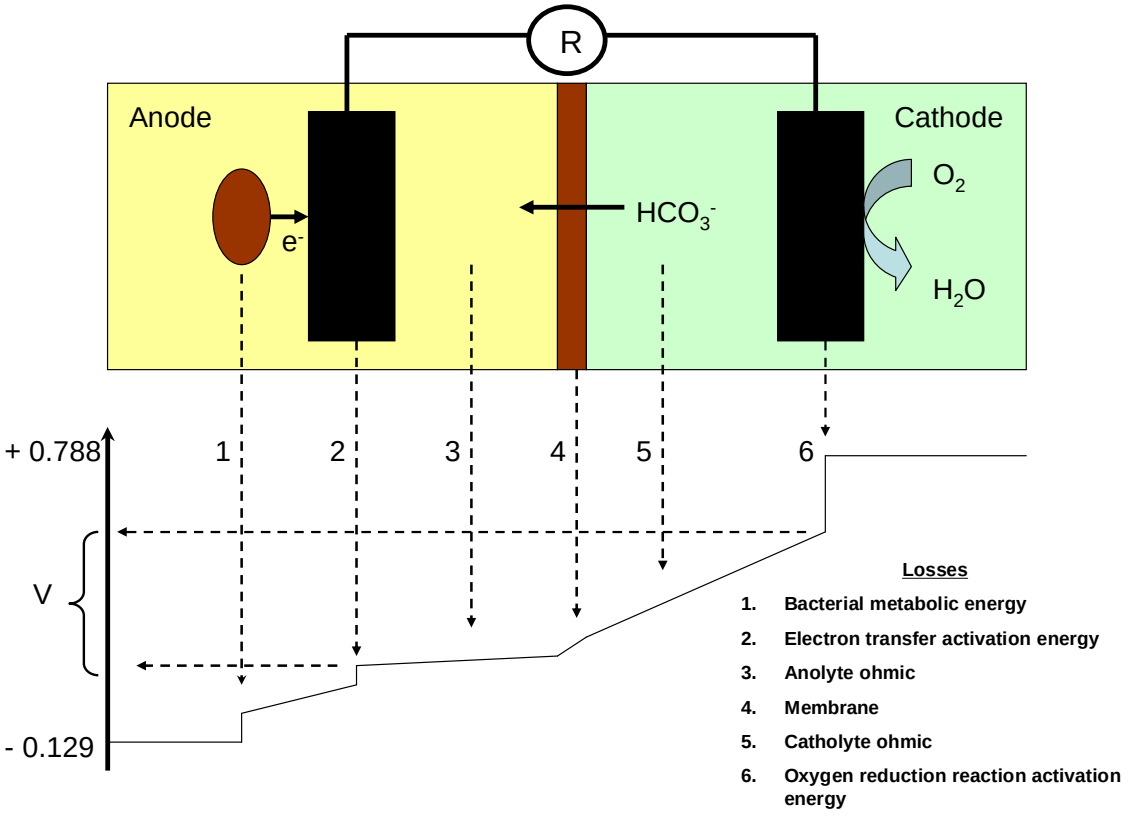

Figure 3-1. MFC Potential Losses Illustration[3]

2) Coulombic Efficiencies

The actual versus theoretical coulombic efficiencies were calculated to understand the MFC electron capture efficiency and possible electron fates of acetate oxidation reaction.

2a) Acetate Coulombic Efficiency

MFC-C Experimental Data:

Feed sCOD*	371 mg/l
Effluent sCOD	288 mg/l
MFC Potential	0.3384 V at 5 ohm resistance
Current	0.068 amperes
Anode Volume	5.8 L
HRT	11.5 hr
Feed Rate	12.15 L/day

*COD – Chemical oxygen demand

Coulombic Efficiency ($\in$) calculation[4]:

$$\in = \frac{MI}{FbqΔCOD} \tag{34}$$

$\in$ = Coulombic Efficiency

M = Molecular Weight of Oxygen / mol O_2

I = Current (amperes)

F = Faraday's constant (96,485 amperes-sec/mol e^-)

b = # electrons exchanged per mole O_2

q = Volumetric flow rate (cm^3/sec)

$\triangle$COD = Influent – effluent COD (mg O_2/cm^3)

Coulombic efficiency based on the above experimental data:

$$\in = \frac{(32{,}000\ mg\ O_2 / mol\ O_2)\,(0.068\ amperes)}{(96{,}485\ amperes \cdot \sec)\,(4\ mol\ e^- / mol\ O_2)\,(0.1406\ cm^3 / \sec)\,(0.083\ mg\ O_2)/cm^3)}$$

$$\in = 48.3\%$$

Current density:

$$= (\frac{0.067\ amperes}{5.8\ L}) \times 1000\ L/m^3 = 11.6\ A/m^3 \qquad (35)$$

Power density:

$$= \frac{(Cell\ Potential)(Current)}{Anode\ volume} \qquad (36)$$

$$= \frac{(0.3384\ V)(0.068\ A)}{5.8\ L} \times 1000\ L/m^3 = 3.97\ W/m^3$$

2b) What does 100% coulombic efficiency from acetate to carbon dioxide look like?

100% coulombic efficiency would require the conversion of 100% of the COD removal to current. Using the operating data (Table 3-1), assuming 100% of the feed COD is removed, and solving for the current using equation (34).

$$I(current) = \frac{(1.0)\,(96{,}485\ amperes\text{-}\sec)\,(4\ mol\ e^-/mole\ O_2)}{(32{,}000\ mg\ O_2/mol\ O_2)} \times \qquad (37)$$

$$(0.1406\ cm^3/\sec)\,(0.371\ mg\ O_2/cm^3)$$

$$I = 0.629\ A$$

Current density:

$$= (\frac{0.629\ A}{5.8\ L}) \times 1000\ L/m^3 = 108.4\ A/m^3 \qquad (38)$$

Power density:

$$= \frac{(Cell\ Potential)(Current)}{Anode\ volume} \qquad (39)$$

$$= \frac{(0.3384\ V)(0.629\ A)}{5.8\ L} \times 1000\ L/m^3 = 36.7\ W/m^3$$

2c) Show possible fate of acetate relative to coulombic efficiency

From section 2a, the MFC-C coulombic efficiency under steady operating conditions was calculated to be 48%. The remaining 52% of the electrons transferred may be accounted for by 1. bacterial anabolism, 2. cathode to anode oxygen transport, and 3. methanogenesis. Each will be considered below.

1. Bacterial Anabolism

The energy required for bacterial anabolism depends on the bacteria, growth rates, and environmental conditions. MFC workers have shown that very high coulombic efficiencies (> 95%) are possible for established anodic bacterial communities fed soluble wastewater substrates (acetate and glucose).[5] While some of the high coulombic efficiency data may not reflect steady state conditions, the data does indicate that an established bacterial community's anabolic energy requirement may be relatively low when fed acetate (<5%). Thus, while the specific MFC-A and C bacterial anabolic/catabolic energy balance cannot be determined, data suggests that the anabolic energy requirement may be relatively small. This conclusion is supported by long term MFC operations (9 months) in which there was not a progressively larger anodic biomass, which would be the case if the bacterial metabolism was primarily anabolism.

2. Cathode to anode oxygen transport

If we assume that cathode to anode oxygen transport is mediated by diffusion, Fick's law can be used to estimate the amount of oxygen transferred.

$$N_i = D_i (dC_i / dx) \quad (40)$$

where, N_i = Flux of oxygen in water

D_i = Diffusion coefficient of oxygen in water (1.97×10^{-5} cm^2-s^{-1})[6]

dC_i = Oxygen concentration difference across AEM (2.21×10^{-4} mol O_2/L)

= 2.21×10^{-7} mol O_2/cm^3

(From section 4d)

dx = Membrane thickness (0.05 cm)

$$N_i = D_i \, dC_i/dx$$

$$N_i = (1.97 \times 10^{-5} \ cm^2\text{-}s^{-1}) \frac{(2.21 \times 10^{-7} \ mol \ O_2/cm^3)}{(0.05 \ cm)}$$

$$N_i = 8.7 \times 10^{-11} \ \frac{mol \ O_2}{cm^2 \cdot s}$$

Now, the total oxygen flux across the membrane can be estimated for a 12-hour HRT by using the diffusion volumetric flux.

Diffusion volumetric flux = diffusion flux x time x membrane area (41)

$$= (8.7 \times 10^{-11} \ \frac{mol \ O_2}{cm^2 \cdot s}) \ (43{,}200s) \ (1570 \ cm^2)$$

$$= 5.9 \ \text{x} \ 10^{-3} \ mol \ O_2$$

$$= 5.9 \ \text{x} \ 10^{-3} \ mol \ O_2 \ \text{x} \ \frac{32 g \ O_2}{mol \ O_2} = 0.189 \ \text{g} \ O_2 \quad (42)$$

The 0.189g of oxygen (189 mg O_2) diffusing across the membrane during a 12-hour period equates to 31 mg O_2/L of COD uptake or 37% of the total electrons transferred (72% of the unaccounted for coulombic efficiency). If, however, membrane oxygen crossover were to fully account for the remaining electrons, approximately 262 mg O_2 would have to cross the membrane in 12 hours (34). Thus, diffusion alone may not account for this amount of oxygen transport, particularly if the membrane partially retards transport.

One possible explanation for the additional oxygen transport, involves the electroosmotic flux of bicarbonate ions (discussed in section 5b) across the AEM. When bicarbonate ions migrate from the cathode to anode, it is conceivable that they "drag" water molecules along with them. Because the catholyte water is saturated with dissolved oxygen, it is possible that dissolved oxygen is present in the water moving adjacent to the bicarbonate ions (beyond the hydration radius of water), thereby accompanying the bicarbonate ions across the membrane. This phenomenon could account for a greater oxygen transport than calculated. However, we did not test this.

3. Methanogenesis

The biogas production volume was very small and could not account for a significant affect to the coulombic efficiency (Details provided in section 4c).

2d) Why is the UMFC Nernst equation prediction of potential lower than the actual potential?

An anode overpotential is one possible explanation, but anode conditions were consistently maintained for the pressured and non-pressured experiments. Thus, the anode potential was equivalent for pressured and non-pressured cases. Another more probable explanation for the difference in actual versus Nernst equation predicted fuel cell potential is a decrease in the irreversible activation losses at the cathode electrode, especially at lower temperatures. The decrease in the cathode electrode's irreversible activation losses is related to the exchange current density, which refers to the steady state forward and backward flow of electrons between reactants and products at the electrode surface. With an increase in the oxygen partial pressure, the exchange current density increases, reflecting a more active cathode electron flux. The more active cathode requires a lower overpotential to energize cathode electron transfer reactions. Thus, increasing exchange current density (by increasing the oxygen partial pressure, increasing the cathode temperature, or by using more effective cathode catalysts) lowers the irreversible activation losses required to energize chemical reactions.[7]

3) Solution Chemistry

The solution chemistry section emphasizes the MFC carbon dioxide solution chemistry because of the application to Chapter 5 (Carbon dioxide addition to microbial fuel cell cathodes maintains stable catholyte pH and improves anolyte pH, total alkalinity, and conductivity)

The applicable MFC half reactions follow,

Anode Half Reaction:

$$CH_3COO^- + 4H_2O \rightarrow 2HCO_3^- + 9H^+ + 8e^- \quad (20)$$

Cathode Half Reaction (written to show electron balance):

$$2O_2 + 4H_2O + 8e^- \rightarrow 8OH^- \quad (23)$$

Net MFC Reaction:

$$CH_3COO^- + 8H_2O + 2O_2 \rightarrow 2HCO_3^- + 9H^+ + 8OH^- \quad (28)$$

3a) pH effect on cathode:

The anode and cathode half reactions communicate in two ways.

1) Via an external electrical circuit that conducts electrons from the anode to the cathode and
2) Via an anion exchange membrane (AEM) that conducts anions from the cathode to the anode to maintain fuel cell electroneutrality.

With an AEM, every electron transferred from the anode to cathode must be charge balanced by an anion transferred from the cathode to anode.[8-10]

Because MFC-C has a catholyte cathode, it will be used for the following illustration. The MFC-C catholyte uses circulated ultra-pure water exposed to air in the

MFC-C cathode tube and CO_2 gas in the carbon dioxide contact vessel. With water, air, and carbon dioxide, the only anions available for electroneutrality maintenance are hydroxide ions (water dissociation) or bicarbonate ions (CO_2 dissolution). For now, the diffusion of ions from the anode to cathode will be ignored.

Water dissociation[11]: $$K_w = 10^{-14} = [H^+][OH^-] \quad (43)$$

CO_2 Dissolution (Henry's Law)[11]: $$P_{CO_2} = K_{HCO_2}[CO_2] \quad (44)$$

Where,

$$K_{HCO_2} = 29.79 L \cdot atm / mol$$

To determine the catholyte pH resulting from the CO_2 dissolution, six equations are required. First, as shown above is the water dissociation equation (43). Second is the use of Henry's Law for CO_2 dissolution in water (44). The third equation describes the hydration of CO_2 in water to H_2CO_3.[11]

$$CO_2 + H_2O \rightarrow H_2CO_3 \quad (45)$$

$$\frac{[H_2CO_3]}{[CO_2]} = K_h = 1.70 \times 10^{-3} \text{ (hydration equilibrium constant)} \quad (46)$$

The fourth equation relates the dissociation of H_2CO_3 to H^+ and HCO_3^-.[11]

$$H_2CO_3 \rightarrow H^+ + HCO_3^- \quad (47)$$

$$\frac{[H^+][HCO_3^-]}{[H_2CO_3]} = K_{a1} = 2.5 \times 10^{-4} \text{ (dissociation constant one)} \quad (48)$$

The fifth equation relates the dissociation of HCO_3^- to H^+ and CO_3^{2-}.[11]

$$HCO_3^- \rightarrow H^+ + CO_3^{2-} \quad (49)$$

$$\frac{[H^+][CO_3^{2-}]}{[HCO_3^-]} = K_{a2} = 5.6 \times 10^{-11} \text{ (dissociation constant two)} \quad (50)$$

The sixth equation denotes the charge balance.[11]

$$[H^+] = [OH^-] + [HCO_3^-] + 2[CO_3^{2-}] \tag{51}$$

Since the MFC-C catholyte pH < 6, the carbonate concentration will be neglected.

Starting with the charge balance equation:

$$[H^+] = [OH^-] + [HCO_3^-] \tag{52}$$

Substitute the water dissociation equation (43) for [OH^-].

$$[H^+] = \frac{10^{-14}}{[H^+] + [HCO_3^-]} \tag{53}$$

Substitute the bicarbonate dissolution equation (48) for [HCO_3^-].

$$[H^+] = \frac{10^{-14}}{[H^+]} + \frac{[H_2CO_3]K_{a1}}{[H^+]} \tag{54}$$

Substitute the hydration equilibrium equation (47) for [H_2CO_3].

$$[H^+] = \frac{10^{-14}}{[H^+]} + \frac{[CO_2]K_hK_{a1}}{[H^+]} \tag{55}$$

Substitute the carbon dioxide dissolution equation (44) for [CO_2].

$$[H^+] = \frac{10^{-14}}{[H^+]} + \frac{P_{CO_2}K_hK_{a1}}{K_{HCO_2}[H^+]} \tag{56}$$

Simplifying and rearranging terms yields;

$$[H^+] = (10^{-14} + \frac{P_{CO_2}K_hK_{a1}}{K_{HCO_2}})^{1/2} \tag{57}$$

The above equation indicates that solution pH is dependent on the carbon dioxide partial pressure. Because the MFC-C catholyte is circulated with exposure to air and 100% carbon dioxide gas, the carbon dioxide partial pressure will be bound on the low side by

the atmospheric carbon dioxide concentration (P_{CO2} = 3.85 x 10^{-4} atm) and on the high side by 100% carbon dioxide (P_{CO2} = 1.0 atm). Calculations showing the carbon dioxide partial pressure effect on catholyte pH follow.

pH at atmospheric carbon dioxide partial pressure (P_{CO2} = 3.85 x 10^{-4} atm):

$$[H^+] = (10^{-14} + \frac{K_h K_{a1} P_{CO_2}}{K_{HCO_2}})^{1/2} \quad (57)$$

$$[H^+] = (10^{-14} + \frac{(1.70\times10^{-8})(2.5\times10^{-4})(3.85\times10^{-4})}{29.76\ L\text{-}atm/mol})^{1/2}$$

$$[H^+] = 2.24\times10^{-8}$$

$$pH = 5.63$$

$$[HCO_3^-] = 2.44\times10^{-8}$$

pH at 100% carbon dioxide partial pressure (P_{CO2} = 1.0 atm) :

$$[H^+] = (10^{-14} + \frac{K_h K_{a1} P_{CO_2}}{K_{HCO_2}})^{1/2} \quad (57)$$

$$[H^+] = (10^{-14} + \frac{(1.70\times10^{-8})(2.5\times10^{-4})(1.0atm)}{29.76\ L\text{-}atm/mol})^{1/2}$$

$$[H^+] = 1.19\times10^{-4}$$

$$pH = 3.92$$

$$[HCO_3^-] = 1.2\times10^{-4}$$

Thus, assuming equilibrium conditions and no influence from anolyte to catholyte ion diffusion, the MFC-C catholyte pH will theoretically vary between pH 3.92 and 5.63. If anolyte to catholyte diffusion becomes prominent, the ions transferred to the catholyte will affect the charge balance and likely raise the pH.

Previous studies have shown that MFC electroneutrality is mediated by the ions in the highest concentrations.[9,10] Because the MFCs in this study use anion exchange membranes (AEM), the catholyte anions in the highest concentration will mediate electroneutrality. Therefore, bicarbonate ions will maintain electroneutrality since $[HCO_3^-] >> [OH^-]$ at acidic pH values. Using the above illustrations with air and 100% carbon dioxide exposure, the bicarbonate ion concentrations for MFC-A and MFC-C are 2.44×10^{-6} M (based on CO_2 partial pressure in the atmosphere) and 1.2×10^{-4} M, respectively. Thus, on a concentration basis, MFC-A has fewer bicarbonate ions available for charge transfer than MFC-C. This is evident from pH data, where the pH levels for MFC-A and C were 8.32 and 5.25, respectively.

The pH effect on the MFC-C catholyte can now be considered with the inclusion of the oxygen reduction electron transfer and electroneutrality anion transfer. We will start with the cathode oxygen reduction reaction (per mol acetate);

$$2O_2 + 4H_2O + 8e^- \rightarrow 8OH^- \quad (23)$$

In the above reaction, electrons transfer from the anode and oxygen is reduced to hydroxide ions. Since the hydroxide ion concentration increases, the pH will increase. To maintain electroneutrality, eight catholyte bicarbonate ions will transfer from the cathode to anode (Fig. 3-2).

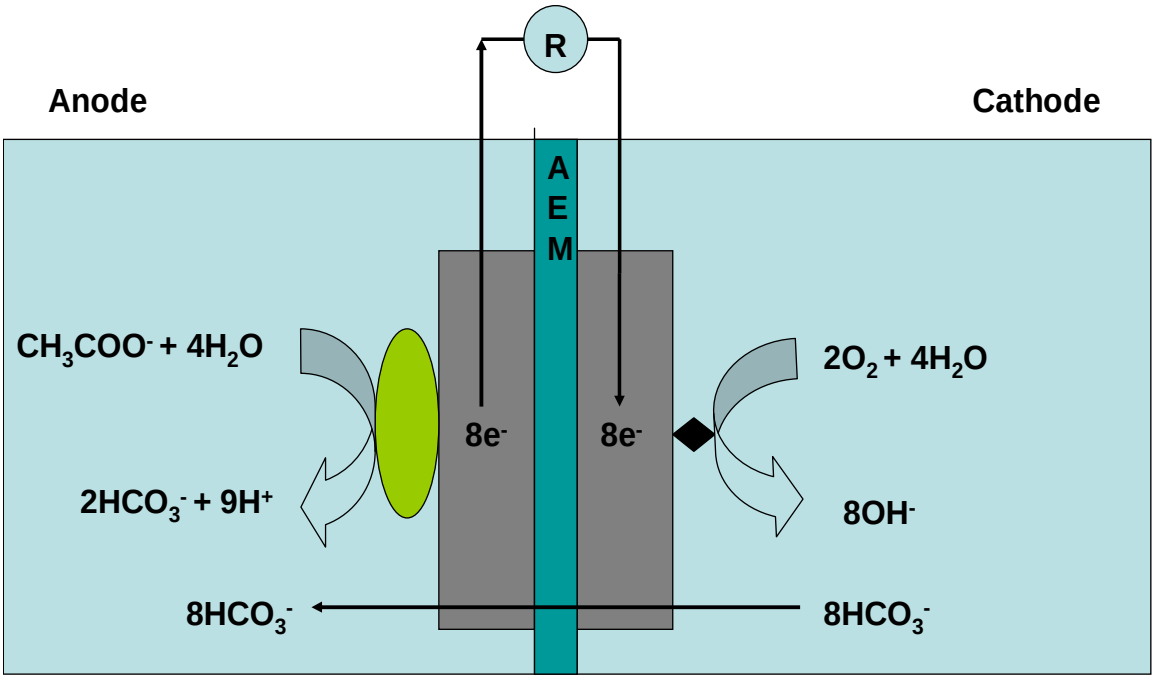

Figure 3-2. MFC ion transfer illustration. MFC cathode and anode reaction stoichiometry with bicarbonate ion migration to maintain electroneutrality.

The catholyte, however, is not static; it is circulated between the MFC-C cathode chamber and the carbon dioxide contact vessel. The catholyte leaving MFC-C, therefore has a higher pH (hydroxide ion increase) and lower alkalinity (bicarbonate ion deficit) than the catholyte entering MFC-C (Fig.3-3).

The catholyte entering the carbon dioxide contact vessel is exposed to 100% carbon dioxide gas. Assuming that the catholyte was at CO_2 equilibrium before being pumped to MFC-C, the catholyte returning from MFC-C is no longer at equilibrium because it has gained 8 hydroxide ions and lost 8 bicarbonate ions. To return to equilibrium, 8 CO_2 molecules must dissolve (Henry's Law), form H_2CO_3 (carbon dioxide

hydration), and then dissociate (dissociation constant 1) into H^+ and HCO_3^-. The addition of the dissolved carbon dioxide with the incoming catholyte is shown in Fig. 3-3.

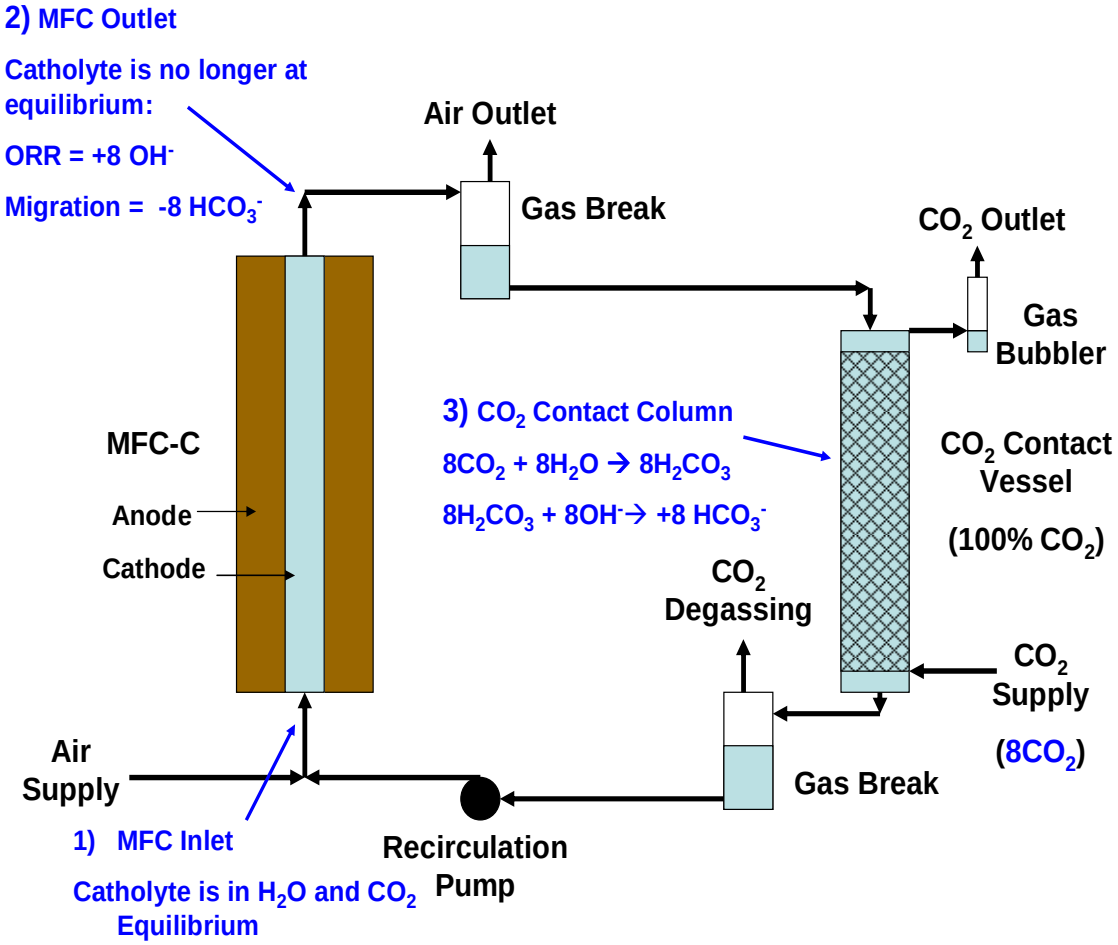

Figure 3-3. MFC and Carbon Dioxide Contactor Catholyte Recirculation

1) The circulation process begins with the catholyte being at CO_2 equilibrium before entering the MFC. 2) Within the MFC, catholyte bicarbonate ions migrate to the anode concurrently with hydroxide ion generation from the oxygen reduction reaction. Thus, the catholyte leaving the MFC is no longer at equilibrium since it has gained 8 hydroxide ions and lost 8 bicarbonate ions (per molecule of acetate oxidized). 3) Within the CO_2 contact column, CO_2 absorbs and hydrates to H_2CO_3. The H_2CO_3 reacts with the hydroxide ion to generate bicarbonate ions and the bicarbonate ion production replaces the bicarbonate ions lost to migration, thus restoring equilibrium.

The carbon dioxide dissolution and dissociation replenishes the hydroxide ion production in the oxygen reduction reaction and makes bicarbonate ions available for electroneutrality transfer to the anode. Thus, the catholyte pH should remain stable so long as equilibrium conditions are maintained. Experimental data indicates the MFC-C catholyte pH has remained very stable (pH = ~5.5). This is in stark contrast with the cathode pH increases experienced by other MFC researchers.[9,10,12,13]

There is also evidence of cation transport from the anode to the cathode. Catholyte samples indicate 0.56 mg Na^+/L and 0.11 mg K^+/L. This data became significant in understanding catholyte pH trends during the MFC start-up.

3b) pH effect on anode:

In the MFC-C anode, acetate is oxidized to bicarbonate and electrons are released in the reaction (Fig. 3-2). Protons (nine) are generated at a faster rate than the bicarbonate ions (two), which could decrease the anolyte pH.

$$CH_3COO^- + 4H_2O \rightarrow 2HCO_3^- + 9H^+ + 8e^- \quad (20)$$

The MFC-C anolyte interacts with the catholyte by donating eight electrons and receiving eight bicarbonate ions as illustrated in Fig. 3-2. The net anolyte ion composition after the electron transfer and bicarbonate ion exchange (per mole of acetate) can be shown as.

$$10HCO_3^- + 9H^+ \qquad \text{or,} \qquad HCO_3^- + 9CO_2 \quad (58)$$

The above reaction indicates that the net anolyte bicarbonate ion increase (2 from the oxidation reaction plus 8 from bicarbonate ion migration) exceeds the proton generation by one alkalinity unit. Therefore, the anolyte alkalinity and pH should increase rather than decrease because of the bicarbonate ion migration. Experimental data indicate the

cathode to anode bicarbonate ion migration increased the anolyte effluent pH (6.83 versus 6.70), conductivity (2.56 versus 2.32 milliMHO), and total alkalinity (358 versus 294 as mg $CaCO_3$/L) compared to the MFC feed solution. This illustration shows that for every mole of acetate oxidized; one mole and nine moles of carbon dioxide will be sequestered and recycled, respectively (assuming a 100% coulombic efficiency). The recycled carbon dioxide can theoretically be recaptured and reused for additional catholyte pH control.[13]

3c) pH and the Nernst Equation:

The Nernst Equation (19) can be used to predict the potential impact solely from the change in pH.

$$E = E^{o} + \frac{RT}{nF} \ln \left[\frac{\{C\}^{\gamma} \{D\}^{\delta}}{\{A\}^{\alpha} \{B\}^{\beta}} \right] \tag{19}$$

Consider the cell potential change resulting from a one unit catholyte pH change from 5.25 to 6.25. From section 1d, the actual anode potential was -0.129 V (pH = 6.83) (31) and the cathode potential was 0.788 V (pH = 5.25) (32). The anode potential will remain constant in this example.

Anode potential at pH = 6.83:

$$E = -0.129\,V \tag{31}$$

Cathode potential at pH = 6.25:

$$E = 1.253V - \frac{(8.314\,J/mol - K)\,(298\,K)}{(4e^{-})\,(96{,}485\,C/mol)} \ln \frac{[\mathrm{OH^-}]^4}{[O_2]} \tag{32}$$

$$E = 1.253V - (6.42 \text{ x } 10^{-3} \text{ V}) \ln \frac{\left[1.78 \text{ x } 10^{-8}\right]^4}{\left[2.65 \text{ x } 10^{-4}\right]} \quad (59)$$

$$E = 1.253V - 0.405V$$

$$E = 0.848 \ V = 848 \ mV$$

Thus, the cathode and cell potential difference due to a one unit catholyte pH change is

$$\begin{aligned} \textit{Cathode potential at pH} &= 6.25 = 0.848 \ V \\ \textit{Cathode potential at pH} &= 5.25 = 0.788 \ V \\ &\quad \_\_\_\_\_ \\ &= 0.06 \ V \textit{ cell potential difference per unit pH} \\ &= \frac{0.06 \ V}{pH} \end{aligned}$$

3d) Can $CaCO_3$ precipitate while using atmospheric pressure carbon dioxide for pH control?

$CaCO_3$ cannot precipitate when using atmospheric carbon dioxide for pH control because the carbon dioxide is exposed to ultrapure water. Further, calcium ion diffusion from the anode to cathode across the anion exchange membrane is unlikely. Thus, calcium precipitation is not anticipated.

If calcium ions were present in the MFC-C catholyte at pH = 5.25 and $[HCO_3^-]$ = 1.08 x 10^{-3}, the calcium carbonate concentration would be,

$$HCO_3^- \rightarrow H^+ + CO_3^{2-} \quad (49)$$

$$\frac{[H^+][CO_3^-]}{[HCO_3^-]} = K_{a2} = 5.61 \times 10^{-11} \quad \text{(Dissociation Constant two)} \quad (50)$$

$$[CO_3^{2-}] = \frac{[HCO_3^-](5.61\times10^{-11})}{[H^+]}$$

$$= \frac{[1.08\times10^{-3}](5.61\times10^{-11})}{[5.62\times10^{-6}]}$$

$$[CO_3^{2-}] = 1.08\times10^{-8}\ mol/L$$

Based on the $CaCO_3$ equilibrium constant,[11]

$$K_{sp} = 3.31\times10^{-9} = [Ca^{2+}][CO_3^{2-}] = [Ca^{2+}][1.08\times10^{-8}] \quad (60)$$

$$[Ca^{2+}] = 0.306\ \ M$$

Thus, if the Ca^{2+} concentration was equal to or greater than 0.306M, the solution would be supersaturated, and $CaCO_3$(s) would precipitate.

3e) Cathode alkalinity change from hydroxide ion generation

The cathode oxygen reduction reaction indicates one mole of hydroxide ions are generated for every mole of electrons donated from the cathode electrode.

$$2O_2 + 4H_2O + 8e^- \rightarrow 8OH^- \quad (23)$$

From section 4b it was determined that 4.24 x 10^{17} e^-/s (79) are transferred as current, which indicates 7.04 x 10^{-7} mol OH^-/s is produced in the cathode oxygen reduction reaction.

$$\frac{4.24\times10^{17}\ e^-}{s}\times\frac{1\ mol\ e^-}{6.02\times10^{23}\ e^-}\times\frac{8\ mol\ OH^-}{8\ moles\ e^-} \quad (61)$$

$$= \frac{7.04\times10^{-7}\ mol\ OH^-}{s}$$

From section 4e, it was determined that 1.6 L of water passes through the cathode tube in 6.68 minutes. Thus, the hydroxide ion generation in this duration equals;

$$\frac{\left(\frac{7.04\times10^{-7}\ mol\ OH^{-}}{s}\times 400.8\ s\right)}{1.6\ L} = 1.76\times10^{-4}\ mol\ OH^{-}/L \qquad (62)$$

With the acidic pH, the above hydroxide ion generation rate can be considered as the equivalent proton consumption rate (7.04×10^{-7} mol H^+/s). The catholyte bicarbonate ion concentration can be found by considering the total alkalinity equation assuming no other ions are present in the catholyte;

$$Alk_T = [HCO_3^-] + 2[CO_3^{2-}] + 2[HPO_4^{2-}] + [H_2PO_4^-] + [OH^-] - [H^+] \qquad (63)$$

At pH = 5.25, the carbonate and hydroxide ion concentration can be neglected. Likewise, the phosphate ion concentration was assumed to be negligible, thus the phosphate alkalinity contribution will be neglected. Therefore, the total alkalinity equation can then be simplified to;

$$Alk_T = [HCO_3^-] + [H^+] \qquad (64)$$

The total alkalinity of the catholyte was measured at 66 mg/L (as mg $CaCO_3$/L). Converting this measurement to the bicarbonate concentration yields;

$$\frac{66\ \text{mg CaCO}_3}{L}\times\frac{1\ \text{mmol CaCO}_3}{1\times10^2\ \text{mg CaCO}_3}\times\frac{1\ \text{mmol CO}_3^{2-}}{1\ \text{mmol CaCO}_3}\ \text{x}\ \frac{2\ \text{meq alk}}{1\ mmol\ CO_3^{2-}} = 1.32\ \text{meq}/L \qquad (65)$$

The total alkalinity equation can now be solved in terms of the bicarbonate ion concentration at the cathode effluent. Since all of the alkalinity is bicarbonate alkalinity at pH = 5.24, $ALK_T = 1.32 \times 10^{-3}$ HCO_3^-.

$$Alk_T = [HCO_3^-] - [H^+] \qquad (64)$$

$$\frac{1.32\times10^{-3}\ mol\ HCO_3^-}{L} = [HCO_3^-] - [5.62\times10^{-6}] \quad (66)$$

$$[HCO_3^-] = 1.31\times10^{-3}\ \text{M}$$

From (62), 1.76 x 10^{-4} mol OH^-/L is consumed in the cathode, which can now be shown to equal 1.76 x 10^{-4} mol HCO_3^-/L. Converting this concentration to the total alkalinity (as mg $CaCO_3$/L) and assuming a negligible pH change equals;

$$\frac{0.176\ mmol\ HCO_3^-}{L}\times\frac{1\ mmol\ CO_3^{2-}}{2\ meq\ \text{Alk}}\times\frac{1\ mmol\ CaCO_3}{1\ mmol\ CO_3^{2-}}\ \text{x}\ \frac{100\ \text{mg}\ \text{CaCO}_3}{1\ \text{mmol}\ \text{CaCO}_3} = \quad (67)$$

$$8.8\ mg\ CaCO_3/L$$

Thus, the cathode alkalinity decrease from the hydroxide ion generation equals 8.8 mg/L (as mg $CaCO_3$/L). Since the cathode oxygen reduction reaction and bicarbonate ion migration consume alkalinity, the catholyte pH should decrease. The catholyte pH in the experiment, however, remained stable, which indicates that the bicarbonate ions were replenished by CO_2 dissolution, hydration, and dissociation in the CO_2 contact column.

4) Develop the MFC governing equations.

The simplified process flow diagram (Fig. 3-4) will be used to illustrate the system boundaries for the application of the governing equations.

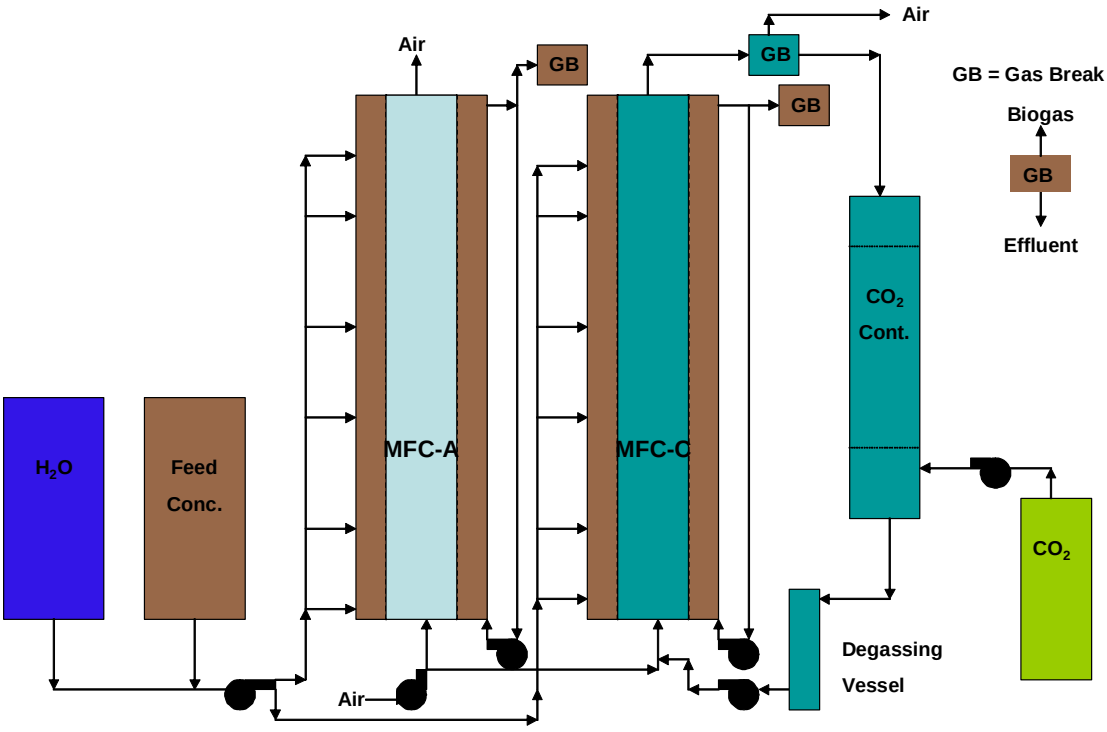

Figure 3-4. MFC Simplified Process Flow Diagram. Feed (a mixture of feed concentrate plus dilution water) is pumped to the MFCs and distributed along the length of the column with six injection nozzles. Within the MFCs, the anolyte is internally circulated from the top to the bottom of the column. The anolyte exits the MFC through a gas break to separate the biogas. The effluent is routed to a sewer drain. Air is pumped into the MFC cathode chambers in equal amounts. For MFC-A, the cathode chamber is air filled. For MFC-C, the cathode chamber is filled with reverse osmosis water (catholyte). Upon entering the bottom of MFC-C, the air and circulating catholyte are mixed together in a tee connection. The catholyte exits the top of MFC-C through a gas break to separate the air from the catholyte. The catholyte, then flows to the CO_2 contact column where the catholyte is exposed to 100% CO_2 gas. Exposure to the CO_2 gas replenishes bicarbonate ions and alkalinity lost in the MFC to maintain a

stable catholyte pH. The degassing vessel at the outlet of the CO_2 contactor column removes excess CO_2, which limits the dissolved oxygen uptake. This enables an increase in the dissolved oxygen concentration of the catholyte returning to the MFC.

4a) MFC Governing equations:

To describe an electrochemical system, the following effects need to be considered: species fluxes, mass conservation, current, electroneutrality, electrode kinetics, and hydrodynamics.[1,2] While important to electrochemical cell operation, electrode kinetics will not be addressed in this discussion because of the focus on membrane processes. Also, the four governing equations (i.e., 70; 71; 72; and 73) proposed assume dilute concentrations of electroactive species, therefore solute to solute interactions are assumed to be negligible.[1,2]

Equation (70) describes the catholyte to anolyte ion flux, with the terms of the equation reflecting three different processes: ion migration resulting from an electric field, ion diffusion, and ion convection.

$$N_i = -z_i u_i F c_i \nabla\Phi - D_i \nabla c_i + c_i v \qquad (70)$$

where, N_i = Flux of species i (mol/s-cm^2)

z_i = Charge of ion i (charge number)

u_i = ion mobility (cm^2-mol/J-s)

F = Faradays Constant 96,485 C/equiv

c_i = Concentration of species i (mol/cm^3)

$\nabla\Phi$ = Potential gradient (V)

D_i = Diffusivity of species i (cm^2/s)

v = bulk fluid velocity (cm/s)

Equation (71) describes the current created by the motion of charged species.

$$i = F\sum z_i N_i \tag{71}$$

where, i = Current density (Amps/cm^2)

F = Faradays Constant (96,485 C/equiv)

z_i = Charge of ion i (charge number)

N_i = Flux of species i (mol/s-cm^2)

Equation (72) addresses the material balance in the bulk solution.

$$\frac{\partial c_i}{\partial t} = -\nabla \cdot N_i + R_i \tag{72}$$

where, Ri = Chemical reaction occurring in solution (mol/cm^3-s)

Lastly, because of the large electrical forces between charged species, a significant charge separation cannot occur. Thus, in the bulk solution, electroneutrality is assumed and reflected in equation (73).

$$\sum_i z_i c_i = 0 \tag{73}$$

The four equations address the electrochemical system effects previously noted with the exception of the electrode kinetics. To apply these equations to the Brewery MFC data, more simplifying assumptions will be made. First, because there is no catholyte to anolyte pressure gradient, the water velocity (v) is assumed to be zero. Second, a homogeneous anolyte oxidation reaction will be assumed reflecting the anode CSTR assumption. Third, all anolyte and catholyte solution concentrations are assumed to be homogeneous, again reflecting the CSTR assumption.

The current density defined in terms of the species flux is obtained by substituting equation (70) into equation (71).

$$i = -F^2 \nabla \Phi \sum z_i^2 u_i c_i - F \sum z_i D_i \nabla c_i + Fv \sum z_i c_i \quad (74)$$

The last term can be assigned a value of zero by the electroneutrality assumption (73). If the concentration gradient is assumed to be zero for the electron transfer, the equation would reduce to;

$$i = -F^2 \nabla \Phi \sum z_i^2 u_i c_i \quad (75)$$

or,

$$i = -K \nabla \Phi \quad (76)$$

where, $K = F^2 \sum z_i^2 u_i c_i$

Equation 75 is Ohm's law, which indicates that the current density is proportional to the gradient of the potential. For the charge transfer of ions, a concentration gradient may be present and the diffusion term would need to be included in the equation.

4b) System mass balance:

A system mass balance was performed to understand the MFC influent and effluent fluxes.

Consider MFC-C and the anolyte recirculation line in Fig. 3-4 as the control volume.

Rate of mass efflux from MFC-C

- Rate of mass flow into MFC-C

+ Rate of accumulation of mass within MFC-C

= 0

Influent:	Effluent:
Feed solution	Effluent liquid
Oxygen (air)	Effluent gas
Carbon dioxide	Carbon dioxide as bicarbonate

Accumulation:

Because the MFC-C biomass is very small (invisible to the naked eye) and the experimental data was taken over a period of a few hours, the mass accumulation of acetate, biomass, oxygen and carbon dioxide are assumed to equal zero.

Influent rates:

Influent feed rate:

$$12{,}150\ cm^8/day\ x\ 1\ g/cm^8 = 12{,}150\ g/day \tag{77}$$

Oxygen consumption rate:

The cathode oxygen reduction reaction stoichiometry indicated one mole of oxygen is consumed for every four electrons donated from the cathode electrode.

$$2O_2 + 4H_2O + 8e^- \rightarrow 8OH^- \tag{23}$$

The electrons transferred can be determined from the current, which is found by using Ohm's Law, I = V/R.

$$\frac{0.3384V}{5\Omega} = 0.068\ A \tag{78}$$

Because 1.0 A equals one 1.0 C/s and 1.0 C/s equals 6.242 x 10^{18} electrons, the electron flow to the cathode can be determined from the current.

$$0.068\ A = 0.068\,C/s \times 6.242 \times 10^{18} e^{-}/C \tag{79}$$
$$= 4.24 \times 10^{17}\, e^{-}/s$$

$$4.24 \text{ x } 10^{17}\ \text{e}^{-}/\text{s} \times 1\,\text{mol e}^{-}/6.023 \text{ x } 10^{23}\ \text{e}^{-} \times 1\,\text{mol O}_2/4\ \text{moles e}^{-} \tag{80}$$

$$= 1.76\ \times\ 10^{-7}\ moles\ O_2/s$$

$$1.76\ x\ 10^{-7}\ moles\ O_2/s \times 32 g\ O_2/mol\ O_2 \times\ 86{,}400\ s/day \tag{81}$$

$$= 0.48\ g\ O_2\ consumed/day$$

Carbon dioxide consumption rate:

Like oxygen, the carbon dioxide consumption is related to the current because of the charge balance (section 3a). It was determined that one CO_2 molecule dissolves for every electron transferred from the anode to cathode. The electron transfer (4.24 x 10^{17} e^{-}/s) was determined in the oxygen illustration above (79).

$$\frac{4.24 \times 10^{17} e^{-}}{s} \times \frac{1 mol\ e^{-}}{6.023 \times 10^{23}\ e^{-}} \times \frac{1 mol\ CO_2}{1 mol\ e^{-}} = 7.03 \times 10^{-7}\ moles\ CO_2/s \tag{82}$$

$$\frac{7.03\ x\ 10^{-7}\ moles\ CO_2}{s} \times \frac{44\ g\ CO_2}{1\ mol\ CO_2} \times \frac{86{,}400\ s}{day} \tag{83}$$

$$= 2.67\ g\ CO_2\ consumed/day$$

Because carbon dioxide is transformed to bicarbonate, the bicarbonate addition can be calculated.

$$\frac{2.67\ g\ CO_2}{day} \times \frac{1\ mol\ CO_2}{44\ g\ CO_2} \times \frac{1\ mol\ HCO_3^-}{mol\ CO_2} \times \frac{61\ g\ HCO_3^-}{mol\ HCO_3^-} \tag{84}$$

$$= 3.70\ g\ HCO_3^-\ /\ day$$

Effluent Rates:

Effluent rate:

$$12{,}150\ \ cm^3/day\ x\ 1\ g/cm^3\ = 12{,}150\ g/day \tag{76}$$

Effluent gas:

Only 1 cm^3 of biogas was detected exiting the MFC. The mass is negligible compared to the feed effluent.

Alkalinity addition:

The alkalinity addition is equivalent to the bicarbonate addition calculated above (3.70 g HCO_3^-/day) and is not significant to the mass balance.

4c) Anode carbon balance:

The carbon balance was calculated to understand the MFC carbon inputs, transformations by chemical reactions, and dispositions.

Consider the MFC-C anode (Fig. 3-4), including the anolyte recirculation system, as the control volume.

Rate of carbon efflux from MFC

- Rate of carbon flow into MFC

+ Rate of accumulation of carbon within MFC

= 0

Carbon influent sources and rates:

The feed solution contains acetic acid and bicarbonate.

Acetic acid:

The influent COD can be used to determine the concentration of acetic acid in the feed stream by using the net reaction stoichiometry:

$$CH_3COO^- + 8H_2O + 2O_2 \rightarrow 2HCO_3^- + 9H^+ \; 8OH^- \tag{28}$$

$$\frac{371\ mg\ O_2}{1} \times \frac{1\ mol\ O_2}{32{,}000\ mg\ O_2} \times \frac{1\ mol\ H\text{-}Ac}{2\ mol\ O_2} \times \frac{2\ mol\ C}{1\ mol\ H\text{-}Ac} \times \frac{1000\ mmol}{1\ mol} = 11.6\ mmol\ C \tag{85}$$

$$11.6\ mmol\ C \times 12.15 L/day$$

$$= 140.9\ mmol\ C\ from\ acetic\ acid/day$$

Bicarbonate:

The influent bicarbonate concentration can be determined based on the sodium bicarbonate contained in the feed solution.

$$\frac{1.0\text{ g NaHCO}_8}{L}\times\frac{1\ mol\ \text{NaHCO}_3}{84\text{ g NaHCO}_3}\times\frac{\text{mol C}}{\text{mol NaHCO}_3}\times\frac{1000\ mmol}{1\ mol}=11.9\ mmol\ C \qquad (86)$$

$$11.9\ mmol\ C\times 12.15 L/day = \ 144.6\ mmol\ C\ from\ NaHCO_3/day$$

Total influent carbon:

The total influent carbon rate = $140.9+144.6=285.5\ mmol\ C/day$.

Carbon effluent sources and rates:

The carbon effluent sources include the unmineralized portion of the acetic acid as measured by the effluent water soluble COD, the effluent bicarbonate ions, and the carbon in the biogas. Each of these streams is addressed below.

Unmineralized acetic acid:

The effluent soluble COD reflects the unmineralized portion of the acetic acid by the net reaction stoichiometry:

$$CH_3COO^- + 8H_2O + 2O_2 \rightarrow 2HCO_3^- + 9H^+ + 8OH^- \qquad (28)$$

$$\frac{288\ mg\ O_2}{1}\times\frac{1\ mol\ O_2}{32{,}000\ mg\ O_2}\times\frac{1\ mol\ H\text{-}Ac}{2\ mol\ O_2}\times\frac{2\ mol\ C}{1\ mol\ H\text{-}Ac}\times\frac{1000\ mmol}{1\ mol}=9\ mmol\ C \qquad (87)$$

$$9\ mmol\ C/L\times 12.15 L/day = \ 109.4\ mmol\ C/day$$

Bicarbonate:

The effluent bicarbonate equals the influent sodium bicarbonate (144.6 mmol C from $NaHCO_3$/day) (86) plus the bicarbonate produced via electroneutrality maintenance, which was previously calculated (3.70 g HCO_3^- /day) (84).

$$\frac{3.70 \text{ g } HCO_3^-}{day} \times \frac{1\ mol\ HCO_3^-}{64 \text{ g } HCO_3^-} \times \frac{1 \text{ mol C}}{\text{mol } HCO_3^-} \times \frac{1000\ mmol}{1\ mol} = 60.7\ mmol\ C/da\ y \qquad (88)$$

Therefore, the total carbon from bicarbonate in the effluent is,

$$144.6\ mmol\ C/day + 60.7\ mmol\ C/day = 205.3\ mmol\ C/day$$

Biogas carbon dioxide and methane production rate

The biogas production rate will include methane and carbon dioxide measured as biogas and biogas saturated gas in the liquid effluent. Only 1.07 cm^3 of biogas was produced during the test period and composition measurement was inaccurate. Therefore, a 70% methane/30% carbon dioxide composition (by volume) will be used for the carbon balance analysis.[8] Soluble carbon dioxide will be reflected in the alkalinity measurement discussed above.

The biogas carbon will be determined using the ideal gas law.

$$n(CH_4) = PV / RT \qquad (89)$$

$$n = \frac{(0.7\ atm\ CH_4)(0.001\ L)}{(0.08026\ L\text{-}atm/mol\text{-}K)(296K)}$$

$$n = 2.95 \times 10^{-6}\ mol\ CH_4/day$$

$$n(CO_2) = PV / RT \tag{90}$$

$$n = \frac{(0.3\ atm\ CH_4)(0.001\ L)}{(0.08026\ L\text{-}atm/mol\text{-}K)(296K)}$$

$$n = 1.26 \times 10^{-5}\ mol\ CO_2/day$$

For methane and carbon dioxide, there is one mol of carbon for each mol of gas, therefore, there is 4.21 x 10^{-5} mols C/day generated as biogas.

The methane saturated in the effluent will be found using the Clark-Glew-Weiss equation, which calculates the mole fraction of methane in a fermentation medium.[14]

$$\ln X = A_0 + A_1(T/100)^{-1} \tag{91}$$

where, X = mol fraction of methane

A_o = -16.1198 K

A_1 = 16.4510 K

T = ^oK

$$\ln X = -16.1198 + 16.4510(296\ K/100)^{-1}$$

$$X = 2.59 \times 10^{-5}\ \text{mole fraction}\ CH_4$$

$$2.59 \times 10^{-5}\ mole\ fraction\ CH_4 = \frac{n\ CH_4}{n\ CH_4 + n\ H_2O} \tag{92}$$

where, n = number of mols

Solving for n CH_4 = 1.44 x 10^{-3} mols CH_4/L

Solving for the carbon,

$$1.44 \times 10^{-3}\ mol\ CH_4/L \times \frac{1\ mol\ C}{1\ mol\ CH_4} = 1.44 \times 10^{-3}\ mols\ C/L$$

$$1.44 \times 10^{-3}\ mol\ CH_4/L \times 12.15 L/day = 1.75 \times 10^{-2}\ mols\ C/L$$

Thus, the total carbon in the biogas plus saturated methane,

$$= 4.11 \times 10^{-5}\ mol\ C/day + 1.75 \times 10^{-2}\ mol\ C/day$$

$$= 1.75 \times 10^{-2}\ mol\ C/day$$

Total effluent carbon:

The total effluent carbon rate = 314.7 mmol C/day.

The 29.2 mmol C/day difference between the influent (285.5 mmol C/day) and effluent carbon (314.7 mmol C/day) likely reflects analytical inaccuracies with test methods.

4d) Anode oxidation rate constant (reaction engineering approach)

MFC-C performance data from Table 3-1 will be used to determine the anode acetate oxidation rate constant using a steady-state flow system continuous stirred tank reactor (CSTR) approach.[15] The accumulation of carbon is not considered in this analysis. The anode half reaction is as follows,

$$CH_3COO^- + 4H_2O \rightarrow 2HCO_3^- + 9H^+ + 8e^- \quad (20)$$

Definitions:

X = Conversion, moles of acetate reacted/moles of acetate fed

F_{Ao} = Molar flow rate acetate to the MFC (mmol/hr)

$F_{Ao}X$ = molar rate of acetate reacting in the MFC (mmol/hr)

Conservation of mass statement;[15]

Molar flow rate of acetate to MFC	-	Molar rate at which acetate is consumed in the MFC	=	Molar flow rate of acetate exiting the MFC
F_{Ao}	–	$F_{Ao}X$	=	F_A

(93)

Rearranging terms of the mass conservation statement,

$F_A = F_{Ao}(1-X)$ (The relation between the molar flow rate and conversion)

$F_A = F_{Ao} - F_{Ao}X$

$F_A - F_{Ao} = F_{Ao}X$ (94)

CSTR design equation;[15]

$$V = F_{Ao} - \frac{F_A}{-r_A} \tag{95}$$

where, V = volume (L)

A = Acetate

F_{Ao} = Molar flow rate of acetate to the reactor ($F_{Ao} = C_{Ao}Q$) (mmol/hr)

C_A = Concentration of acetate, (mmol)

Q = Volumetric flow rate to and from MFC (L/hr)

F_A = Molar flow rate of acetate from the reactor ($F_A = C_AQ$) (mmol/hr)

r_A = Acetate oxidation rate (mmol/hr-L)

Rearranging terms of the CSTR design equation,

$$-r_AV = F_{Ao} - F_A \tag{96}$$

Now, set the $F_{Ao} - F_A$ terms from the mass conservation (94) and CSTR design equations (96) equal to each other;

$$V = \frac{F_{Ao}X}{(-r_A)_{EXIT}} \tag{97}$$

Applying the MFC-C performance data,

V = 5.8 L

F_{Ao} = 2.93 mmol acetate/hr

X = $C_{Ao} - C_A$ = 5.8 mmol – 4.5 mmol = 1.3 mmol acetate reacted

= 1.3 mmol acetate reacted / 5.8 mmol acetate fed

X = 0.22

Solving for the MFC performance data, the acetate oxidation rate can be found.

$$(-r_A)_{EXIT} = \frac{-F_{Ao}X}{V} = 2.93\ mmol\ acetate/hr \times 0.22/5.8\ L \tag{98}$$

$$(-r_A)_{EXIT} = -0.11\ mmol\ acetate/hr \cdot L$$

where, $(r_A)_{EXIT} = (r_A)_{REACTOR}$ for a CSTR.

With a known reaction rate, an assumed first order reaction with acetate, and a constant temperature, the anode reaction rate constant k_A can be calculated.

$$-(r_A)_{EXIT} = k_A C_{Ao}(1-X) \tag{99}$$

$$k_A = \frac{-(r_A)_{EXIT}}{C_{Ao}(1-X)}$$

$$k_A = \frac{-(-0.11 mmol\ \text{acetate/hr} \cdot \text{L})}{5.8 mmol\ \text{acetate}(1-0.22)}$$

$$k_A = 0.024 hr^{-1}$$

4e) Oxygen reduction rate constant (reaction engineering approach)

The cathode oxygen reduction reaction stoichiometry indicates one mole of oxygen is consumed for every four electrons donated from the cathode electrode.

$$2O_2 + 4H_2O + 8e^- \rightarrow 8OH^- \tag{23}$$

From section 4b, the oxygen consumption was determined to equal 0.48 g O_2 consumed/day (81).

Although the MFC cathode is tubular, a steady-state CSTR approach (97) will be taken as opposed to a tubular flow reactor (PFR) approach, because the catholyte is well mixed with air.[15]

$$V = \frac{F_{Ao} X}{(-r_A)_{EXIT}} \tag{97}$$

Where, V = volume = 1.6 L.

F_{Oo} = Molar flow rate of oxygen to the reactor ($F_{Oo} = C_{0o}Q$) (mmol/hr)

X = Conversion, moles of oxygen reacted/moles of oxygen fed

r_O = Oxygen oxidation rate (mmol/hr-L)

The molar flow rate of oxygen to the reactor ($F_{Oo} = C_{0o}Q$) can be found by assuming that the water enters the reactor saturated with oxygen (8.4 mg/L);

$$\frac{8.4\ mg\ O_2}{L} \times \frac{1g}{1000\ mg} \times \frac{1\ mol\ O_2}{32\ g\ O_2} = 2.65 \times 10^{-4}\ mol\ O_2/L$$

2.65×10^{-4} mol O_2/L x 345 L/day = 9.14×10^{-2} mol O_2/day

Because the flow rate is constant through the reactor, the oxygen reaction must occur within the time the catholyte enters and leaves the cathode tube. The catholyte recirculation flow is 345 L/day and the tube volume is 1.6 L, which indicates an HRT of 6.68 min. The 0.48 g O_2 consumed/day can now be applied to cathode tube.

$$\frac{0.48\ g\ O_2}{day} \times \frac{1\ day}{1440\ \text{min}} \times \frac{1000\ mg}{g} \times 6.68\,\text{min} = 2.23\ mg\ O_2 \tag{100}$$

$$2.23\ mg\ O_2 \times \frac{1g}{1000\ mg} \times \frac{1\ mol\ O_2}{32\ g\ O_2} = 6.97 \times 10^{-5}\ mol\ O_2$$

6.97 x 10^{-5} mol O_2 is consumed in 6.68 minutes. In this time, 1.6 L of water passes through the cathode tube. Therefore, the oxygen concentration removed from the catholyte is;

$$\frac{6.97\times10^{-5}\ mol\ O_2}{1.6L} = 4.36\times10^{-5} mol\ O_2 / L$$

The reactor conversion can now be determined;

$$X = \frac{moles\ of\ oxygen\ reacted}{moles\ of\ oxygen\ fed}$$

$$\mathrm{X} = \frac{4.36\times10^{-5}\,\mathrm{mol\,O_2}/L}{2.65\times10^{-4}\,\mathrm{mol\,O_2}/L} \qquad (101)$$

$$\mathrm{X} = 0.16$$

The oxygen reduction rate can now be calculated.

$$(-r_O) = \frac{F_{Oo}X}{V} \qquad (97)$$

$$(-r_O) = \frac{9.14\times10^{-2} mol\ O_2/day(0.16)}{1.6L}$$

$$(-r_O) = 9.16\times10^{-3} mol\ \mathrm{O_2} / day - L$$

$$r_O = 9.16\times10^{-3} mol\ \mathrm{O_2} / day - L$$

Thus, the oxygen supplied to the catholyte is not rate limiting.

4e1) Carbon dioxide uptake rate

From section 4a, the carbon dioxide uptake rate was calculated to be 2.67 g CO_2 consumed/day. The carbon dioxide dissolves and dissociates in the carbon dioxide contact vessel (liquid volume = 0.15L). The HRT of the carbon dioxide contact vessel is 36 seconds (0.15 L/365 L/day). Thus, the carbon dioxide uptake in the vessel proceeds at the rate of;

$$\frac{2.67\ g\ CO_2}{day} \times \frac{1\ day}{86{,}400\ s} \times \frac{36\ \text{sec}}{0.15\ L} = 7.42 \times 10^{-3}\ g\ CO_2/L \qquad (102)$$

On a mole basis:

$$\frac{7.42 \times 10^{-3}\ g\ CO_2}{L} \times \frac{1\ mole\ CO_2}{44 g\ CO_2} = 1.69 \times 10^{-4}\ mols\ CO_2/L \qquad (103)$$

Using the ideal gas law (n = PV/RT), the CO_2 uptake can be calculated:

$$\frac{1.69 \times 10^{-4} mols\ CO_2}{L} = \frac{(1.0 atm)(V)}{(0.08206 L - atm/molK)(295 K)} \qquad (104)$$

$$Vol = 4.09 \times 10^{-3}\ L\ CO_2\ /L\text{-}day$$

$$4.09 \times 10^{-3} \frac{L\ CO_2}{L\text{-}day} \times 365 \frac{L}{day}$$

$$= 1.49\ L\ CO_2\ /\ day$$

4f) Determine the catholyte oxygen and carbon dioxide gas-liquid transfer rates.

Carbon dioxide:

$$CO_2 + H_2O \leftrightarrow H_2CO_3 \tag{45}$$

$$\frac{[H_2CO_3]}{[CO_2]} = K_h = 1.70 \times 10^{-3} \text{ (hydration equilibrium constant)} \tag{46}$$

Hydration forward reaction rate constant = $k_f = 0.039\ s^{-1}$ [16]

Hydration reverse reaction rate constant = $k_r = 23\ s^{-1}$ [16]

$$\frac{d[H_2CO_3]}{dt} = k_f [CO_2] \tag{105}$$

where, $[CO_2] = \frac{P_{CO_2}}{K_{HCO_2}}$ from Henry's law ($K_{HCO_2} = 29.76 L - atm/mol$)

substituting and solving for P_{CO_2} = 1.0 atm;

$$\frac{d[H_2CO_3]}{dt} = k_f \frac{P_{CO_2}}{K_{HCO_2}} \tag{106}$$

$$\frac{d[H_2CO_3]}{dt} = 0.039\ s^{-1} \frac{1.0\ atm}{29.76\ L\text{-}atm/mol}$$

$$\frac{d[H_2CO_3]}{dt} = 1.31 \times 10^{-3}\ mol\ H_2CO_3/L - s$$

Because 1.0 mol of CO_2 dissolves and dissociates for every mol of H_2CO_3 formed, the CO_2 dissolution rate equals;

$$\frac{d[CO_2]}{dt} = 1.31 \times 10^{-3}\ mol\ CO_2 / L - s$$

From section 4b, it was determined that the MFC-C catholyte CO_2 consumption rate equaled 7.03 x 10^{-7} moles CO_2/s (82). Thus, the catholyte CO_2 consumption rate is much slower than the CO_2 dissolution and hydration rate.

$$1.31\times10^{-3}\, mol\, CO_2 / L - s \rangle\rangle 7.03\times10^{-7}\, moles\, CO_2 / s$$

Thus,

$$\left.\frac{d[CO_2]}{dt}\right|_{hydration} \rangle\rangle \left.\frac{d[CO_2]}{dt}\right|_{consumed}$$

This finding is significant to my study because the rate of CO_2 hydration is not rate limiting, thus a stable catholyte pH can be sustained.

Oxygen:

The oxygen gas-liquid transfer rate is proportional to the difference between the saturated and actual dissolved oxygen concentration. The relationship can be described with the following mass balance equation;

$$\frac{dC_O}{dt} = K_a (C_{sat} - C_w) \qquad (107)$$

where,

dC_O/dt = time rate of change of the dissolved oxygen concentration

K_a = mass transfer coefficient for dissolved oxygen (T^{-1}) = 5.6 /hr [17]

C_{Osat} = saturated dissolved oxygen concentration

C_{Ow} = dissolved oxygen concentration of water

From section 4d, the catholyte tube inlet and outlet oxygen concentration was determined to be 2.65 x 10^{-4} mol O_2/L and 6.97 x 10^{-5} mol O_2/L, respectively. Therefore, the above mass balance equation gives;

$$\frac{dC_O}{dt} = (5.61/\text{hr})\,(2.65\times10^{-4}\,mol\,O_2/L - 6.67\times10^{-5}\,mol\,O_2/L \qquad (108)$$

$$= 1.1\times10^{-3}\,mol\,O_2/L - hr$$

The above oxygen dissolution rate is lower than the rate of oxygen addition if the catholyte was anaerobic. With zero oxygen, the time rate of change of the dissolved oxygen concentration would give,

$$\frac{dC_O}{dt} = (5.61/\text{hr})\,(2.65\times10^{-4}\,mol\,O_2/L - 0 mol\,O_2/L) \qquad (109)$$

$$= 1.5\times10^{-3}\,mol\,O_2/L - hr$$

Thus, the actual oxygen uptake is less than the potential oxygen uptake.

4g) Are the oxygen and carbon dioxide at equilibrium?

The data provided in section 4e indicate carbon dioxide and oxygen utilization rates are much lower than the replenishment rates. This indicates that the gas transport is not limiting CO_2 hydration or the oxygen reduction reaction rates. Since the hydration or reaction rates are not limiting, the gases can be considered to be in equilibrium and not limiting the MFC power density.

5) Membrane processes

5a) Bicarbonate ion flux

Ion transport across the ion exchange membrane is necessary to maintain MFC electroneutrality. With an AEM, the anion transfer from the cathode to anode must equal the electron transfer from the anode to cathode. As developed in section 4b, the anode to cathode electron flux equals 4.24 x 10^{17} e^-/s (79). Because HCO_3^- is the predominant catholyte anion (section 3a), the bicarbonate ion flux must equal the electron flux to maintain the MFC-C charge balance (4.24 x 10^{17} HCO_3^-/s).

On a unit surface area basis, the membrane anion flux equals:

$$\frac{4.24\times10^{17}\ HCO_3^-\ /\ s}{2\pi\ rh} \tag{110}$$

$$= \frac{4.24\times10^{17}\ HCO_3^-\ /\ s}{2\pi\ (2.5\,cm)\,(100\,cm)}$$

$$= 2.69\times10^{14}\ HCO_3^-\ ions\ /\ s-cm^2$$

5b) What membrane processes are considered?

The MFC electroneutrality requirement is the primary driver for bicarbonate ion transfer across the AEM. The membrane bicarbonate ion transfer is influenced by the following processes. Diffusion, however, is the primary driver of ionic transport unless the ionic concentration is very low. For very low concentrations, the electroosmotic drag becomes more significant.

-electroosmotic drag (reflects the number of water molecules accompanying the movement of each ion)

-diffusion due to the concentration gradient

-convection due to the pressure gradient

These processes can be described by a form of the Nernst-Planck equation:[18,19]

$$N_i = -z_i \frac{F}{RT} D_i C_i \left(\frac{d\phi_m}{dx}\right) - D_i \left(\frac{dC_i}{dx}\right) + vC_i \qquad (111)$$

where, N_i = Flux of species i (HCO_3^-)

z_i = Charge number of species i (-1)

F = Faraday's number (96,485 C/mol)

R = Universal Gas Constant (8.314 J/mol-K)

D_i = Diffusion coefficient of HCO_3^- (1.18×10^{-5} cm^2-s^{-1})[21]

C_i = Concentration of HCO_3^- (6.6×10^{-5} mol/L) (120)

dC_i = Concentration difference of HCO_3^- (1.68×10^{-2} mol/L) (121)

Φ_m = Electrical potential across the membrane (0.3384 V)

dx = Membrane thickness (0.05 cm)

T = Temperature (295 K)

v = Velocity of water, which is generated by the electrical potential and the pressure gradient (Insufficient information to calculate the water velocity resulting from the electrical potential. The water velocity resulting from the pressure gradient is zero, because the anode and cathode operate at the same pressure.)

The velocity of water can also be expressed by Schogl's equation:

$$v = k\frac{\phi}{\mu} z_f c_f F(\frac{d\phi_m}{dx}) - \frac{k_p}{\mu}\frac{dp}{dx} \quad (112)$$

where, k_Φ = Electrokinetic permeability*

μ = Pore-fluid viscosity

z_f = Fixed site charge*

c_f = Fixed-charge concentration*

k_p = Hydraulic permeability*

p = Hydraulic pressure

* Membrane specific information not available

The three terms of the Nernst Planck equation reflect the three processes influencing the bicarbonate ion transfer.

$$Electroosmotic\ drag_{(ED)} = -z_i \frac{F}{RT} D_i C_i (\frac{d\varphi_m}{dx}) \quad (113)$$

$$Diffusion_{(D)} = -D_i(\frac{dC_i}{dx}) \quad (114)$$

$$Convection_{(C)} = vC_i \quad (115)$$

The Nernst-Planck equation can be solved (leaving the water velocity as an unknown),

$$N_i = -z_i \frac{F}{RT} D_i C_i (\frac{d\phi_m}{dx}) - D_i(\frac{dC_i}{dx}) + vC_i \quad (111)$$

$$N_{i\ ED} = -(1)\frac{(96{,}485\ C/mol)}{(8.314\ J/mol\text{-}K)(295K)} \times (1.18\times10^{-5}\ cm^2/s)(6.6\times10^{-5}\ mol/L)(\frac{0.3384V}{0.05cm}) \quad (116)$$

$$N_{i\ ED} = -2.07\times10^{-7}\ mol/L\ \text{cm/s}$$

$$N_{i\,D} = -(1.18\times10^{-5}\,cm^2/s)(1.68\times10^{-2}\,mol/L)/(0.05cm) \quad (117)$$

$$N_{i\,D} = 3.97\times10^{-6}\,mol/L\ \ cm/s$$

$$N_{i\,C} = +v(6.6\times10^{-5}\,mol/L) \quad (118)$$

$$N_i = -2.07\times10^{-7}\,mol/L\ \ cm/s - 3.97\times10^{-6}\,mol/L\ \ cm/s + v(6.6\times10^{-5}\,mol/L)$$

$$N_i = 1.9\times10^{-6}\,mol/L\ \ cm/s + v(6.6\times10^{-5}\,mol/L)$$

5b) What gradients are present across the membrane?

The MFC-C membrane gradients are illustrated in Fig. 3-5 below. The bicarbonate ion concentration gradient exists from the anolyte to catholyte. Electroneutrality with an AEM, however, requires that the bicarbonate ions flow from the catholyte to anolyte, counter to the ion gradient, to maintain the MFC charge balance. The transfer of bicarbonate ions against the concentration gradient increases the internal resistance and negatively impacts MFC power. All anion transfers across the AEM are shown with green arrows, indicating a favorable passage through the AEM. Protons, however, are retarded in their movement across the AEM and are therefore, shown with a red arrow. The solution conductivity is shown to reflect the significant ionic concentration difference between the anolyte and catholyte. There is no pressure gradient because the anolyte and catholyte have equivalent hydraulic heads.

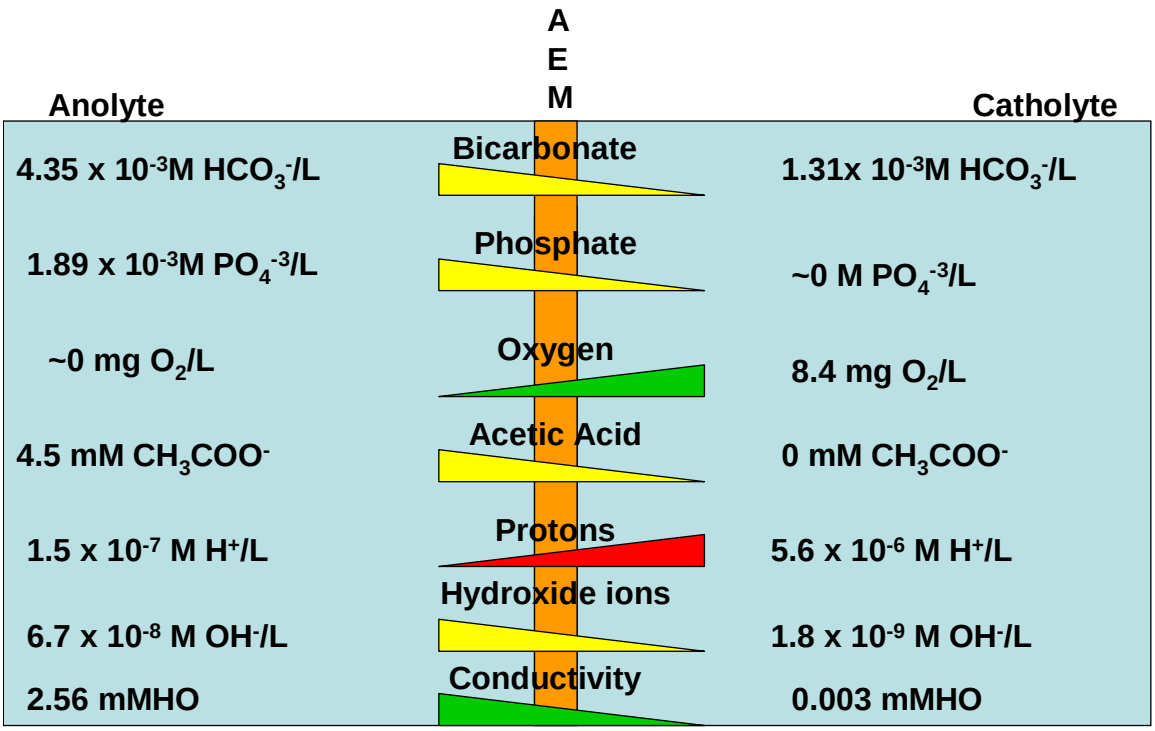

Figure 3-5. MFC Transmembrane Ion Concentrations and Conductivity Gradient bars reflect the diffusion direction based on the ion concentration gradient across the membrane. Green - Diffusion with the concentration gradient, Yellow - Diffusion is retarded by anion migration counter the ionic concentration gradient, and Red - Diffusion is retarded by the membrane

For MFC-C, the cathode to anode bicarbonate ion flux necessary to maintain MFC electroneutrality was determined in section 4e (2.69 x 10^{14} HCO_3^- ions/s-cm^2). The influence of the bicarbonate ion concentration gradient can be determined by Fick's law.

$$W_{HCO_3} = -D_{AB}\left(\frac{dC}{dx}\right) \tag{119}$$

where,

W_{HCO_3} = Bicarbonate molar flux

D_{AB} = Diffusivity of HCO_3^- in water (1.18 x 10^{-5} cm^2-s^{-1})[20]

dC/dx = Difference in the HCO_3^- concentration across the membrane divided by the membrane thickness of 0.05 cm.

The difference in the HCO_3^- concentration across the membrane assumes that all of the catholyte alkalinity is bicarbonate alkalinity and the anolyte alkalinity is based on 205.3 mmol C/day from section 4c (88).

Anolyte bicarbonate concentration:

$$= 205.3\ mmol\ C/day \times \frac{1\ mmol\ HCO_3^-}{1\ mmol\ C} \times \frac{1\ day}{12.15\ L}$$

$$= 16.9\ mmol\ HCO_3^- \quad (120)$$

Catholyte bicarbonate concentration:

$$= \frac{66\ mg\ CaCO_3}{L} \times \frac{1\ mol\ CaCO_3}{1.0 \times 10^6\ CaCO_3} \times \frac{2\ mol\ HCO_3^-}{1\ mol\ CaCO_3}$$

$$= \frac{0.132\ mmol\ HCO_3^-}{L} \quad (121)$$

Bicarbonate concentration difference:

$$= 16.9\ mmol\ HCO_3^- - 0.132\ mmol\ HCO_3^- = 16.77\ mmol \quad (122)$$

$$= 1.68 \times 10^{-2}\ mol\ HCO_3^-/L$$

Thus,

$$W_{HCO_3} = -(1.18\times10^{-5}\ cm^2/s)\frac{(1.68\times10^{-5}\ mol\ HCO_3^-/cm^3)}{.05\ cm}\ x\ 1570 cm^2 \quad (119)$$

$$W_{HCO_3} = 6.22\times10^{-6}\ M\ HCO_3^-/s\ \textit{(from the anode to the cathode)}$$

From section 4e, the cathode to anode bicarbonate flux was determined to equal 2.69 x 10^{14} HCO_3^- ions/s-cm^2.

$$= 4.45\times10^{-10}\ \text{mols}\ HCO_3^-/s\bullet cm^2\times1570\,\text{cm}^2 \quad (123)$$

$$= 6.99\times10^{-7}\ \textit{mols}\ HCO_3^-/s\ \textit{(from cathode to anode)}$$

Thus, the bicarbonate ion concentration gradient across the membrane indicates diffusion from the anode to cathode. The bicarbonate ion electromigration flux, however, is based on the potential across the membrane and transport is from the cathode to the anode. The net bicarbonate ion flux (based on experimental data) transports from the cathode to anode.

5c) Bicarbonate ion concentration based on pH and alkalinity

Catholyte

The catholyte bicarbonate ion concentration can be found by considering the total alkalinity equation assuming no other ions are present in the catholyte;

$$Alk_T = [HCO_3^-] + 2[CO_3^{2-}] + 2[HPO_4^{2-}] + [H_2PO_4^-] + [OH^-] - [H^+] \quad (63)$$

At pH = 5.25, the carbonate and hydroxide ion concentration can be neglected. Likewise, the phosphate ion concentration is assumed to be negligible, and therefore the phosphate alkalinity contribution will be neglected. Therefore, the total alkalinity equation can then be simplified to;

$$Alk_T = [HCO_3^-] - [H^+] \quad (64)$$

The total alkalinity of the catholyte was measured at 66 mg/L (as mg $CaCO_3$/L). Converting this measurement to the bicarbonate concentration yields;

$$\frac{66 \text{ mg } CaCO_3}{L} \times \frac{1 \text{ mol } CaCO_3}{1\times10^5 \text{ mg } CaCO_3} \times \frac{2 \text{ meq } HCO_3^-}{1 \text{ meq } CaCO_3} \quad (124)$$

$$= 1.32\times10^{-3} \text{ mol } HCO_3^- / L$$

The total alkalinity equation can now be solved in terms of the bicarbonate ion concentration at the cathode effluent.

$$Alk_T = [HCO_3^-] - [H^+] \quad (64)$$

$$\frac{1.32\times10^{-3} \ mol \ HCO_3^-}{L} = [HCO_3^-] - [5.62\times10^{-6}] \quad (125)$$

$$[HCO_3^-] = 1.31\times10^{-3}$$

Anolyte

To understand the anolyte alkalinity change, the MFC feed (anolyte feed) stream must first be understood using the Total Alkalinity Equation.

$$Alk_T = [HCO_3^-] + 2[CO_3^{2-}] + 2[HPO_4^{2-}] + [H_2PO_4^-] + [OH^-] - [H^+] \quad (63)$$

The MFC feed total alkalinity was measured at 294 mg/L (as mg $CaCO_3$/L) and pH = 6.70. With the acidic pH, the carbonate and hydroxide ion concentrations will be assumed to be negligible, particularly given the high bicarbonate and phosphate ions concentrations. The total alkalinity equation can now be simplified to;

$$Alk_T = [HCO_3^-] + 2[HPO_4^{2-}] + [H_2PO_4^-] - [H^+] \quad (126)$$

The total alkalinity (294 mg $CaCO_3$/L) can be converted to bicarbonate alkalinity;

$$\frac{294\ mg\ CaCO_3}{L} \times \frac{1\ mol\ CaCO_3}{1\times10^5\ mg\ CaCO_3} \times \frac{2\ eq\ HCO_3^-}{1\ eq\ CaCO_3} \tag{127}$$

$$= 5.88\times10^{-3}\ mol\ HCO_3^-/L$$

The bicarbonate and phosphate ion concentrations can be determined from the feed composition.

$$\frac{1.0\ g\ NaHCO_3}{L} \times \frac{1\ mol\ NaHCO_3}{83\ g\ NaHCO_3} \times \frac{1\ mol\ HCO_3^-}{1\ mol\ NaHCO_3} \tag{128}$$

$$= 0.012\ M\ HCO_3^-$$

$$0.33\ \text{g}\ K_2HPO_4 \times \frac{1\ mol\ K_2HPO_4}{174.2\ g\ K_2HPO_4} \times \frac{1\ mol\ PO_4^{-3}}{1\ mol\ K_2HPO_4} \tag{129}$$

$$= 0.0019\ M\ PO_4^{-3}$$

The relative concentration of $H_2PO_4^-$ and HPO_4^{-2} can be determined from the acid/base equilibrium at pH = 6.7.

$$[H_2PO_4^-] = 0.00113\ M$$

$$[HPO_4^{-2}] = \frac{0.00077\ M}{0.0019\ M}$$

The total alkalinity equation can now be considered with the MFC data.

$$Alk_T = [HCO_3^-] + 2[HPO_4^{-2}] + [H_2PO_4^-] - [H^+] \tag{125}$$

$$5.88\times10^{-3}\ M\ HCO_3^- = 0.012\ M\ HCO_3^- + 2(0.00077\ M\ HPO_4^{-2})$$

$$+ 0.00113\ M\ H_2PO_4^- - 1.99\times10^{-7}\ H^+$$

Simplifying;

$$5.88\times10^{-3}\ M \neq 1.47\times10^{-2}\ M$$

The measured MFC feed total alkalinity is 60% less than the predicted alkalinity. The likely explanation for this is the release of carbon dioxide when the sodium bicarbonate is added to the acidic feed solution, because the sodium bicarbonate is added after the acetic acid. The total alkalinity equation can be balanced assuming the phosphate is conserved and the excess of alkalinity is all composed of bicarbonate alkalinity, which is not conserved. Thus, solving for the unknown bicarbonate alkalinity;

$$5.88\times10^{-3}\ \text{M}\ HCO_3^- = X\ \text{M}\ HCO_3^- + 2(0.00077\ \text{M}\ HPO_4^{-2}) + 0.00113\,\text{M}\ H_2PO_4^- - 1.99\times10^{-7}\ H^+$$

$$[HCO_3^-] = 3.2\times10^{-3}\ M$$

This result indicates that a portion of the sodium bicarbonate added to the feed solution is lost through the degassing of carbon dioxide.

The total alkalinity of the MFC-C anolyte effluent is 358 mg/l (as mg $CaCO_3$/L) at pH = 6.83. With the acidic pH, the carbonate and hydroxide ion concentrations will again be assumed to be negligible given the relatively higher bicarbonate and phosphate ions concentrations. Thus, the simplified total alkalinity equation will be used;

$$Alk_T = [HCO_3^-] + 2[HPO_4^{-2}] + [H_2PO_4^-] - [H^+] \tag{125}$$

The total alkalinity (358 mg $CaCO_3$/L) can be converted to bicarbonate alkalinity.

$$\frac{358\ \text{mg CaCO}_3}{L}\times\frac{1\,\text{mol CaCO}_3}{1\times10^5\ \text{mg CaCO}_3}\times\frac{2\ \text{eq HCO}_3^-}{1\,\text{eq CaCO}_3} \tag{130}$$

$$= 7.16\times10^{-3}\ mol\ HCO_3^-/L$$

The phosphate ion concentration is assumed to be conserved in the anolyte, although a small amount may diffuse to the catholyte through the AEM. The relative concentration

of the mono and di-basic phosphate does, however, change with the pH because of the acid/base equilibrium.

$$[H_2PO_4^-] = 0.00099\ M$$

$$[HPO_4^{-2}] = \frac{0.00091\ M}{0.0019\ \text{M}}$$

The bicarbonate ion concentration in the anolyte effluent can now be calculated using the total alkalinity equation.

$$Alk_T = [HCO_3^-] + 2[HPO_4^{-2}] + [H_2PO_4^-] - [H^+] \quad (125)$$

$$7.16 \times 10^{-3}\ \text{mol}\ HCO_3^-\ /\ L = X\ \text{M}\ HCO_3^- + 2(0.00091\ \text{M}\ HPO_4^{-2})$$

$$+ 0.00099\ M\ H_2PO_4^- - 1.49 \times 10^{-7}\ M\ H^+$$

$$[HCO_3^-] = 4.35 \times 10^{-3}\ M$$

Thus, the anolyte bicarbonate ion concentration increases from 3.2 x 10^{-3} to 4.35 x 10^{-3} M HCO_3^- between the MFC feed and effluent. Within the MFC anode, the anolyte alkalinity is influenced by two processes, cathode to anode bicarbonate ion migration and acetic acid oxidation. The bicarbonate ion migration was calculated to be 3.70 g HCO_3^- /day (0.0607 M HCO_3^-/day) based on the MFC current. The 0.0607 M HCO_3^-/day ion flux can be calculated on a per liter basis by using the anolyte flow rate of 12.15 L/day.

$$\frac{0.0607\ M\ HCO_3^-/day}{12.15\ L/day} = 0.005\ M\ HCO_3^-/L \quad (131)$$

The acetic acid oxidation produces more protons than bicarbonate ions, which would decrease the pH and consume alkalinity.

$$CH_3COO^- + 4H_2O \rightarrow 2HCO_3^- + 9H^+ + 8e^-$$

or, rewritten as;

$$CH_3COO^- + 4H_2O \rightarrow 2CO_2 + 7H^+ + 8e^-$$

5mmol acetic acid was fed to the MFC, 10.6% of which was transformed to electricity based on the measured sCOD reduction and 48% coulombic efficiency. Therefore 0.53 mmol of acetic acid was transformed in the MFC. Considering the acetic acid oxidation stoichiometry, 7 mols of protons are released for every 1 mol of acetic acid consumed. Thus, there is a 3.7 mmol increase in the anolyte proton concentration (0.53mmol acetic acid x 7 mmol H=/1 mmol HAc), which is equivalent to a 3.7 mmol (0.0037 M) anolyte alkalinity decrease. The anolyte alkalinity, therefore, increases by 0.005 M from the bicarbonate ion migration and decreases by 0.0037 M from acetic acid oxidation reaction yielding a net 0.0013 M alkalinity increase.

Considering the total anolyte system, the following "alkalinity balance" is proposed.

Feed Alkalinity + Ion Migration Alkalinity – Acetic Acid Oxidation Alkalinity =

Effluent Alkalinty

$$3.2\times10^{-3}\ \text{M}\ HCO_3^- + 0.005\ \text{M}\ HCO_3^- - 0.0037\ \text{M}\ HCO_3^- = \quad (132)$$

$$4.5\times10^{-3}\ \text{M}\ HCO_3^-$$

The predicted anolyte effluent total alkalinity of 4.5 x 10^{-3} M HCO_3^-/L is in reasonable agreement with the measured 4.35 x 10^{-3} mol HCO_3^-/L total alkalinity.

6) Energy comparisons

6a) Oxygen requirement for fuel cell vs. activated sludge system

From section 4b, the oxygen consumption was 0.48 g O_2 consumed/day (81) for an 83 mg/L wastewater COD reduction and a 12 hour HRT. The total COD removed equals;

$$83\ mg\ COD/L \times 12.15\ L/day \times \frac{1g}{1000\ mg} = 1.01g\ COD/day\ removed \tag{133}$$

Thus, on a unit COD basis, the oxygen requirement is;

$$\frac{(0.48\ g\ O_2/day)}{(1.01\ g\ COD/day)} = \frac{0.48\ g\ O_2}{1\ g\ COD} \tag{134}$$

To provide this amount of oxygen to MFC-C, 50 ml/min of air (10.5 ml O_2/min) was supplied.

$$\frac{(10.5\ ml\ O_2)}{(\ \min\ )} \times \frac{1440\ \min}{day} \times \frac{1L}{1000\ mL} \times \frac{1.429\ g\ O_2}{L} = 21.6\ g\ O_2/day \tag{135}$$

Thus, the total oxygen supplied per gram of COD removed equals 21.6 g O_2 / 1.01 g COD, or 21.4 g O_2/1 g COD.

For commercial municipal activated sludge wastewater treatment, 0.5 to 0.6 kg O_2 /kg BOD is required to transform soluble carbon (BOD)[6]. Because easily biodegradable acetate is the sole MFC-C carbon source, it is reasonable to assume that the MFC-C COD equals the BOD for comparison purposes. Thus, the MFC-C oxygen requirement is ~40x higher than the oxygen required for municipal wastewater treatment. The higher MFC oxygen requirement may be attributed to inefficient laboratory catholyte mixing (larger

bubble size, less agitation), indirect electron transfer from the electron donor to oxygen with the MFC, and MFC oxygen mass transport limitations to the platinum reaction sites.

6b) Energy requirement for catholyte vs. air cathode MFC

MFC-A and C were operated with identical amounts of feed, air, and anolyte recirculation during the comparison test. Therefore, the energy input for those functions were equivalent for both MFCs. MFC-C catholyte, however, requires circulation for pH control. Thus, the energy required to drive the MFC-C catholyte recirculation pump is the only energy input difference between the two MFCs.

Energy Balance (All power in Watts)

Pump	**MFC-A**	**MFC-C**
Feed	8.25	8.25
Anolyte Recirculation	4.95	4.95
Catholyte Recirculation	NA	16.5
Air	12.1	12.1
Total Energy Input	25.3	41.8
Total Energy Output	0.0107	0.0229
Net Energy Consumption	25.29	41.78
Net Energy Balance Ratio (output/input)	4.2×10^{-4}	5.5×10^{-4}

6c) Is the catholyte cathode better than air cathode?

The section 6b energy balance data indicates MFC-A has lower energy consumption than MFC-C. MFC-A also has a greater %COD reduction, which shows that the energy required per unit COD reduction is lower for MFC-A than C. Advantages with MFC-C include a higher coulombic efficiency (48 versus 28%) and more stable pH control (5.25 versus 8.23) than MFC-A. Thus, while the experimental data indicates that MFC-A required less energy than MFC-C, the MFC-C pH stability relative to MFC-A yields superior power densities and wastewater treatment.

7) Microbiology

7a) Biochemical pathways to electricity

Within bacteria, acetate is transformed to acetyl-CoA and enters the citric acid cycle to be oxidized to carbon dioxide (catabolism) or synthesized into more complex molecules (anabolism) for cell synthesis (See Fig. 3-6 and 3-7). The reducing equivalents produced from the citric acid cycle (e.g., NADH) must be re-oxidized (NAD^+) for the cell to produce energy for cell maintenance and growth. Anaerobic bacteria can regenerate reducing equivalents in at least two ways;

i) substrate level phosphorylation, or

ii) oxidative phosphorylation.

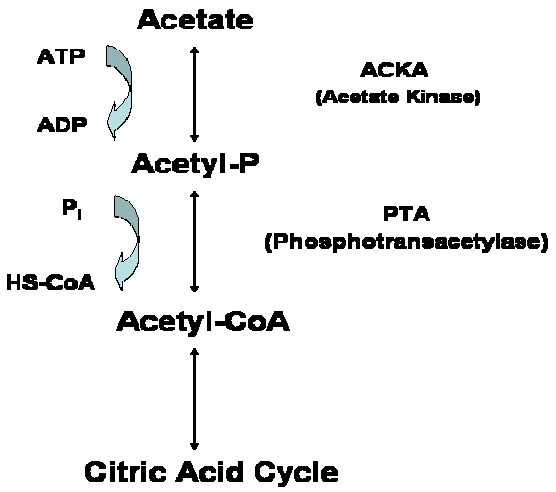

Figure 3-6. Transformation of acetate to Acetyl-CoA for entry into the citric acid cycle[22] (http://www.biologicalprocedures.com)

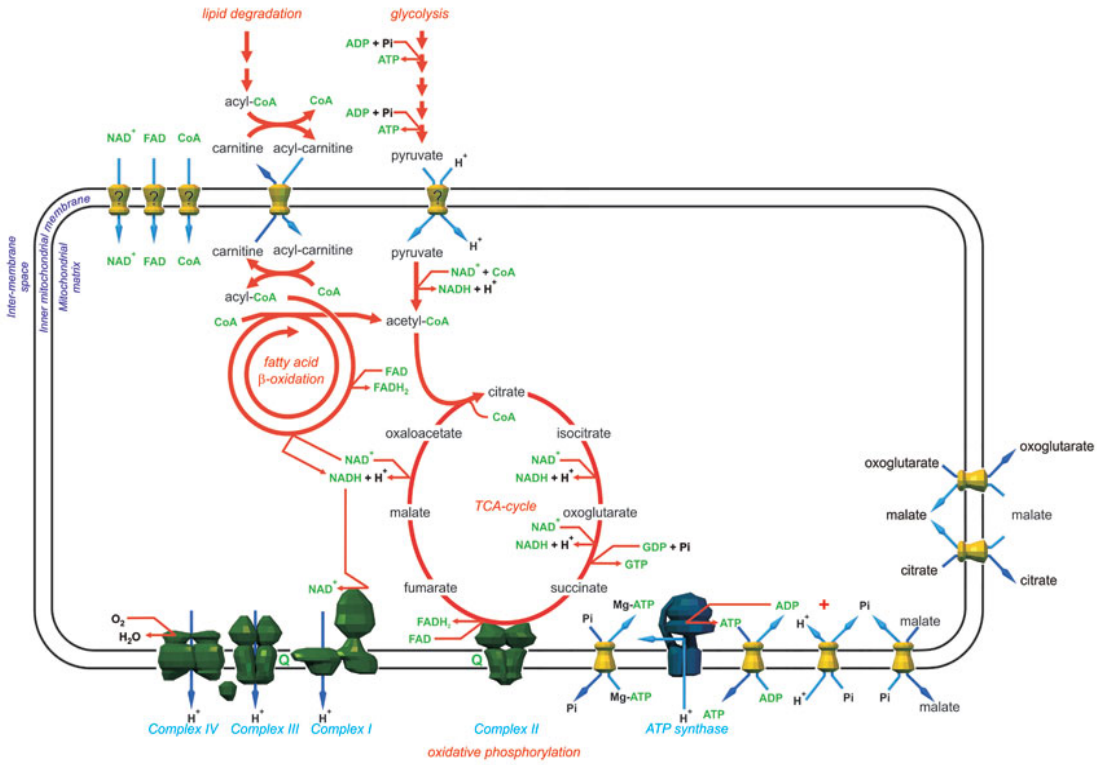

Figure 3-7. Citric acid cycle and electron transport chain with oxidative phosphorylation illustration.[23]

(http://www.mrc-dunn.cam.ac.uk/images/energymetabolism-large.jpg)

Substrate level phosphorylation involves the transfer of phosphate from a donor molecule directly to ATP. Oxidative phosphorylation produces ATP with the electron transport chain, which concurrently transports electrons while expelling protons outside the cell membrane. The expelled protons create a proton gradient, or proton motive force (PMF), which generates ATP by means of ATP synthase. An example from a eukaryotic organism is presented (See Fig. 3-7). The electrons transferred from reducing equivalents travel through the electron transport chain to the terminal electron acceptor, which in an MFC is the anode electrode. In fact, the anode electrode acts as an intermediate electron

acceptor as the electrons travel through an external electric circuit to the cathode electrode where oxygen, the terminal electron acceptor, is reduced to hydroxide ions.

In summary, the biochemical pathway from acetate to electricity requires the following;

1) The oxidation of acetate to carbon dioxide via the citric acid cycle with the simultaneous generation of reducing equivalents,
2) Oxidation of the reducing equivalents at the electron transport chain,
3) Transfer of electrons to the intermediate anode electrode,
4) Conduction of the electrons by an external circuit, and
5) The reduction of oxygen to hydroxide ions.

7b) Biochemical pathways to other carbon substrates

As shown in Fig. 3-7, bacterial anabolism originates with carbon from the citric acid cycle. The citric acid cycle then supplies building block molecules for macromolecule synthesis.

7c) Biochemical pathways to biogas

Besides the carbon dioxide generated in the Krebs cycle (Section 7a), methane is produced by bacteria and archaea within the MFC anaerobic anode by methanogenesis. Methane production can proceed by the conversion of acetate to methane and carbon dioxide by acetotrophic bacteria,

$$CH_3COOH \rightarrow CH_4 + CO_2 \qquad \Delta G = -131\ KJ/mol \tag{136}$$

or the conversion of hydrogen and carbon dioxide to methane by chemolithotrophs.

$$4H_2 + CO_2 \rightarrow CH_4 + 2H_2O \qquad \Delta G = -31\ KJ/mol \tag{137}$$

While the above fermentation reactions are energetically favorable, they are not as energetically favorable as the acetate oxidation reaction that utilizes the MFC anode electrode as an intermediate electron acceptor (electricigenic bacteria).

$$CH_3COO^- + 8H_2O + 2O_2 \rightarrow 2HCO_3^- + 9H^+ + 8OH^- \qquad \Delta G^{\circ\prime} = -753\ KJ/mol \tag{28}$$

Electricigenic bacteria, using the anode electrode as the intermediate electron acceptor for oxidative phosphorylation, gain more energy than fermenting bacteria, which use substrate level phosphorylation. Because of the energetic advantage of electricigens, MFCs are operated to promote electricigens in favor of fermenting bacteria. This is primarily achieved by slowly introducing the feed carbon source, not overfeeding, and monitoring the percent COD reduction.

7d) Show half reaction stoichiometry with overall fate of carbon

Details of the acetate fates are discussed in sections 1b, 2b, 7a, 7b, and 7c and are summarized below along with the reaction stoichiometry if available.

1) Acetate oxidation on the MFC anode;

$$CH_3COO^- + 4H_2O \rightarrow 2HCO_3^- + 9H^+ + 8e^- \tag{20}$$

2) Acetate oxidation from cathode oxygen crossover and feed dissolved oxygen;

$$CH_3COO^- + 8H_2O + 2O_2 \rightarrow 2HCO_3^- + 9H^+ + 8OH^- \tag{28}$$

3) Acetoclastic Methanogenesis;

$$CH_3COOH \rightarrow CH_4 + CO_2 \quad (137)$$

4)Hydrogenotrophic methanogenesis;

$$4H_2 + CO_2 \rightarrow CH_4 + 2H_2O \quad (138)$$

5) Acetate conversion to biomass by the citric acid cycle;

$$CH_3COOH \rightarrow nCH_2O \quad (139)$$

Table 3-1. Brewery MFC Performance Data April 15, 2009

Comprehensive MFC data acquired during steady state operation at 5 ohm resistance

Potential Data (Avg of 100 data points within the test window)

MFC-A	**MFC-A**	**MFC-C**
Cell Potential (V)	0.2312	0.3384
Anode Potential (V)	-0.3155	-0.2887
Cathode Potential (V)	NA	0.2095

Current, Power, and Coulombic Efficiency Data

Parameter	**MFC-A**	**MFC-C**
Current (Amps)	0.0462	0.0677
Current density (A/m^3)	7.96	11.67
Power (Watts)	0.0107	0.0229
Power density (W/m^3)	1.8	3.95
Coulombic Efficiency (%)	28	48

Feed and Effluent COD, pH, Alkalinity, Conductivity, and VFA data

Test	**Feed**	**MFC-A Effluent**	**MFC-C Effluent**
Total COD (mg/L)	366	294	322
sCOD (mg/L)	371	271	288
% sCOD removal		27	22
pH	6.70	6.73	6.83
Total Alkalinity (as mg $CaCO_3$/L)	294	338	358
Conductivity (milliMHO)	2.32	2.4	2.56
VFA (as mg Acetic Acid/L)	290	258	218

Table 3-1

Catholyte Properties

Test	MFC-A	MFC-C
pH	8.32	5.25
Alkalinity (mg/L)	NA	66
Conductivity (milliMHO)	NA	0.0028
Ion Analysis		TBD

Flow Rates

Process	MFC-A	MFC-C
Feed Rate (L/day)	11.7	12.15
Catholyte Recirculation (L/day)	NA	345
Anolyte Recirculation (L/day)	10.9	10.9
Air Supply (L/day)	72	72
Carbon Dioxide (L/day)	NA	46
Feed Concentrate - Total (L/day)	5.9	

Biogas

Volume = 1.07 cm^3

Composition = Insufficient sample size

References:

(1) Thauer, R. K.; Jungermann, K.; Decker, K., Energy conservation in chemotrophic anaerobic bacteria. *Bacteriol. Rev.* 1977, *41*, 100-180.

(2) Lipkowski, J., *Electrocatalysis*; Wiley-VCH: New York, NY, 1998.

(3) Rabaey, K.; Verstraete, W., Microbial fuel cells: Novel biotechnology for energy generation. *Trends Biotechnol.* 2005, *23*, 291-298.

(4) Logan, B. E.; Hamelers, B.; Rozendal, R.; Schröder, U.; Keller, J.; Freguia, S.; Aelterman, P.; Verstraete, W.; Rabaey, K., Microbial fuel cells: Methodology and technology. *Environ. Sci. Technol.* 2006, *40*, 5181-5192.

(5) Fornero, J.J.; Rosenbaum, M.; Angenent, L. T., Electric power generation from municipal, food, and animal wastewaters using microbial fuel cells; Submitted as a review paper to *Electroanalysis*, to be published in January, 2010.

(6) Richard, T., http://www.css.cornell.edu/compost/oxygen/oxygen.diff.water.html, 2005; Accessed June, 2009.

(7) Larminie, J.; Dicks, A., *Fuel Cell Systems Explained*; 2nd ed.; John Wiley & Sons Ltd.: Chichester, West Sussex, England, 2003.

(8) Fornero, J. J.; Rosenbaum, M.; Cotta, M. A.; Angenent, L. T., Microbial fuel cell performance with a pressurized cathode chamber. *Environ. Sci. Technol.* 2008, *42*, 8578-8584.

(9) Rozendal, R. A.; Hamelers, H. V. M.; Buisman, C. J. N., Effects of membrane cation transport on pH and microbial fuel cell performance. *Environ. Sci. Technol.* 2006, *40*, 5206-5211.

(10) Zhao, F.; Harnisch, F.; Schröder, U.; Scholz, F.; Bogdanoff, P.; Herrmann, I., Challenges and constraints of using oxygen cathodes in microbial fuel cells. *Environ. Sci. Technol.* 2006; *40*, 5193-5199.

(11) Butler, J., *Ionic Equilibrium*; John Wiley and Sons, Inc.: Cambridge, MA, 1998.

(12) Harnisch, F.; Warmbier, R.; Schneider, R.; Schröder, U., Modeling the ion transfer and polarization of ion exchange membranes in bioelectrochemical systems. *Bioelectrochemistry.* 2009, *75*, 136-141.

(13) Torres, C. I.; Lee, H. S.; Rittmann, B. E., Carbonate species as OH^- carriers for decreasing the pH gradient between cathode and anode in biological fuel cells. *Environ. Sci. Technol.* 2008, *42*, 8773-8777.

(14) Serra, M. C. C.; Pessoa, F. L. P.; Palavra, A. M. F., Solubility of methane in water and in a medium for the cultivation of methanotrophs bacteria. *J. Chem. Thermodyn.* 2006, *38*, 1629-1633.

(15) Fogler, S., *Elements of Chemical Reaction Engineering*; 2 ed.; Prentice Hall of India: New Dehli, India, 2001.

(16) Welch, M. J., Tracer studies with radioactive oxygen-15. Exchange between carbon dioxide and water. *J. Phys. Chem.* 1969, *73*, 3351-3356.

(17) Hill, G. A., Oxygen mass transfer correlations for pure and salt water in a well-mixed vessel. *Ind. Eng. Chem. Res.* 2009, *48*, 3696-3699.

(18) Spiegel, C., *Designing and Building Fuel Cells*; McGraw-Hill: New York, NY, 2007.

(19) Speigel, C., *PEM Fuel Cell Modeling and Simulation using MATLAB*; Elsevier: Burlington, MA., 2008.

(20) Millero, F., *The Physical Chemistry of Natural Waters*; Wiley-Interscience: New York, NY, 2001.

(21) Clesceri, L. S.; Greenberg, A. E.; Eaton, A. D., *Standard Methods for the Examination of Water and Wastewater*; 20th ed.; American Public Health Association: Washington, D.C., 1998.

(22) Keating, D. H.; Shulla, A.; Klein, A. H.; Wolfe, A. J., Optimized two-dimensional thin layer chromatography to monitor the intracellular concentration of acetyl phosphate and other small phosphorylated molecules. *Biol. Proced. Online* 2008, 36-46.

(23) Dunn, M., *Metabolic energy generation from lipids*; http://www.mrc-dunn.cam.ac.uk/research/mitochondrial_carriers/lipids.php. Accessed July, 2009.

Chapter 4

Microbial Fuel Cell Performance with a Pressurized Cathode Chamber

Fornero J. J., Rosenbaum M., Cotta M. A., and Angenent L. T. (2008). Microbial fuel cell performance with a pressurized cathode. *Environmental Science and Technology*, Vol. 42, No. 22, pp. 8578–8584.

Abstract

Microbial fuel cell (MFC) power densities are often constrained by the oxygen reduction reaction rate on the cathode electrode. One important factor for this is the normally low solubility of oxygen in the aqueous cathode solution, which creates mass transport limitation and hinders oxygen reduction at the electrocatalyst (platinum, Pt). Here, we increased the air pressure in the cathode chamber to increase the solubility and consequently the availability of oxygen, which is a function of the partial pressure. Under stable anode and cathode conditions, a MFC was tested with an anion exchange membrane (AEM) and a cation exchange membrane (CEM) at atmospheric pressure, +17.24 kPa (2.5 psig), and +34.48 kPa (5.0 psig) overpressure of air. The cell potential at an external resistance of 100 Ω increased from 0.423 V to 0.553 V by increasing the cathode pressure from atmospheric pressure to 17.24 kPa for a MFC with AEM, and this resulted in a 70% increase in the power density (4.29 versus 7.29 W/m^3). In addition, the

MFC produced 66 - 108% more power with AEM in comparison to CEM under the same operating conditions. Results from this study demonstrate that higher MFC power densities can be realized by increasing the cathode air pressure if the membrane oxygen diffusion to the anode can be controlled.

Introduction

Persistent high energy prices and the desire for environmental sustainability will likely challenge traditional engineering practices that were developed in an era of relatively low energy costs. One such area is conventional secondary treatment of wastewater with activated sludge systems. It was estimated that wastewater treatment consumes ~1.5% of the total electricity usage in the U.S. and that activated sludge aeration requires ~50% of that energy.[1] Microbial fuel cell (MFC) technology holds promise as a viable alternative to secondary activated sludge systems because of the ability to simultaneously treat wastewater and generate electricity.[2-5] Thus, one priority for the development and application of MFC technology is to transform wastewater treatment from an energy consuming process to a sustainable, energy neutral or energy producing, process.

Recently, novel MFC designs have been proposed to further increase their power densities.[3,6-9] These designs share a common feature of proximate anode and cathode electrodes to reduce the voltage drop associated with the resistance of the flow of ions through the electrolyte (i.e., ohmic losses). Ion transfer between the anode and cathode is necessary to maintain fuel cell electroneutrality because of the movement of negatively charged electrons from the anode to the cathode. To achieve this counterbalance, either

negative charge equivalents (anions/hydroxide ions) travel from the cathode to the anode, or positive charge equivalents (cations/protons) move from the anode to the cathode depending on the selection of the ion exchange membrane material (anion exchange membrane [AEM] versus cation exchange membrane [CEM]). Because MFCs operate near neutral pH in the anode and cathode chambers, ions other than hydroxide ions or protons are present at higher concentrations than the hydroxide ions or protons themselves (~10^{-6}M to ~10^{-8}M) in wastewater and buffer solutions, respectively. Therefore, the trans-membrane transport of nonhydroxide/nonproton ion species is the dominant mechanism to maintain electroneutrality in MFCs.[10-12]

Improvements to the cathode design in MFCs have also lead to considerable power density increases. To date, cathode designs have mainly used two different terminal electron acceptors; oxygen and nonsustainable chemicals, such as ferricyanide.[5,12] Cathode designs using oxygen as the terminal electron acceptor include cathodes with oxygen reduction catalysts submerged in an electrolyte (i.e., electrolyte cathodes)[*10,12,13*], air cathodes with oxygen-reduction catalysts[*3,14,15*], and biocathodes.[6,16,17] The primary limitation of power densities for oxygen as the electron acceptor results from the activation losses (i.e., voltage losses associated with the electrode electron transfer reactions) at the (bio)catalyst reaction sites.[18] Another limitation of oxygen cathodes with respect to the power density, especially for electrolyte cathodes, are the mass transport losses of oxygen to the catalyst reaction sites on the cathode electrode.[10,14] The relatively low solubility of oxygen affects the activation and oxygen mass transport losses in the cathode electrolyte. Because the solubility of air and consequent availability of

oxygen at the reaction sites are a function of their partial pressure, a pressurized cathode chamber should increase MFC power densities. Indeed, higher oxygen partial pressures, which increase oxygen reduction catalyst site occupancy, are routinely utilized for proton exchange membrane fuel cells with hydrogen as the energy carrier.[18]

Here, we studied the effect of a pressurized cathode chamber in a MFC on the power density by using an electrolyte cathode with an oxygen reduction catalyst configuration. In addition, the requirement of a membrane to prevent the crossover of oxygen from the pressurized cathode to the pressurized anaerobic anode was tested. We, therefore, chose a previously published MFC design with an upflow hydraulic pattern for which the ion exchange membranes (AEM or CEM) could be exchanged or removed without disturbing the anode during a long-term operating period of nine months.[19] Steady anode operating conditions were necessary to isolate and study the effects of changing cathode conditions. Before removing the membrane, however, the effect of the anode effluent as the catholyte in place of the phosphate buffer solution was taken into consideration. For all conditions, supporting performance data was gathered for power generation (power density, current density, potential, and coulombic efficiency) and waste treatment characterization (chemical oxygen demand [COD], volatile fatty acids [VFA], pH, and CH_4/CO_2 gas production).

Materials and Methods

Setup

The upflow MFC (UMFC) consisted of two chambers, an anaerobic anode chamber on the bottom (480 cm^3 total; 420 cm^3 net anode volume) and a cathode chamber (260 cm^3 total; 250 cm^3 net cathode volume) on the top.[19] The anode electrode consisted of 8.0 m of carbon fiber (unsized fiber, Zoltek, St. Louis, MO) inserted randomly into the anode chamber. The cathode electrode was made of parallel sheets of carbon paper (AVCARB P75 Carbon fiber paper, Ballard Material Products, Inc., Lowell, MA) (521 cm^2 total surface area) secured by carbon fiber (Zoltek) to the electrode external conductor (Fig. B1, Appendix B). The cathode electrode was coated with 0.0189 mol/m^2 (3.65 g/m^2) of platinum (Pt) by chemical deposition of Pt with 0.976 mmol (0.4 g) chloroplatinic acid hexahydrate ($H_2PtCl_6 \bullet 6H_20$) (Sigma Aldrich), according to Gharibi et al..[20] The $H_2PtCl_6 \bullet 6H_20$ was first dissolved in deionized water, followed by immersion of the carbon paper electrode in the solution. The solution was then ultrasonicated and heated to 80°C. A sodium formate solution (40 g/l) (Sigma Aldrich, St. Louis, MO) was added to the $H_2PtCl_6 \bullet 6H_20$ solution, ultrasonicated, and heated for one hour to reduce Pt. The carbon electrode was then removed and dried overnight at 105°C. For experiments A-H (see experimental design), no Nafion® coating was applied. Only prior to experiments I-K, two coatings of Nafion® (5% solution) were applied to the cathode electrode to protect the Pt catalyst from the anolyte. Ion exchange membranes consisted of either AEM or CEM (AMI-7001, CMI-7000 Membranes International, Glen Rock, NJ) (28.26 cm^2). The ***anode*** effluent line outlet was positioned 1.4 m above the ion exchange membrane to maintain a 13.79 kPa backpressure on the anode compartment. This anode backpressure was designed to reduce the cathode to anode oxygen diffusion during operating periods with a pressurized cathode and should not adversely affect the microbial

community.[21] Anodic biogas production was measured with a gas meter (Ritter MGC-1 Milligas Counter, Bochum, Germany) and gas composition samples were taken through a septum that was placed after a liquid/gas separator located in the anode effluent tubing. ***Cathode*** air pressure was increased by using a pressure regulator (Lowes Kobalt Mini Regulator, Mooresville, NC). Compressed air was continuously sparged through an air diffuser (Lee's, San Marcos, CA).

Operation

The inoculum was a homogenized granular sludge from an upflow anaerobic bioreactor at a brewery (Anheuser Busch, Inc., St. Louis, MO). The UMFC was fed a sucrose synthetic wastewater with a chemical oxygen demand (COD) concentration of 900 mg/L and a continuous flow rate of 550 ml/day. The anode hydraulic retention time (HRT) was 18 h. The synthetic wastewater consisted of (per liter of deionized water): sucrose, 0.8 g; yeast extract (Difco Laboratories, Inc., Detroit, MI), 0.006 g; NH_4Cl, 0.033 g; K_2SO_4, 0.006 g; $FeCl_2 \cdot 4H_2O$, 0.033 g; iron citrate, 0.011 g; NaCl, 5.0 g; KCl, 0.1 g; $CaCl_2$, 0.1 g; $MgCl_2 \cdot 6H_2O$, 0.1 g; 0.040 M phosphate buffer; and trace elements, 1.0 ml modified from.[22,23] The anolyte conductivity at 25 °C was 8.9 mS/cm. Anolyte was recirculated with a flow rate of 75 ml/min throughout the experiment. The anode temperature was maintained at 35±1ºC with an external recirculation heater (Scientific Model 1104 VWR, West Chester, PA). The cathode electrode was submersed in a 700 mM phosphate buffered catholyte solution (Sigma-Aldrich, St. Louis, MO) and continuously replenished at a rate of 160 ml/day to maintain a constant pH level of 7.6 throughout the experiment with this catholyte. The catholyte conductivity at 25 °C was 124.5 mS/cm. Peristaltic

pumps were used for both the anolyte recirculation and catholyte replenishment (Cole Parmer, Vernon Hills, IL). Sustainable fuel cell operating periods used a 100-Ω external resistor.

Analyses

The potential (E) across a resistor (R) was measured using a digital multimeter (2700 + 7700 multiplexer, Keithley Instruments, Inc., Cleveland, OH). The current density was calculated as $I = E/RV$ and the power density was calculated as $P = E^2/RV$, where V was the net liquid volume of the anode chamber. The polarization curve was developed by changing the external resistor stepwise from open circuit to 20 Ω. The internal (R_i) resistance was determined using the steady discharging method.[24] Influent total COD, effluent soluble COD (SCOD), VFA, pH, and conductivity were measured according to procedures described in *Standard Methods*.[25] For the conductivity measurements a self-contained conductivity meter was used (Series 11, Oakton Instruments, Vernon Hills, IL). Gas analysis was performed with gas chromatography (Gow-Mac Model 69-350, 4" x 1/8" o.d. 20% DC-200 on Chromosorb P AW-DMCS, 80/100 mesh column, Bethlehem, PA). All analyses were performed in triplicate with the exception of the biogas production and pH for which daily measurements were recorded.

The theoretical increase in the cathode potential with increasing air pressure was calculated with the Nernst equation. This equation was used in its simplified form because all other performance variables (temperature, feed rate, feed composition,

recirculation rate, reactor configuration) were maintained constant with the exception of the pressure:[18]

$$\Delta E = \frac{RT}{4F} \ln(\frac{P_2}{P_1})$$

where E = potential; R= universal gas constant; T = temperature; F = Faraday's constant; and P_i = absolute cathode pressure.

Experimental Design

The study was conducted over a nine-month period of time, with the following experimental sequence: experiment A: 34.48 kPa with AEM; B: 17.24 kPa with AEM; C: nonreplenished catholyte pH test with AEM at 17.24 kPa (the continuous catholyte replenishment was temporarily switched off); D: atmospheric pressure with AEM; E: atmospheric pressure with CEM; F: 34.38 kPa with CEM; G: 17.24 kPa with CEM; H: nonreplenished catholyte pH test with CEM at 17.24 kPa (the continuous catholyte replenishment was temporarily switched off); I: atmospheric pressure with Nafion coated cathode with CEM and phosphate buffered catalyst; J: atmospheric pressure with Nafion coated cathode with CEM and anolyte effluent as catholyte; and K: atmospheric pressure without a membrane and with the anode effluent flowing from the anode to the cathode in an upward mode (Fig. B2, Appendix B). The recirculation of the anolyte was sustained during experiments J and K.

Results and Discussion

Pressurized Cathode Chamber Increases MFC Power Densities

The highest power density of our study (7.29 W/m^3) was achieved with 17.24 kPa of cathode pressure and an AEM (Fig. 4-1 and Table 4-1). The power density at a 17.24-kPa pressure represented a 70% and 13% improvement in comparison to atmospheric pressure and 34.48 kPa, respectively (experiments B, D, and A). Further, the fuel cell open circuit potential (OCP) at 17.24 kPa with the AEM was 0.931 V, and this is to our knowledge the highest recorded for a platinum oxygen-reducing cathode in a MFC (Fig. 4-1A and Table 4-1). As anticipated, the cathode potential increased with increasing air pressure, reflecting the increasing catholyte dissolved oxygen concentrations (Table B1, Appendix B). The cathode OCP (versus Ag/AgCl, sat. KCL, 0.195V versus standard hydrogen electrode [SHE]) was 0.3059, 0.3261, and 0.3545 V for atmospheric pressure, 17.24 kPa, and 34.48 kPa, respectively (Fig. B3, Appendix B). With CEM, the highest power density (3.49W/m^3) also occurred at 17.24 kPa compared to atmospheric pressure and 34.48 kPa (Fig. 4-1D and Table 4-1) (experiments G, E, and F). The power density with the 17.24 kPa cathode pressure represented a 35% and 10% improvement compared to atmospheric pressure and 34.48 kPa, respectively.

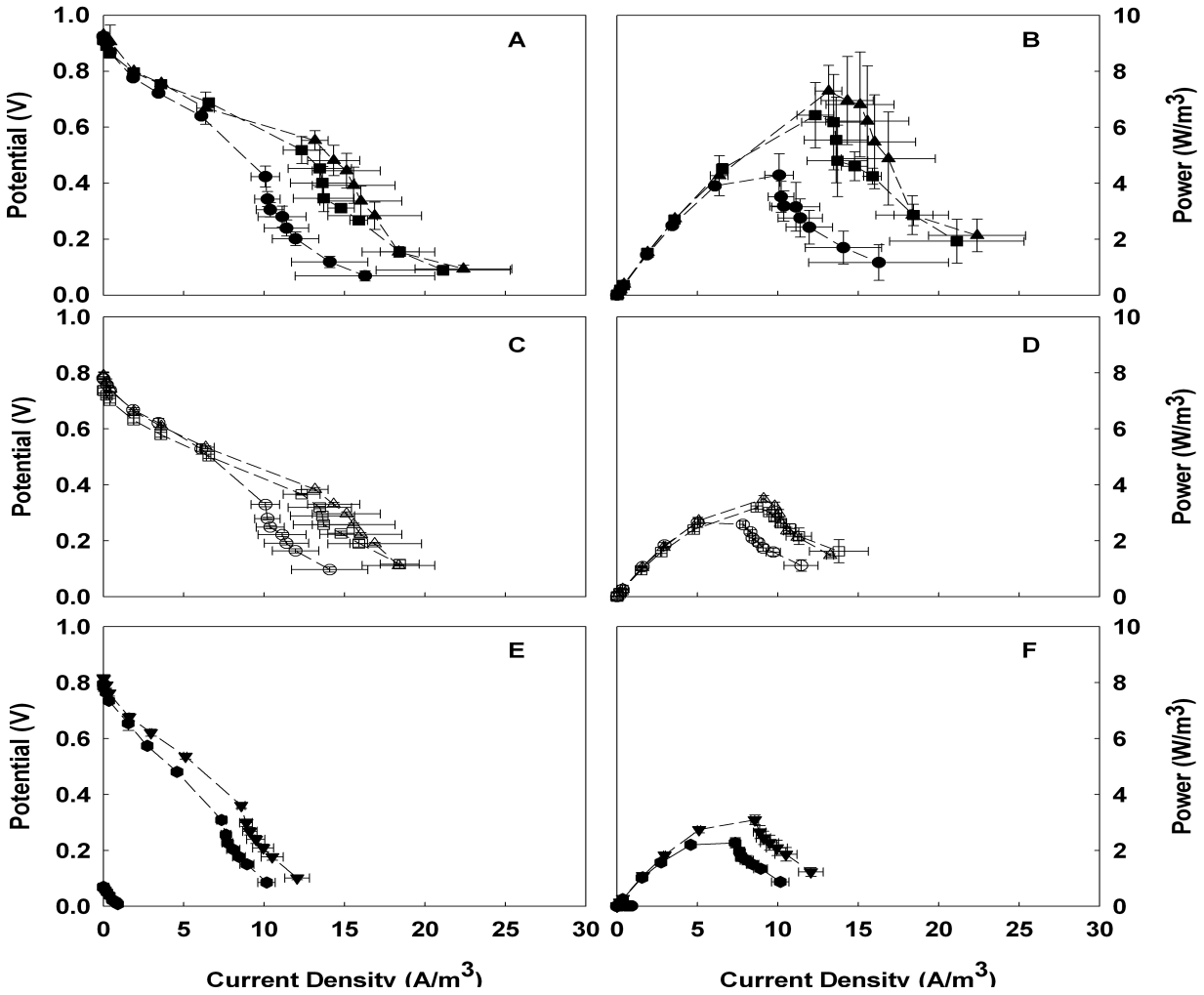

Figure 4-1. UMFC Polarization and Power Curves. **(**A) Polarization curve with AEM; (B) power curve with AEM. AEM data represented with solid symbols: (■) 34.48 kPa; (▲) 17.24 kPa; and (●) atmospheric pressure; **(**C) polarization curve with CEM; (D) power curve with CEM. CEM data is shown with hollow symbols: (□) 34.48 kPa; (△) 17.24 kPa; and (○) atmospheric pressure; (E) polarization curve with atmospheric pressure cathode: (▼) Nafion coated cathode electrode with phosphate buffered catholyte; (⬣) Nafion coated cathode with anolyte effluent catholyte; and (●) Membrane removed; (F) power curve with atmospheric pressure cathode: (▼) Nafion coated cathode electrode with phosphate buffered catholyte; (⬣) Nafion coated cathode with anolyte effluent catholyte; and (●) membrane removed. Data points represent an average of three experiments with the accompanying standard deviation error bars (presented as a color image in Fig. B5, Appendix B).

We predicted with the Nernst equation that an increase in pressure from atmospheric pressure to 17.24 kPa and 34.48 kPa would increase the cathode cell potential by 0.0010 V and 0.0019 V respectively. However, our experimental data showed higher than predicted cathode potential increases of 0.0202 V and 0.0468 V for 17.24 kPa and 34.48 kPa, which represents a 20- and 25-fold increase over the Nernst equation predicted potentials, respectively. The difference in actual versus predicted potentials was explained for fuel cells by a decrease in the irreversible activation losses at the cathode electrode, especially at lower temperatures.[18] The decrease in the cathode electrode's irreversible activation losses is related to the exchange current density, which refers to the steady state forward and backward flow of electrons between reactants and products at the electrode surface. With an increase in the oxygen partial pressure, the exchange current density increased, reflecting a more active cathode electron flux. The more active cathode requires a lower overpotential to energize cathode electron transfer reactions. Thus, increasing exchange current density (by increasing the oxygen partial pressure, increasing the cathode temperature, or by using more effective cathode catalysts) lowers the irreversible activation losses required to energize chemical reactions.[18]

We anticipated increasing MFC power densities with increasing cathode pressure. Our data, however, showed that power densities decreased as the cathode pressure was increased from 17.24 to 34.48 kPa. At 100 Ω of external resistance, the cathode potential increased from 141 to 179 mV (Fig. B3, Appendix B) and the corresponding MFC potentials decreased from 553 to 518 mV (Table 4-1) when the pressure was increased from 17.24 to 34.48 kPa. The differences between the cathode and MFC potentials

indirectly indicate an anode potential of -412 and -339mV for 17.24 and 34.48 kPa, respectively. We believe that the lower anode potential (-339 mV) is most likely the result of increased oxygen crossover through the ion exchange membrane at higher pressures. We found experimentally that oxygen diffusion increased with increasing differential pressures across the membrane (Fig. B4, Appendix B), supporting the theory that oxygen diffusion at the highest cathode pressure (34.48 kPa) negatively impacted performance. A similar phenomenon of lower overall cell potentials at a higher cathode potential was found in a sediment fuel cell study that used a rotating cathode. The cathode potential was improved by increasing the speed of cathode rotation, however, the overall fuel cell potential declined because of the increased oxygen concentrations in the sediment.[26] Since diffusion of oxygen over the ionic membrane is affected by both oxygen concentration and pressure gradients, a backpressure on the anode compartment was utilized to minimize oxygen diffusion from the cathode to the anode. The negative effect of the oxygen diffusion at 17.24 kPa was reduced because of a 13.79 kPa backpressure on the anode chamber and a resulting catholyte to anolyte pressure gradient of only 3.45 kPa. This pressure gradient increased to 20.69 kPa with the 34.48 kPa cathode, and thereby increasing the oxygen diffusion. Our data, thus, suggest that equalizing and optimizing the pressures in the cathode and anode chambers can further increase the overall cell potential and power densities.

Anolyte Effluent as Catholyte and Membraneless Operation Reduce MFC Power Densities

Three additional experiments were conducted with an atmospheric pressure cathode and a 13.79 kPa anode (constant backpressure throughout the entire experimental period): (1) a baseline experiment with a CEM and phosphate buffered catholyte (experiment I); (2) CEM and anolyte effluent (experiment J); and (3) the removal of CEM (experiment K). We observed a 26.5% decrease in the power density with the change from the phosphate buffered catholyte (experiment I) to the anode effluent catholyte (experiment J) because of immediate and longer term effects, which are discussed in detail in the supporting information (Appendix B). In addition, operation without a membrane (experiment K) resulted in a 99.5% decrease in the power density compared to experiment J with CEM and anolyte effluent as catholyte (0.01 versus 3.09 W/m^3) and 99.6% to the baseline experiment I (Table 4-1), which strongly suggests that removing the ion-exchange membrane in a MFC with an electrolyte cathode and oxygen reduction catalyst severely deteriorates the power density due to oxygen cross over, cathode insulation, and/or catalyst poisoning (see discussion in the supporting information, Appendix B).

Ion Gradients Influence Internal Resistance and Power Densities

With ion transport being imperative to maintain electroneutrality, ohmic losses become important because they contribute to MFC total system losses. Ohmic losses in MFCs are influenced by the: 1. ionic transport processes within the anolyte and catholyte (i.e., solution losses due to diffusion and electro-migration processes)[10-12]; and 2. ionic transport processes across the exchange membrane (i.e., membrane losses due to the specific material features of the membrane and characteristics of the electrolyte solutions).[27] Our upflow microbial fuel cell had concentration and hydraulic pressure

gradients over the ion exchange membrane (because of different anolyte and catholyte solutions and operating conditions, see Fig. 4-2), which can be either a driving force or restraint for ion movement from one compartment to the other. We maintained identical ion and hydraulic pressure gradients with constant anolyte and catholyte solutions (i.e., 0.08 M and 1.19 M monovalent equivalents, respectively) during the comparison experiments with AEM and CEM, and thus we anticipate similar solution losses. Kim et al.[27] found comparable internal resistances for the same AEM and CEM materials without ion gradients across the membranes. Therefore, since the solution losses and specific material membrane losses were similar between AEM and CEM experiments, we anticipate different membrane losses due to the impact of the ion gradient and to a lesser extent (due to a modest 3.45 kPa pressure differential) the hydraulic pressure gradient: the choice of AEM versus CEM will dictate whether anions or cations, respectively, travel selectively across the ion exchange membrane to maintain fuel cell electroneutrality.[10-12] In our study with AEM, anion transport was favorable *with* the concentration and hydraulic pressure gradients (Fig. 4-2A), while with CEM cations (nonprotons) were transported *against* the concentration and hydraulic pressure gradients (Fig. 4-2B). Thus, a favorable ion gradient will result in lower membrane losses compared to a nonfavorable ion gradient.

Indeed, our results consistently yielded higher power densities for the AEM compared to the CEM (Fig. 4-1A, 4-1C, and Table 4-1). More specifically for experiments B and G with 17.24 kPa, a lower internal resistance of 61.2 Ω for AEM compared to 93.6 Ω for CEM was estimated. As explained above, the favorable anion versus the nonfavorable

cation gradient in our study accounts for the ~30 Ω difference in internal resistance. This quantitative difference was caused by our choice of composition and concentration of phosphate buffer solution in the cathode chamber, and would have been less pronounced if we had used a lower concentration phosphate solution in the cathode. In a real-world situation, the ion gradients between the anode and cathodes are dependent on the encountered wastewater solution (anolyte) and selected catholyte. Based on these solutions the engineer should decide between AEM and CEM to minimize the overall MFC resistance.

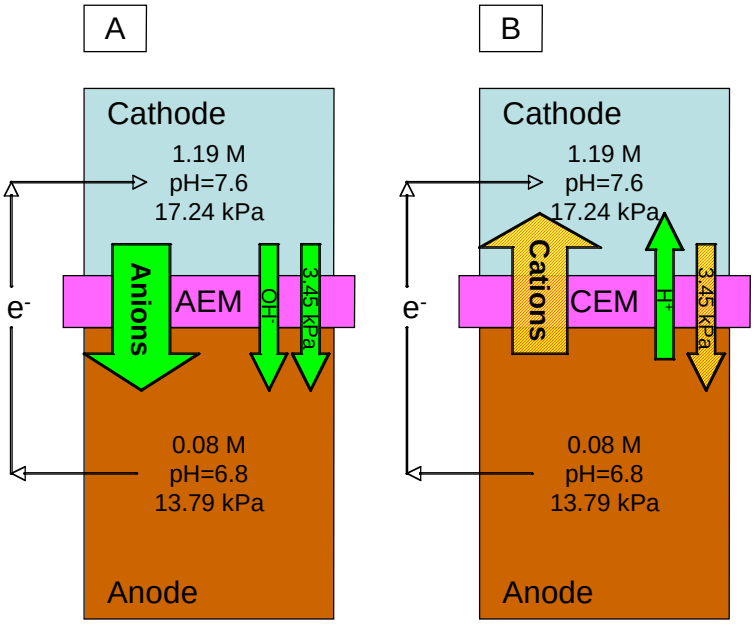

Figure 4-2. UMFC Monovalent Ion Charge Equivalents and Ion Transport. Monovalent charge equivalents (cation, anion, proton, and hydroxide ions) and hydraulic pressures are illustrated for the UMFC during experiment B and G. The direction, size, and shading of the arrows reflect the dominant ion transport mechanisms to achieve fuel cell electroneutralilty; (A) electroneutrality maintenance with the AEM requires the movement of negatively charged ions from the cathode to the anode. The large downward anion arrow represents the favorable transport of anions with the concentration gradient; and (B) electroneutrality maintenance with the CEM requires the movement of

positively charged ions from the anode to the cathode. The large upward cation arrow is cross-hatched because cation transport were moving against the ion concentration gradient. The pressure gradients were less important (smaller arrow) and were a driving force for AEM or a restraint (cross-hatched) for CEM to move ions across the membrane. Proton and hydroxide ion gradients were equivalent for both membranes, and are much less important at neutral pH levels (smaller arrows).

Monovalent Ions Show Lower Charge Transfer Resistance than Divalent Ions

Measurement of catholyte pH trends with a nonreplenished phosphate buffered catholyte (experiments C and H), showed an anticipated increase in pH levels over time for both the AEM and CEM (at 17.24 kPa) (Fig. 4-3). Such increases in pH reflect proton consuming oxygen reduction reactions in the cathode (while hydroxide ions and protons do not transfer to maintain electroneutrality). The slightly greater pH increase for the AEM compared to the CEM was accounted for by the higher current densities with the AEM (Fig. 4-3A). Cathode potential for both AEM and CEM over time during batch operating conditions showed a slow decrease as the pH increased, which follows the Nernst equation (0.34 mV/pH AEM; 0.69 mV/pH CEM measured versus 0.59 mV/pH predicted). The overall cell potential profiles for the UMFC with AEM and CEM, however, differed considerably from each other. The cell potential decline with the AEM was initially rapid and then approximated the cathode potential decrease (Fig 4-3A). With the CEM, however, the cell potential decline continually corresponded with the decrease in the cathode potential (Fig. 4-3B). The difference in the cell potential profiles could not be attributed to the pH, cathode potential, or the initial ion concentrations because these variables were similar for the AEM and CEM experiments. Therefore, we hypothesized that ionic transport processes across the exchange membrane were

influencing the cell potential. Indeed, we could explain the difference in cell potential profiles by a preferential transfer of monovalent versus divalent ions crossing the membrane due to the smaller radius of the monovalent ion compared to the divalent ion.

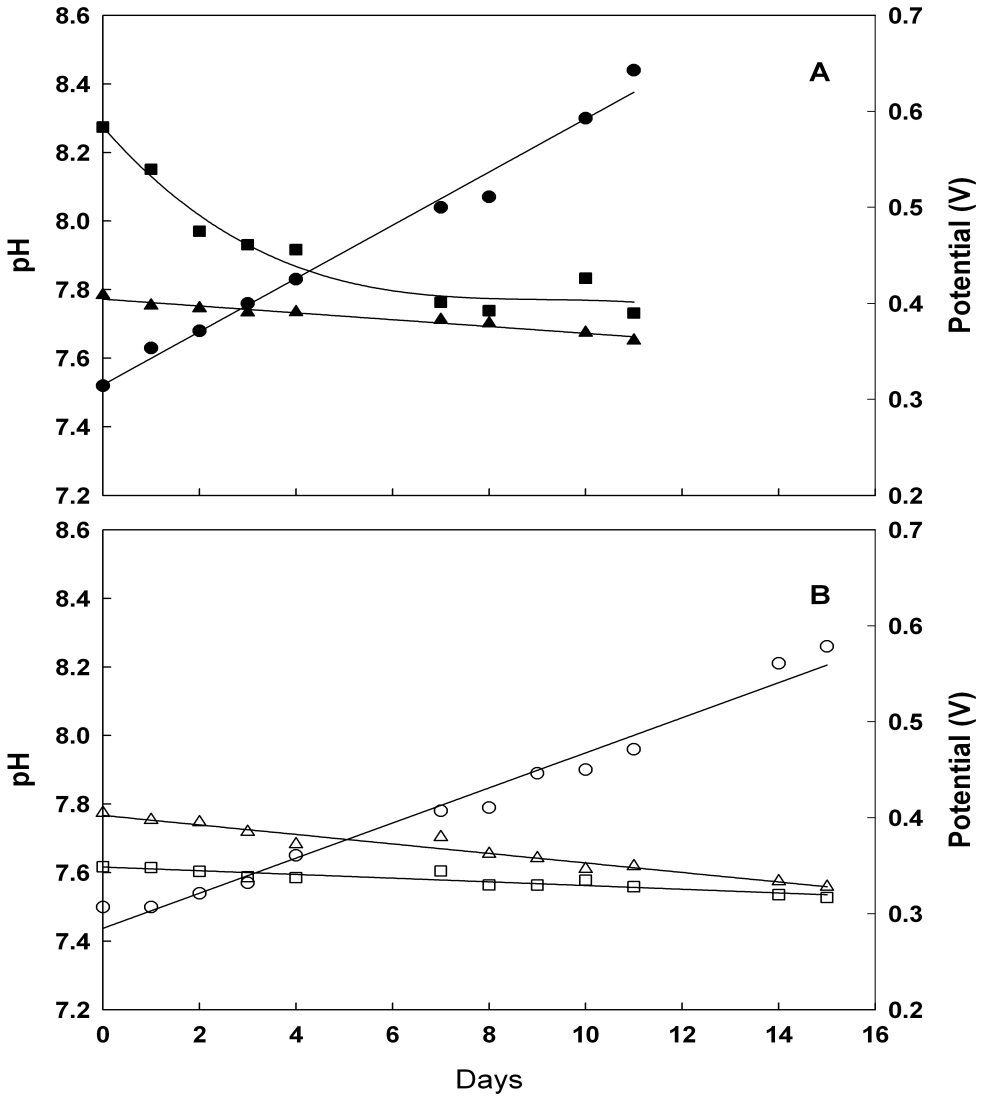

Figure 4-3. pH Trends, Cathode Potentials, and Overall Cell Potentials with Nonreplenished Phosphate Buffered Catholyte. (A) AEM data for experiment C represented with solid symbols; and (B) CEM data for experiment H represented with hollow symbols. Squares (■ AEM; □ CEM) indicate the overall potential across the fuel cell, triangles (▲ AEM; △ CEM) indicate the cathode potential, and circles (● AEM; ○, CEM) the catholyte pH.

The pH increase from 7.5 to 8.2 in the nonreplenished cathode greatly influenced the equilibrium of monovalent ($H_2PO_4^-$) and divalent (HPO_4^{2-}) phosphate ions (the monovalent/divalent ratio decreased from 0.35 to 0.07 based on the acid/base equilibrium). The resulting increase in the concentration of divalent phosphate ions coincided with the rapid decrease in the MFC potential with AEM. This indicates increasing resistance losses with the membrane transfer of divalent anions compared to monovalent anions because of the larger radius of the divalent phosphate ions in comparison to the monovalent. The number of tightly bounded water molecules that move with the ion as it diffuses is 1.91 and 3.95 for the monovalent and divalent phosphate ions, respectively, resulting in equivalent hydrated sphere radius of 3.02 and 3.27 Å.[28] This observation is supported by Rozendal et al.[12], who measured cation transport across a Nafion 117 membrane to maintain electroneutrality, and also found that the monovalent cations (Na^+, K^+, and NH_4^+) transferred more readily than the divalent cations (Ca^{2+} and Mg^{2+}). This selectivity of monovalent versus divalent ions reflects the differences in equivalent hydration radius of these ions.[28] For the CEM, cation transport from the anode to cathode is required to maintain fuel cell electroneutrality. Whereas the nonreplenished cathode had a changing pH, the anode, which was replenished, had a stable pH in these experiments. Thus, the monovalent to divalent cation equilibrium for the anolyte in the UMFC with CEM ion transport was constant because the anode chamber was continuously replenished, resulting in an overall cell potential decrease that closely matched the decrease in the cathode potential (Fig. 4-3).

Wastewater Treatment

The COD removal rates with UMFC treatment were high (93.1 – 97.7%) regardless of cathode pressure, type of membrane, or the presence/absence of a membrane (Table 4-2). Relatively low coulombic efficiencies (3.6 – 8.6% in Table 4-1) indicate that electricigens were not the primary COD consuming microbes in the UMFC. Instead, methanogens were the primary COD removing microbes indicated by a methane content of 70% in the off gas from the anode chamber. Other factors that contributed to the high COD removals were the presence of facultative anaerobes utilizing the oxygen that diffused through the ion exchange membranes at higher cathode air pressures, and the accumulation of biomass due to cellular growth. As anticipated, coulombic efficiencies positively correlated with power densities and MFC potential at 100 Ω of external resistance (Table 4-1). The relatively low coulombic efficiencies indicate that this work was performed with a nonoptimized MFC for research purposes. This design was chosen because the membrane had to be replaced or removed without disturbing the anode. Similar relative increases in overall power densities are anticipated with a more optimized design, and for example an anticipated potential increase from 0.4 to 0.5 V at 10-Ω resistance will increase the power density by 25% based on Ohm's Law. However, many questions remain for future MFC research before implementation as a wastewater treatment device: Are the gains in MFC power densities economical considering the energy required to pressurize air? What is the optimum cathode pressure? Are there effective cathode and anode pressure balancing designs that will enable the benefits of higher cathode air pressures while minimizing the negative effects of oxygen diffusion? Can catholyte composition and ion gradients be designed to minimize ohmic resistance?

The knowledge gained from this study, and addressing the above questions, will help advance MFC design, potentially leading to more sustainable wastewater treatment processes.

Acknowledgements

The financial support for this work was provided through a specific collaborative agreement between Washington University in St. Louis and the Fermentation Biotechnology Research Unit, USDA, Agricultural Research Service, Peoria, Illinois and the National Science Foundation through grant no. 0645021. We thank Sarah Dryden and anonymous reviewers for critically evaluating the manuscript.

Experiment	Cathode Air Pressure (kPa)	Exchange Membrane	OCP (mV)[1]	Maximum Power Density (W/m^3)[1]	Maximum Current Density (A/m^3)[1]	Potential @100Ω (mV)[1]	Coulombic Efficiency (%)[2]
A	34.48	AEM	913 (2)	6.43 (1.17)	12.34 (1.15)	518 (48)	7.9
B	17.24	AEM	931 (9)	7.29 (0.93)	13.16 (0.83)	553 (35)	8.6
D	Atm	AEM	925 (6)	4.29 (0.77)	10.07 (0.89)	423 (37)	6.8
F	34.48	CEM	737 (9)	3.18 (0.06)	8.70 (0.08)	366 (3)	5.4
G	17.24	CEM	790 (12)	3.49 (0.12)	9.12 (0.13)	383 (7)	6.3
E	Atm	CEM	780 (6)	2.58 (0.12)	7.83 (0.18)	329 (8)	3.6
I	Atm	CEM-NC[3]	816 (11)	3.09 (0.17)	8.57 (0.11)	360 (10)	6.5
J	Atm	CEM-AC[4]	795 (2)	2.27 (0.18)	7.35 (0.29)	309 (12)	3.8
K	Atm	None	70 (13)	0.01	0.37 (0.03)	23 (1)	0.2

[1] Single standard deviations noted in parenthesis.
[2] Coulombic efficiency calculated with average maximum current density and average COD removal data.
[3] NC – Nafion coated cathode electrode
[4] AC – Anolyte to cathode configuration

Table 4-1. UMFC Electrical Performance Data

Experiment	Cathode Air Pressure (kPa)	Exchange Membrane	% COD Removal[1]	Effluent VFA (mg/l)[1]	cm^3 Gas/mg COD Feed	Effluent Gas Composition $\%CH_4$ / $\%CO_2$	
A	34.48	AEM	93.7 (0.7)	38.5 (8.1)	0.109	NA	
B	17.24	AEM	95.2 (0.8)	73.9 (3.2)	0.085	NA	
D	Atm	AEM	93.6 (3.0)	48.5 (14.2)	0.091	NA	
F	34.48	CEM	97.6 (0.7)	50.4 (26.3)	0.147	77.2 / 8.6	
G	17.24	CEM	93.1 (6.3)	46.9 (0.0)	0.172	71.6 / 8.8	
E	Atm	CEM	96.4 (13.8)	55.3(23.8)	0.097	73.1 / 8.0	
I	Atm	CEM-NC[2]	NA	47.9 (21.2)	0.013	73.0 / 8.0	
J	Atm	CEM-AC[3]	97.7 (1.8)	18.7 (7.5)	0.008	70.7 / 7.5	
K	Atm	None	93.8 (2.7)	25.4 (11.9)	0.001	NA	

[1] Single standard deviations noted in parenthesis.
[2] NC – Nafion coated cathode electrode
[3] AC – Anolyte to cathode configuration

Table 4-2. UMFC Wastewater Treatment Data

References:

(1) Burton, F. L., Water and wastewater industries: Characteristics and energy management opportunities, Electric Power Research Institute, Inc. (EPRI), Community Environmental Center, 1996.

(2) Logan, B. E., Biologically extracting energy from wastewater: Biohydrogen production and microbial fuel cells. *Environ. Sci. Technol.* 2004, *38*, 160A-167A.

(3) Liu, H.; Logan, B. E., Electricity generation using an air-cathode single chamber microbial fuel cell in the presence and absence of a proton exchange membrane. *Environ. Sci. Technol.* 2004, *38*, 4040-4046.

(4) Rabaey, K.; Lissens, G.; Siciliano, S. D.; Verstraete, W., A microbial fuel cell capable of converting glucose to electricity at high rate and efficiency. *Biotechnol. Lett.* 2003, *25*, 1531-1535.

(5) Rabaey, K.; Verstraete, W., Microbial fuel cells: Novel biotechnology for energy generation. *Trends Biotechnol.* 2005, *23*, 291-298.

(6) Clauwaert, P.; Van der Ha, D.; Boon, N.; Verbeken, K.; Verhaege, M.; Rabaey, K.; Verstraete, W., Open air biocathode enables effective electricity generation with microbial fuel cells. *Environ. Sci. Technol.* 2007, *41*, 7564-7569.

(7) Rabaey, K.; Clauwaert, P.; Aelterman, P.; Verstraete, W., Tubular microbial fuel cells for efficient electricity generation. *Environ. Sci. Technol.* 2005, *39*, 8077-8082.

(8) Logan, B. E.; Cheng, S.; Watson, V.; Estadt, G., Graphite fiber brush anodes for increased power production in air-cathode microbial fuel cells. *Environ. Sci. Technol.* 2007, *41*, 3341-3346.

(9) He, Z.; Wagner, N.; Minteer, S. D.; Angenent, L. T., The upflow microbial fuel cell with an interior cathode: Assessment of the internal resistance by impedance spectroscopy. *Environ. Sci. Technol.* 2006, *40*, 5212-5217.

(10) Zhao, F.; Harnisch, F.; Schröder, U.; Scholz, F.; Bogdanoff, P.; Hermann, I., Challenges and constraints of using oxygen cathodes in microbial fuel cells. *Environ. Sci. Technol.* 2006, *40*, 5193-5199.

(11) Harnisch, F.; Schröder, U.; Scholz, F., The suitability of monopolar and bipolar ion exchange membranes as separators for biological fuel cells. *Environ. Sci. Technol.* 2008, *42*, 1740-1746.

(12) Rozendal, R. A.; Hamelers, H. V. M.; Buisman, C. J. N., Effects of membrane cation transport on pH and microbial fuel cell performance. *Environ. Sci. Technol.* 2006, *40*, 5206-5211.

(13) Min, B.; Kim, J.; Oh, S.; Regan, J. M.; Logan, B. E., Electricity generation from swine wastewater using microbial fuel cells. *Water Res.* 2005, *39*, 4961-4968.

(14) Liu, H.; Ramnarayanan, R.; Logan, B. E., Production of electricity during wastewater treatment using a single chamber microbial fuel cell. *Environ. Sci. Technol.* 2004, *38*, 228-235.

(15) Feng, Y.; Wang, X.; Logan, B. E.; Lee, H., Brewery wastewater treatment using air-cathode microbial fuel cells. *Appl. Microbiol. Biotechnol.* 2008, *78*, 873-880.

(16) He, Z.; Angenent, L. T., Application of bacterial biocathodes in microbial fuel cells. *Electroanalysis.* 2006, *18*, 2009-2015.

(17) Rozendal, R. A.; Jeremiasse, A. W.; Hamelers, H. V.; Buisman, C. J., Hydrogen production with a microbial biocathode. *Environ. Sci. Technol.* 2008, *42*, 629-634.

(18) Larminie, J.; Dicks, A., *Fuel Cell Systems Explained*; 2nd ed.; John Wiley & Sons, Ltd.: Chichester, West Sussex, England, 2003.

(19) He, Z.; Minteer, S. D.; Angenent, L. T., Electricity generation from artificial wastewater with an upflow microbial fuel cell. *Environ. Sci. Technol.* 2005, *39*, 5262-5267.

(20) Gharibi, H.; Mirzaie, R. A.; Shams, E.; Zhiani, M.; Khairmand, M., Preparation of platinum electrocatalysts using carbon supports for oxygen reduction at a gas-diffusion electrode. *J. Power Sources.* 2005, *139*, 61-66.

(21) Wood, E. J. F., *Marine Microbial Ecology*; Reinhold Publishing Company: New York, NY, 1965.

(22) Angenent, L. T.; Sung, S., Development of anaerobic migrating blanket reactor (AMBR), a novel anaerobic treatment system. *Water Res.* 2001, *35*, 1739-1747.

(23) Zehnder, A. J. B.; Huser, B. A.; Brock, T. D.; Wuhrmann, K., Characterization of an acetate-decarboxylating, non-hydrogen-oxidizing methane bacterium. *Arch. Microbiol.* 1980, *124*, 1-11.

(24) Liang, P.; Huang, X.; Fan, M. Z.; Cao, X. X.; Wang, C., Composition and distribution of internal resistance in three types of microbial fuel cells. *Appl. Microbiol. Biotechnol.* 2007, *77*, 551-558.

(25) Clesceri, L. S.; Greenberg, A. E.; Eaton, A. D., *Standard Methods for the Examination of Water and Wastewater*; 20th ed,; American Public Health Association: Washington, D. C., 1998.

(26) He, Z.; Shao, H.; Angenent, L. T., Increased power production from a sediment microbial fuel cell with a rotating cathode. *Biosens. Bioelectron.* 2007, *22*, 3252-3255.

(27) Kim, J. R.; Cheng, S.; Oh, S. E.; Logan, B. E., Power generation using different cation, anion, and ultrafiltration membranes in microbial fuel cells. *Environ. Sci. Technol.* 2007, *41*, 1004-1009.

(28) Kiriukhin, M. Y.; Collins, K. D., Dynamic hydration numbers for biologically important ions. *Biophys. Chem.* 2002, *99*, 155-168.

Chapter 5

Carbon Dioxide Addition to Microbial Fuel Cell Cathodes Maintains Sustainable Catholyte pH and Improves Anolyte pH, Alkalinity, and Conductivity

Fornero J. J., Rosenbaum M., Cotta M. A., and Angenent L. T., Carbon Dioxide Addition to Microbial Fuel Cell Cathodes Maintains Sustainable Catholyte pH and Improves Anolyte pH, Alkalinity, and Conductivity. In preparation for *Environmental Science and Technology*.

Abstract

Anode to cathode pH imbalances significantly contribute to potential losses in bioelectrochemical systems (BES). Our objective was to determine if adding carbon dioxide (CO_2) gas to cathode water would create a CO_2/bicarbonate buffered catholyte, which could maintain a stable microbial fuel cell (MFC) catholyte pH and, with the migration of bicarbonate ions, increase the anolyte pH, alkalinity, and conductivity. By adding CO_2 to the MFC catholyte we sustained steady catholyte conditions (pH = 5.94 ± 0.02) over a two week period. Because bicarbonate ions are the dominant catholyte ion species (pH = ~ 5.9), an anion exchange membrane (AEM) was selected to promote

bicarbonate ion migration to maintain MFC electroneutrality. With steady state operating conditions, the bicarbonate ion migration increased the anolyte pH (6.57 to 6.96, ΔpH = 0.39 ± 0.31), total alkalinity (494 ± 6 to 582 ± 6 as mg $CaCO_3$/L), and conductivity (1.53 ± 0.49 to 2.16 ± 0.03 mS), relative to the feed properties. Our results show that with a CO_2/bicarbonate buffered catholyte and AEM, we could control the MFC catholyte pH to reduce the pH imbalance and increase the anolyte pH, total alkalinity, and conductivity. These are favorable qualities for decreasing BES potential losses and increasing power densities. Results also demonstrate ion migration as the rate limiting step in achieving higher power densities for this system.

In addition, we compared the performance of a catholyte-cathode to an air-cathode using two identical MFCs. Catholyte-cathode MFC maximum power densities were higher than the air-cathode, with the aqueous catholyte plus CO_2 addition (4.31± 0.26 W/m^3) or 0.1 M phosphate buffer catholyte (pH = 6.46) (5.76 ± 0.52 W/m^3) MFCs being greater than the air/CO_2 mixture (2.53 ± 0.23 W/m^3) or air-only configuration (1.03 ± 0.16 W/m^3) MFCs.

Introduction

Bioelectrochemical system (BES) technology holds promise to produce environmentally benign and sustainable energy, replace energy intensive processes, and produce chemical products.[1-7] A BES can be configured as a microbial fuel cell (MFC) or as a microbial electrolysis cell (MEC) by adding an externally applied potential.[8-10] With either configuration, the microbial oxidation of organic substrates supplies electrons to the anode electrode. These electrons travel via an external circuit from the anode to

the cathode electrode to participate in a reduction reaction.[3,4,6,11] Concurrent with the flow of electrons is the flow of ions across the ion exchange membrane, which is required to maintain BES electroneutrality.

Because the BES ion flux is composed of cations or anions other than protons or hydroxide ions (dependent upon ion exchange membrane selection), pH imbalances between the cathode and anode are to be anticipated.[12-16] For a BES with an oxygen reduction reaction (ORR) cathode and AEM, the initial catholyte hydroxide ion concentration will typically be much lower than the anion concentration. Thus, anions other than the hydroxide ions will mediate the BES charge balance, which causes the catholyte pH to increase because of hydroxide ion generation by the ORR. The catholyte pH will continue to increase, likewise increasing the BES pH imbalance, until the catholyte hydroxide ion concentration is sufficient (pH > ~ 11) to contribute toward electroneutrality maintenance or a buffer replenishment is provided. Since pH imbalances result in a 59 mV/pH loss in the BES cell potential, minimizing pH imbalances is required for maximizing BES power densities. Strategies used to reduce BES pH imbalances include membrane selection, catholyte buffers, and cathode product generation.[7,12,14-17] Membrane selection strategies attempt to favorably influence the transport of protons and hydroxide ions to minimize the pH imbalance. As shown, however, protons and hydroxide ions are typically to low in concentration to mediate electroneutrality. Buffer selection strategies moderate pH imbalances by stabilizing the catholyte pH. While buffers can moderate pH increases in the short term, longer duration operations require a buffer replenishment strategy. Ions from buffer chemical additions can also participate in BES electroneutrality maintenance, as occurs when phosphate

buffers are used in combination with an AEM.[18] The cathode to anode phosphate ion migration not only reduces the buffer concentration, but also affects anolyte properties. A product generation strategy exploits the pH imbalance by generating products, such as sodium hydroxide in the cathode.[2] In this case, the BES pH imbalance potential loss remains, but may be compensated for by an applied potential.

Air-cathode MFCs are equally susceptible to pH imbalance potential losses as compared to catholyte-cathode MFCs. Given the relatively small liquid volumes permeating across the membrane, pH imbalances may even become more prominent than catholyte MFCs.[19] To mitigate a pH imbalance, Torres et al. performed a ground-breaking air-cathode MFC study with an AEM and demonstrated the concept of adding carbon dioxide (CO_2) to the cathode influent air.[20] The addition of CO_2 to the catholyte produced carbonate species (CO_3^{2-} and HCO_3^-), which acted as the required ions to maintain electroneutrality because these carbonate species became the highest concentration anions in the catholyte. And since the carbonate species acted as hydroxide ion carriers, the carbonates effectively increased the cathode to anode hydroxide ion flux, thereby, reducing the cathode pH and MFC pH imbalance and increasing the power density. However, the cathode pH level remained much higher than the anolyte pH (7.3 – 7.5) because Torres et al. found CO_3^{2-} to be the primary hydroxide ion carrier, which based on the carbonate species equilibrium estimates the pH to be > 10.5 (pH of air-cathode liquid layer not reported).[21] The authors identified that the slow rate of CO_2 absorbtion into the catholyte as a limitation for using carbonate species as hydroxide ion carriers.[20]

Under conditions of sufficient CO_2 absorbtion, we calculated with carbonate equilibrium calculations that the catholyte pH could theoretically be maintained between pH 3.92 and 5.63 (Details in Chapter 3). At these pH levels and an AEM, bicarbonate would be the dominant catholyte anion to maintain electroneutrality. Moreover, if the cathode pH could be maintained below the anode pH, we could reduce the pH imbalance and increase the ORR potential and, therefore, increase the MFC power density. Thus, we hypothesized that a CO_2/bicarbonate buffered catholyte would improve MFC performance in comparison to the CO_2/carbonate buffered catholyte system described by Torres et al. Our objective was, therefore, to determine if by adding carbon dioxide (CO_2) to an aqueous catholyte with an engineering system to provide sufficient CO_2 absorbtion, we would create a CO_2/bicarbonate buffered catholyte system, which could sustainably prevent the formation of an anode to cathode pH imbalance. Further, by maintaining electroneutrality with bicarbonate ions, we anticipated that we would increase the anolyte pH, alkalinity, and conductivity, which are favorable BES qualities for decreasing potential losses, increasing power densities, and improving wastewater treatment. We also wanted to determine the rate limiting step in achieving higher power densities. To test our hypothesis, we used two identical ten-liter MFCs with AEMs; one operated as a catholyte-cathode and the other as an air-cathode. The catholyte-cathode MFC was filled with aqueous catholyte, while the air-cathode MFC only had a small volume of water that permeated from the anolyte. The MFC cathodes were supplied with equivalent volumetric air rates. We circulated the catholyte for the catholyte-cathode MFC continuously to the carbon dioxide contactor column and back (MFC-CC). To compare our system with a conventional system, we also operated the catholyte-cathode

MFC with a phosphate buffer (MFC-CP). The air-cathode MFC was operated in an air/CO_2 (MFC-AC) and air-only (MFC-AO) configuration.

Materials and Methods

Experimental Setup

Two identically constructed tubular MFCs were fabricated for the study (fabrication photos available, Fig. C1 A-H). Each MFC consisted of an inner cathode and an outer anode chamber separated by a 100 cm long x 5 cm diameter tubular AEM (1,570 cm^2 total, 1,453 cm^2 net surface area accounting for the seam) (Material - AMI-7001, Membranes International, Glen Rock, NJ) (Tubular fabrication, Arelco, Prospet, KY). The aerobic cathode chamber (100 cm long x 5 cm diameter) (1,962 cm^3 total; 1,640 cm^3 net cathode volume) and anode chamber (110 cm long x 5 cm inner diameter [ID] x 11 cm outer diameter [OD]) (8,486 cm^3 total; 5,800 cm^3 net anode volume) were contained within a clear polyvinyl chloride pipe. The cathode electrode consisted of a 100 cm x 30 cm graphitized carbon fabric cloth (0.3 m^2 total surface area) (Panex 30 SWB8, Zoltek, St. Louis, MO), which was tightly wrapped, two layers thick, around a 3.7 cm OD rigid polypropylene filtration tube (40% void area, Industrial Netting, Minneapolis, MN.) The cathode electrode was coated with a suspension of 5% platinum (Pt) on activated carbon powder (Acros Organics, Morris Plains, NJ) and Nafion® 117 Solution (5% solution, Fluka Analytical, Sigma Aldrich, St. Louis, MO). The Pt suspension was prepared and manually brushed onto the cathode cloth in 10 cm incremental lengths along the cathode electrode to assure an even Pt distribution (3.33 g Pt/m^2). The anode electrode consisted of a 100 cm x 50 cm graphitized carbon fabric cloth (0.5 m^2 total surface area) tightly

wrapped, two layers thick, around a 6.2 cm OD rigid polypropylene filtration tube (46% void area). The anode electrode was autoclaved prior to use to improve wettability. The cathode and anode carbon fabric cloths were in intimate contact with two 120 cm x 1.5 cm x 0.2 cm graphite foil strips (McMaster Carr, Elmhurst, IL.) located on opposing sides of the filtration tube, which served as the current collectors. The cathode and anode assemblies were fabricated to allow for longitudinal AEM tube swelling (4%) upon exposure to water.

The catholyte-cathode MFC used reverse osmosis (RO) water as a catholyte and had an independent catholyte circulation system (Fig. 3-3) (Fig. C2, Appendix C). Air was injected into the catholyte before introduction into the MFC cathode. Upon exiting the top of the MFC, the catholyte entered a small gas break vessel, which was open to the atmosphere to separate the air from the catholyte. The catholyte then gravity flowed to a clear polyvinyl chloride carbon dioxide contactor column (75 cm long x 6 cm ID) filled with high surface area packing (Fig. C3, Appendix C). Within the carbon dioxide contactor column, the catholyte was exposed to 100% CO_2 gas. Upon exiting the carbon dioxide contact column, the catholyte flowed through another small gas break vessel for CO_2 degassing before returning to the catholyte circulation pump. The air-cathode MFC was supplied with humidified air. A drain line and flask at the bottom of the air-cathode MFC was used to collect permeate water.

Feed to the MFC anodes was distributed via six nozzles (per MFC), evenly spaced and placed on alternating opposing sides along the vertical length of the MFCs (Fig. C2, Appendix C). Each MFC had an independent anolyte recirculation line, which entered the anode chambers independently at the lowest side nozzle and exits from a nozzle on

top of the MFCs. The MFC effluent flowed independently through gas breaks to separate the biogas for measurement prior to anolyte discharge to a sewer drain. Anodic biogas production was measured with a gas meter (Ritter MGC-1 Milligas Counter, Bochum, Germany) and gas composition samples were taken through a septum placed in the anode effluent tubing. The external resistance was applied with resistor boxes (Ohmite Ohm-Ranger, Skokie, IL)

Operation

The anolyte inoculum was a homogenized granular sludge from an upflow anaerobic bioreactor at a brewery (Anheuser Busch-Inbev, Inc., St. Louis, MO). The MFCs were fed an acetate synthetic wastewater with a ~ 480 mg/L total chemical oxygen demand (TCOD) concentration and a continuous flow rate of ~ 12.7 L/day. The anode hydraulic retention time (HRT) was ~ 11 h. A mechanical agitator (Model 5vb, EMI Inc.; Clinton, CT) was used to slowly mix the feed container. The blended synthetic wastewater consisted of (per liter of deionized water) (all chemicals unless noted, Sigma Aldrich, St. Louis, MO.): glacial acetic acid, 0.268 ml; 4 M sodium hydroxide, 0.265 ml; yeast extract (Difco Laboratories, Inc., Detroit, MI), 0.025 g; NH_4Cl, 0.03 g; K_2SO_4, 0.006 g; $FeCl_2$•4 H_2O, 0.033 g; K_2HPO_4, 0.033 g; $NaHCO_3$, 1.0 g; iron citrate, 0.011 g; NaCl, 0.25 g; KCl, 0.1 g; $CaCl_2$, 0.1 g; $MgCl_2$•6 H_2O, 0.1 g; and trace elements, 1.0 ml modified from.[18,22] Anolyte recirculation was maintained at a constant rate (58 ± 0.3 L/day-MFC) for each MFC throughout the study. Air and carbon dioxide pumps were used for the purpose of measuring and controlling the gas flows. Peristaltic pumps were used for all pumping applications (Cole Parmer, Vernon Hills, IL). During steady-state operating periods, the

air-cathode and catholyte-cathode MFCs were operated with an external resistance of 20 Ω (MFC-AO), 10 Ω (MFC-AC), and 6 Ω (MFC-CC and MFC-CP). The air-cathode MFC cathode chamber was flushed with RO water on a weekly basis to prevent the formation of salt deposits. Flush water pH was monitored. The anode temperature was maintained at room temperature (~ 23°C).

Analyses

The potential (*E*) across a resistor (*R*) was measured using a digital multimeter (2700 + 7700 multiplexer, Keithley Instruments, Inc., Cleveland, OH). The current density was calculated as $I = E/RV$ and the power density was calculated as $P = E^2/RV$, where V is the net liquid volume of the cathode and anode chambers. Polarization curves were developed by changing the external resistance stepwise from 11 MΩ to 0 Ω over a seven hour duration. Thirty minute intervals were used between resistance changes for data points adjacent to the maximum MFC power. The internal resistance correlates to the maximum power density found during polarization tests. TCOD, soluble COD (SCOD) (closed-reflux titrimetric method), total alkalinity (TALK) (endpoint pH titration), and volatile fatty acids (VFA) (distillation method), were measured according to procedures described in *Standard Methods*.[23] Conductivity measurements were taken with a conductivity electrode (MI-900, Microelectrodes, Inc., Bedford, NH). Methane and carbon dioxide gas analysis was performed with a gas chromatograph (Gow-Mac Model 69-350, 6' x 1/8" o.d. 80/100 Hayesep Q. mesh Supelco column, Bethlehem, PA). pH is measured with a hand-held meter (Oakton pH 6, Vernon Hills, IL.) Sodium, potassium, and phosphorous were measured using inductively coupled plasma-mass spectrometry

(ICP-MS, Agilent Technologies 7500ce, Santa Clara, CA.). All analyses were performed in triplicate with the exception of the biogas production and pH for which daily measurements were recorded.

Coulombic efficiencies (CE) were calculated according to [18]. Feed and operating conditions, with the exception of polarization tests, were held constant during the steady state testing periods. Equations referred to, include the charge balance

$$\sum_i z_i c_i = 0 \quad (1)$$

and the Nernst-Planck Equation,

$$N_i = -z_i u_i F c_i \nabla\Phi - D_i \nabla c_i + c_i v \quad (2)$$

where, N_i = Flux of species i (mol/s-cm^2)

z_i = Charge of ion i (charge number)

u_i = ion mobility (cm^2-mol/J-s)

F = Faradays Constant 96,485 C/equiv

c_i = Concentration of species i (mol/cm^3)

$\nabla\Phi$ = Potential gradient (V)

D_i = Diffusivity of species i (cm^2/s)

v = bulk fluid velocity (cm/s)

The ion migration flux described by the Nernst Plank equation has three terms; i) ion migration resulting from an electric field, ii) ion diffusion from a concentration gradient, and iii) ion convection from a pressure gradient.[24] pH imbalance potential losses were calculated by calculating the absolute difference between the anode and cathode pH and multiplying by 59 mV/pH.

Experimental Design

Both MFCs were in continuous operation for 10 weeks prior to data gathering to ensure a well developed anodic bacterial community and stable performance. The total operating period for both systems was 20 weeks. The study evaluated the catholyte-cathode MFC performance with an aqueous catholyte in contact with CO_2 (MFC-CC) and 0.1 M phosphate buffer catholyte (pH = 6.46 ± 0.03) (MFC-CP). The air-cathode MFC with an air/CO_2 mixture (MFC-AC) and air-only (MFC-AO) configurations were also evaluated. Experimental data was compared and contrasted for the above operating configurations.

Results and Discussion

Adding CO_2 to aqueous catholyte with AEM maintains stable catholyte pH. Contacting CO_2 gas with a water catholyte enabled a CO_2/bicarbonate buffer replenishment strategy, which resulted in MFC-CC operating with a steady catholyte pH (5.94 ± .02) over the duration of a two week data gathering period (Table 5-1). To maintain the steady pH, daily water replenishments (<3% of catholyte volume) were necessary to counter the catholyte pH increase resulting from anolyte to catholyte cation transport (discussed in next section) and replace evaporation losses. We, thus, showed that the CO_2 dissolution limitation can be simply overcome and that the reduction in catholyte pH yields a superior buffer system than Torres et al.[20] The basis for the stable catholyte pH begins with a consideration of the anolyte and catholyte reaction stoichiometry, and MFC electroneutrality ($\sum_i z_i c_i = 0$) (Fig. 3-2). Because the MFC-CC catholyte consists of water, just exposed to air and CO_2 gas (for now neglecting anolyte to catholyte ion diffusion), the only anions available for electroneutrality maintenance are

hydroxide ions (water dissociation), carbonate ions, or bicarbonate ions (CO_2 absorbtion, hydration, and dissociation). Because BES electroneutrality is mediated by the ions in the highest concentrations, bicarbonate ions will maintain electroneutrality since $[HCO_3^-] >> [CO_3^{-2}]$ and $[HCO_3^-] >> [OH^-]$ at acidic pH values (pH = 5.94 ± 0.02).[25] (Details in Chapter 3).

The catholyte pH remains stable so long as equilibrium conditions are maintained ($[H+] = 1.15 \times 10^{-6}$, $[HCO_3^-] = 8.0 \times 10^{-3}$). Within the MFC-CC cathode chamber oxygen reduction reaction (ORR) ($2O_2 + 4H_2O + 8e^- \rightarrow 8OH^-$), eight electrons received from the anode, and four water molecules plus two oxygen molecules from the catholyte, react to reduce oxygen to eight hydroxide ions (per mol acetate) (Fig. 3-2). Because eight hydroxide ions are produced, the catholyte hydroxide ion concentration increases. To maintain electroneutrality with the anode electron transfer, eight bicarbonate ions migrate from the cathode to anode. The catholyte exiting the cathode chamber, therefore, has a higher hydroxide ion and lower bicarbonate ion concentration than the catholyte entering the cathode. The catholyte however, is not static; it is circulated between the cathode chamber (~ 8 min. HRT) and carbon dioxide contact column. Within the carbon dioxide contact column, the catholyte is exposed to 100% CO_2 gas while passing over a high surface area packing. The 100% CO_2 gas and packing are designed to promote higher gas/liquid transfer rates to ensure sufficient CO_2 absorption. Thus, the catholyte absorbs eight CO_2 molecules, which hydrate and react with the eight hydroxide ions to produce eight bicarbonate ions as a reaction product ($8H_2CO_3 + 8OH- \rightarrow 8\ HCO_3^-$). Thus, the cathode hydroxide ion production is consumed and the bicarbonate ions lost to migration are replenished. Therefore, equilibrium is restored and the pH remains stable.

Cation transfer influences catholyte pH. Ion surveys of the catholyte identified that cations transferred from the anolyte to catholyte, which influenced the MFC-CC catholyte pH. Upon MFC-CC start-up with RO water, the catholyte pH at start-up (~ 5.0) increased at a rate of ~ 0.03 pH/day over the first 32 days of operation to pH ~ 5.9 (Fig. C4, Appendix C). During this period, polarization and catholyte ion concentration tests were performed at catholyte pH = 5.25. A comparison of MFC-CC polarization curves at pH = 5.25 and 5.94 shows a prominent mass transport resistance at higher current densities for the pH = 5.25 test, whereas the pH = 5.94 polarization test does not indicate notable mass transport losses (Fig C5). The catholyte cation concentration test indicated the cation concentration at pH = 5.25 (Na^+ = 0.56 mg/L, K^+ = 0.13 mg/L) was ~ 65 % less than the cation concentration at pH = 5.94 (Na^+ = 1.61 ± 0.04 mg/L, K^+ = 0.40 ± 0.04 mg/L) (Table 5-2), which indicates an increase of the cation concentration with time. Lastly, water replenishments to maintain pH ~5.94 were necessary to stabilize the pH and maximize the MFC potential because the cell potential decreased for pH > 5.95.

To explain this data, we considered three possibilities. The first was that the O_2/bicarbonate buffering could not maintain a stable catholyte pH because the cathode hydroxide ion production rate was greater than the CO_2 hydration rate. A calculation of the rate of CO_2 hydration versus the rate of CO_2 consumption, however, indicated that the dissolution rate was much greater than the consumption rate (calculations in Chapter 3). Second, we speculated that the anode to cathode cation concentration gradient caused cation diffusion from the anode to cathode. While some diffusion likely occurred, significant cation diffusion across the AEM would be retarded because of the positive charge sites within the AEM and the anion migration moving in opposition to the cation

diffusion. Lastly, we hypothesized that cation "forcing" across the AEM may account for the cation transport. With catholyte pH = 5.25, the bicarbonate concentration was relatively low ($[HCO_3^-] = 6.6 \times 10^{-4}$). Thus, with higher MFC-CC current densities, the bicarbonate ion concentration was insufficient to support the anion electroneutrality migration from the cathode to the anode. Since the charge balance is a constraint, cations were "forced" from the anolyte to the catholyte, which raised the catholyte bicarbonate ion concentration (and pH) and enables more anion electromigration. This may explain the high mass transport resistance on the polarization plot at higher current densities (Fig C5). At pH = ~ 5.94, the bicarbonate ion concentration is sufficient to maintain electroneutrality ($[HCO_3^-] = 8.0 \times 10^{-3}$). If the bicarbonate ion concentration was increased above pH = 5.95, the decreasing ORR potential worked against maximizing the MFC power density. Thus for MFC-CC, pH = ~ 5.95 is the equilibrium pH that supports a bicarbonate ion concentration adequate for anion electromigration and a sufficient ORR performance for the maximum power density.

The cation addition (besides protons) to the catholyte affected the CO_2 solution chemistry because cations charge balance bicarbonate ions. Thus, an increase in the cation concentration results in an increase in the bicarbonate ion concentration, which increases the catholyte pH. The cation and bicarbonate ion charge balance also prevents bicarbonate ions from migrating across the membrane. Thus, to control the catholyte to a pH = ~ 5.95 target, regular water replenishments were used to replace evaporation losses and maintain a stable cation concentration via dilution. In fact, the catholyte cation concentration (equivalent sodium bicarbonate concentration) required to attain a specific pH can be predicted as shown by Roosen et al.[26] Thus, replenishment strategies could be

implemented to obtain and maintain a similar pH in the anode and cathode chambers to eliminate the 59 mV/pH potential loss.

Catholyte pH and MFC performance trade-offs. The catholyte pH in a CO_2/bicarbonate buffered water system is important because it affects the ORR potential, pH imbalance, catholyte conductivity (which affects ohmic losses), and anode to cathode ion concentration gradient. The MFC-CC catholyte pH (5.94 ± 0.02) was maintained below the anolyte pH (6.96 ± 0.37) to maximize the cell potential, rather than equilibrate the anolyte and catholyte pH. It is noteworthy that compared to anolyte/catholyte pH equivalence, "acidic" pH imbalance losses are offset by equivalent increases in the ORR potential, whereas "alkaline" pH imbalance potential losses also increase ORR potential losses.[27] Thus, lowering the catholyte pH relative to the anolyte pH improved the ORR potential (60 mV), but likewise increased the pH imbalance losses (60 mV). The lower catholyte pH also decreases the bicarbonate ion concentration, which has negative consequences for both the conductivity and diffusion driving forces of the ion flux (represented by the first and second terms of the Nernst-Planck equation, respectively). Thus, the pH strongly influences MFC performance with a CO_2/bicarbonate buffered catholyte and performance trade-offs are necessary when selecting the catholyte pH.

Anion migration increases anolyte pH, TALK, and conductivity. Under steady state operating conditions (current density = 10.657 ± 1.161 A/m^3 at 6Ω external resistance, feed rate = 12.7 ± 0.4 L/day), the MFC-CC anolyte pH (6.57 to 6.96, ΔpH = 0.39 ± 0.31), TALK (494 ± 6 to 582 ± 6 as mg $CaCO_3$/L), and conductivity (1.53 ± 0.49 to 2.16 ± 0.03 mS) all increased relative to the feed solution (Table 5-1, 5-2, and 5-3). The increases occurred despite the anolyte acetate oxidation reaction, which generates

more protons than bicarbonate ions (Fig. 3-2), and should, thus, normally decrease the pH and TALK. The catholyte to anolyte anion migration stabilized the pH and reversed the TALK decrease. Similar effects to the anolyte pH, TALK, and conductivity relative to the feed solution were also obtained for MFC-AO, MFC-AC, and MFC-CP during steady state operations (Table 5-1).

CO_2/Bicarbonate buffering improves BES wastewater treatment. The migration of bicarbonate ions to the anolyte is beneficial for BES wastewater treatment. First, during the anodic biocatalytic oxidation of organic substrates typically more protons than bicarbonate ions are produced. The proton generation decreases the anolyte pH and lowers the alkalinity, which can increase pH imbalance potential losses, or at an extreme, negatively affect the anode electrode microbial community.[28] Thus, increasing the anolyte pH and alkalinity with bicarbonate (HCO_3^- pKa = 6.3) can decrease the pH imbalance, increase the alkalinity, and help maintain a healthy microbial community. Increasing the wastewater alkalinity is also important for wastewater nitrification, which produces protons and consumes alkalinity. Second, as shown, bicarbonate ion migration increases the anolyte conductivity. Because some wastewaters have a high organic content and a low conductivity, MFC treatment is impaired because of a high anolyte ohmic resistance.[29,30] Increasing the anolyte conductivity decreases the ohmic resistance, which increases power densities. Furthermore, the addition of bicarbonate ions to wastewater (MFC-CC, AC) is compatible with wastewater treatment objectives, whereas phosphate additions (MFC-CP) may require subsequent removal to ensure compliance with effluent discharge permit specifications.

Ion transport is rate limiting step for MFC-CC. We have demonstrated what effects the catholyte pH has on the charge balance ion flux. The ion transport is also affected by the MFC architecture, anolyte properties, and membrane resistance.[12,13,15] Inspection of the Nernst-Planck equation indicates that the potential and ion concentration gradients affect the ion flux. And since electrode spacing affects the gradients, MFC architecture, which affects electrode spacing, affects the ion flux. The shorter the migration path of the charge balancing ions between electrodes, the larger the gradients, and the higher the ion flux. Although MFC-CC had a relatively low external resistance at the maximum power (4Ω), an ion transfer rate limitation is evidenced by comparing the MFC-CC cathode and anode potentials with an increasing current density (Fig. 5-1, upper right).

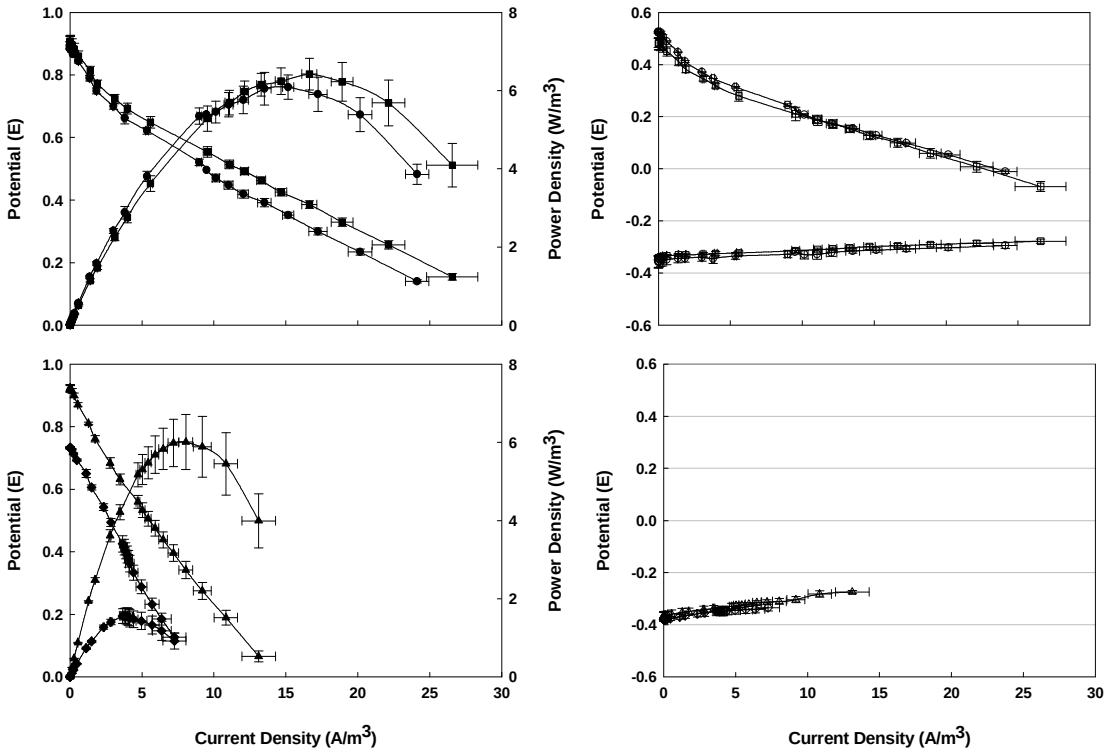

Figure 5-1. Catholyte-cathode (top left) and air-cathode MFC (bottom left) polarization and power plots. Catholyte-cathode MFC (top right) anode and cathode potentials versus the current density. –Air-cathode MFC (bottom right) anode potentials versus the current density. Cathode potential readings could not be obtained for the air-cathodes. Catholyte-cathode MFC symbols include squares for the CO_2/bicarbonate buffered water MFC (MFC-CC) and circles for the phosphate buffered MFC (MFC-CP). Air-cathode MFC symbols include triangles for the air/CO_2 mixture MFC (MFC-AC) and diamonds for the air-only MFC (MFC-AO). The top right plot shows the rapid reduction in the cathode potential indicating a rate limitation that can be attributed to the ion flux. -The top left polarization plot shows that the 0.l M phosphate catholyte-cathode MFC (MFC-CP, squares) power density was greater than the CO_2/bicarbonate MFC (MFC-CC, circles). The power increase is attributed to an increase in the solution conductivity and cathode to anode ion concentration gradient.

The cathode potential approaches zero potential at a much greater rate than the anode potential indicating the cathode is rate limiting. A cathode rate limitation can result from a decreased flow of reactants and products to and from the ORR reaction sites. A review of the polarization curve (Fig. 5-1, upper left) however, does not show prominent mass transfer losses at higher current densities. The cathode can also be rate limited by the ion flux. Since the charge balance requires that the ion flux equal the electron flux (charge equivalence), the electron flux is dependent on the ion flux because ions move much more slowly than electrons. If the ion transport is limited by the electrode spacing, the electron flow will likewise be limited. Thus, if the electron flux to the cathode ORR sites is limited, the ORR potential will decrease and decrease the MFC power density. Therefore, if the ion flux is limited because of MFC architecture and solution compositions (electrode spacing resulting in high ohmic losses), the current flow will be limited, and cathode ORR will be limited, and the power density will be limited.

Contributing to the MFC-CC bicarbonate ion transport limitation, was the i) relatively low bicarbonate ion concentration in the catholyte, which had a low conductivity (0.48 ± 0.34 mS), ii) bicarbonate ion migration moving counter to the bicarbonate ion diffusion (9.3 x 10^{-3} [anode] to 8.0 x 10^{-3} [cathode] M HCO_3^-/L), iii) bicarbonate ion migration moving counter to the phosphate ion diffusion (1.9 x 10^{-3} [anode] to 0 [cathode] mol PO_4^{3-}/L), and to a lesser extent iv) a lower potential gradient because of the pH imbalance (38 mV). For comparison with other studies and to understand the impact of the catholyte ionic species, ionic concentration, and pH, we decided to operate the catholyte-cathode MFC with a 0.1 M phosphate buffer (MFC-CP) with the pH (6.46 ± 0.03) designed closer to the anolyte pH (6.80 ± 0.39). The phosphate buffer increased the catholyte conductivity (8.43 ± 0.2 mS), created a cathode to anode phosphate ion concentration gradient (1.0 x 10^{-1} [cathode] to 1.9 x 10^{-3} [anode] M PO_4^{3-}/L), and reduced the pH imbalance potential loss to 20 mV. Steady state results show that the MFC-CP power density was 34% greater than MFC-CC (5.76 ± 0.52 versus 4.31 ± 0.26 W/m^3) (Table 5-2). The external resistance associated with the maximum power on the polarization curve, however, remained the same as for MFC-CC (4Ω) (Fig. 5-1, upper left). This data suggests that MFC architecture may have a more significant impact on the maximum power external resistance than just the ionic catholyte composition.

Catholyte-cathode power density higher than air-cathode. Catholyte-cathode MFC maximum power densities (and associated external resistance) were higher than the air-cathode, with MFC-CC (4.31± 0.26 W/m^3 [4 Ω]) or MFC-CP (5.76 ± 0.52 W/m^3 [4 Ω]) being greater than MFC-AC (79% air/21% carbon dioxide mixture) (2.53 ± 0.23 W/m^3 [8 Ω]) or MFC-AO (1.03 ± 0.16 W/m^3 [19 Ω]) (Table 5-2). The power density

differences can be attributed to the air-cathode MFC catholyte pH and cathode electrode/AEM spacing. Air-cathode catholyte pH measurements were taken on water that seeped from the anolyte to the cathode and was collected (< 10 ml/day). The MFC-AO catholyte pH value (9.0) was higher than MFC-AC (6.61 ± 0.12). This data indicates MFC-AO pH imbalance potential losses (100 mV) were greater than the MFC-AC losses (20 mV). The spacing between the cathode electrode and AEM also affected the power densities of the air-cathode MFC. Weekly air-cathode water flushes resulted in temporary cell potential increases while the cathode chamber was liquid full. Upon water evacuation, the cell potential would decrease to pre-wash levels (data not shown). This observation indicates that the air-cathode performance was limited by the lack of conductive catholyte between the cathode electrode and AEM. Less than complete catholyte filling of the cathode electrode/AEM void space results in highly inactive cathode surface areas, since the balancing ion transport would be greatly hindered because of ions migrating over a smaller catholyte volume, and more tortuous paths to reach the AEM. This leads to an increase in the ohmic resistance and decrease of the MFC cell potential.

Outlook. We have shown that by adding CO_2 to an aqueous catholyte and AEM, we could control and sustain the MFC catholyte pH to reduce the pH imbalance. This was accomplished by using a CO_2 contactor column with 100% CO_2 to increase the CO_2 partial pressure and high surface area packing to increase the gas/liquid transfer rate. By maintaining the catholyte pH just below the anolyte pH, the ORR potential was increased as anticipated. Promoting bicarbonate migration to the anolyte also increased the anolyte pH, total alkalinity, and conductivity, which are favorable for decreasing BES potential

losses, increasing power densities, and improving BES wastewater treatment. Results also demonstrate ion transport as the rate limiting step in achieving higher power densities. Thus, MFC designs with much higher ion fluxes (lower ohmic losses) are necessary to increase power densities. While MFC-CC had a 4Ω external resistance at the maximum power, we believe order of magnitude reductions in the resistance are necessary. One way to reduce the catholyte ohmic resistance is to increase the bicarbonate ion concentration, which can be done by pressurizing the cathode. Pressurization will increase both the oxygen and carbon dioxide partial pressures and thus increase the dissolved oxygen and bicarbonate ion concentrations. This could lead to improvements in cathode ORR potentials, improved solution conductivity, favorable ion concentration gradients, and convective flow from the cathode to anode.[18]

Acknowledgements

The financial support for this work was provided through a specific collaborative agreement between Largus T. Angenent and the Fermentation Biotechnology Research Unit, USDA, Agricultural Research Service, Peoria, Illinois and the National Science Foundation through grant no. 0645021. We thank Brian Wood of Arelco for the provision of the tubular membranes, Pat Harkins for his significant fabrication contributions, Dan Shannon of Zoltek for the provision of the carbon cloth, and Vipul Borkar for his lab support.

Supporting Information Available

Appendix C.

Table 5-1. Feed, Effluent, and Catholyte Properties

Feed and Effluent Parameters	Feed	MFC-AO	MFC-CC	Feed	MFC-AC	MFC-CP
Total COD (mg/L)	479 ± 28	424 ± 17	384 ± 45	474 ± 17	335 ± 53	254 ± 42
sCOD (mg/L)	487 ± 25	399 ± 26	388 ± 45	492 ± 9	334 ± 36	249 ± 42
% sCOD removal	NA	18 ± 2	20 ± 6	NA	32 ± 6	49 ± 8
pH	6.57 ± 0.18	7.3 ± 0.12	6.59 ± 0.16	6.54 ± 0.02	6.95 ± 0.49	6.8 ± 0.39
Total Alk (as mg $CaCO_3$/L)	494 ± 6	586 ± 8	582 ± 3	495 ± 8	591 ± 38	552 61
Conductivity (mS)	1.53 ± 0.49	2.15 ± 0.12	2.16 ± 0.03	1.67 ± 0.09	1.99 ± 0.07	1.91 0.04
VFA (as mg Acetic Acid/L)	284 ± 23	347 ± 64	292 ± 27	382 ± 74	276 ± 91	297 ± 127
Biogas Volume (cm^3/day)	NA	1	1	NA	NA	NA
Biogas Comp (%CH_4/%CO_2)	NA	70 / 13	71/11	NA	NA	NA
Catholyte Properties						
pH	NA	9.00	5.94 ± 0.02	NA	6.61 ± 0.12	6.46 ± 0.03
MFC-C Inlet pH	NA	NA	5.48 ± 0.07	NA	NA	NA
Total Alk (as mg $CaCO_3$/L)	NA	NA	400 ± 4	NA	NA	1198 ± 67
Conductivity (mS)	NA	NA	0.48 ± 0.34	NA	NA	8.43 ± 0.19
Ion Analysis - Sodium (mg/L)	NA	0.37	1.61 ± 0.04	NA	NA	NA
- Potassium (mg/L)	NA	0.11	0.4 ± 0.04	NA	NA	NA
- Phosphorous (mg/L)	NA	NA	ND	NA	NA	NA

Data ± 1 SD
NA – Not available
ND – Non-detectable

Table 5-2. Current, Power, and Coulombic Efficiency Data

Parameter	MFC-AO	MFC-AC	MFC-CC	MFC-CP
External Resistance (Ω)	20	10	6.7	6
Cell Potential (V)	0.3528 ± 0.0274	0.3841 ± .007	0.4069 ± 0.023	0.4478 ± 0.02
Anode Potential (V)	-0.334 ± 0.0004	-0.2997 ± 0.014	-0.2963 ± 0.016	-0.291 ± 0.011
Cathode Potential (V)	NA	NA	0.1739 ± 0.013	0.1483 ± 0.025
Current (A)	0.017 ± 0.001	0.0384 ± .002	0.062 ± 0.007	0.0747 ± 0.003
Current density (A/m^3)	2.957 ± 0.238	6.63 ± 0.3	10.657 ± 1.161	12.87 ± 0.57
Power (W)	0.006 ± 0.001	0.0147 ± 0.013	0.025 ± 0.001	0.0335 ± 0.003
Power density (W/m^3)	1.015 ± 0.163	2.55 ± 0.23	4.32 ± 0.259	5.77 ± 0.52
Coulombic Efficiency (%)	11.23 ± 2.58	14.1 ± 3.6	37.2 ± 11.48	17.6 ± 2.8

Data ± 1 SD

Table 5-3. MFC Flow Rates

Process	MFC-AO	MFC-AC	MFC-CC	MFC-CP
Feed Rate (L/day)	12.6 ± 0.6	12.9 ± 0.6	12.7 ± 0.4	12.9 ± 0.4
Anolyte Recirculation (L/day)	58 ± 0.3	58 ± 0.3	58 ± 0.3	58 ± 0
Catholyte Recirculation (L/day)	NA	NA	295 ± 0	295 ± 0
Air Supply (L/day)	410 ± 0	410 ± 0	410 ± 0	410 ± 0
Carbon Dioxide (L/day)	NA	108 ± 0	86 ± 0	NA

Data ± 1 SD

References:

(1) Clauwaert, P.; Van der Ha, D.; Boon, N.; Verbeken, K.; Verhaege, M.; Rabaey, K.; Verstraete, W., Biological denitrification in microbial fuel cells. *Environ. Sci. Technol.* 2007, *41*, 7564-7569.

(2) Rozendal, R.; Leonea, E.; Kellera, J.; Rabaey, K., *Electrochem. Comm. 2009.* In press.

(3) He, Z.; Minteer, S. D.; Angenent, L. T., Electricity generation from artificial wastewater using an upflow microbial fuel cell. *Environ. Sci. Technol.* 2005, *39*, 5262-5267.

(4) Logan, B. E., Simultaneous wastewater treatment and biological electricity generation. *Water Sci. Technol.* 2005, *52*, 31-37.

(5) Lovley, D. R., Microbial energizers: Fuel cells that keep on going. *Microbe.* 2006, *1*, 323-329.

(6) Rabaey, K.; Verstraete, W., Microbial fuel cells: Novel biotechnology for energy generation. *Trends Biotechnol.* 2005, *23*, 291-298.

(7) Rozendal, R. A.; Jeremiasse, A. W.; Hamelers, H. V. M.; Buisman, C. J. N., Hydrogen production with a microbial biocathode. *Environ. Sci. Technol.* 2008, *42*, 629-634.

(8) Rozendal, R. A.; Hamelers, H. V. M.; Euverink, G. J. W.; Metz, S. J.; Buisman, C. J. N., Principle and perspectives of hydrogen production through biocatalyzed electrolysis. *Int. J. Hydrogen Energ.* 2006, *31*, 1632-1640.

(9) Ditzig, J.; Liu, H.; Logan, B. E., Production of hydrogen from domestic wastewater using a bioelectrochemically assisted microbial reactor (BEAMR). *Int. J. Hydrogen Energy.* 2007, *32*, 2296-2304.

(10) Call, D.; Logan, B. E., Hydrogen production in a single chamber microbial electrolysis cell lacking a membrane. *Environ. Sci. Technol.* 2008, *42*, 3401-3406.

(11) Lovley, D. R., The microbe electric: Conversion of organic matter to electricity. *Curr. Opin. Biotech.* 2008, *19*, 564-571.

(12) Harnisch, F.; Schröder, U.; Scholz, F., The suitability of monopolar and bipolar ion exchange membranes as separators for biological fuel cells. *Environ. Sci. Technol.* 2008, *42*, 1740-1746.

(13) Harnisch, F.; Warmbier, R.; Schneider, R.; Schröder, U., Modeling the ion transfer and polarization of ion exchange membranes in bioelectrochemical systems. *Bioelectrochemistry. 2009, 75, 136-141*.

(14) Rozendal, R. A.; Hamelers, H. V. M.; Buisman, C. J. N., Effects of membrane cation transport on pH and microbial fuel cell performance. *Environ. Sci. Technol.* 2006, *40*, 5206-5211.

(15) Zhao, F.; Harnisch, F.; Schröder, U.; Scholz, F.; Bogdanoff, P.; Herrmann, I., Challenges and constraints of using oxygen cathodes in microbial fuel cells, *Environ. Sci. Technol.* 2006, 40, 5193-5199.

(16) Kim, J. R.; Cheng, S.; Oh, S. E.; Logan, B. E., Power generation using different cation, anion, and ultrafiltration membranes in microbial fuel cells. *Environ. Sci. Technol.* 2007, *41*, 1004-1009.

(17) Fan, Y. Z.; Hu, H. Q.; Liu, H., Sustainable power generation in microbial fuel cells using bicarbonate buffer and proton transfer mechanisms. *Environ. Sci. Technol.* 2007, *41*, 8154-8158.

(18) Fornero, J. J.; Rosenbaum, M.; Cotta, M. A.; Angenent, L. T., Microbial fuel cell performance with a pressurized cathode chamber. *Environ. Sci. Technol.* 2008, *42*, 8578-8584.

(19) Rozendal, R. A.; Hamelers, H. V. M.; Molenkmp, R. J.; Buisman, J. N., Performance of single chamber biocatalyzed electrolysis with different types of ion exchange membranes. *Water Res.* 2007, *41*, 1984-1994.

(20) Torres, C. I.; Lee, H. S.; Rittmann, B. E., Carbonate species as OH^- carriers for decreasing the pH gradient between cathode and anode in biological fuel cells. *Environ. Sci. Technol.* 2008, *42*, 8773-8777.

(21) Amend, J. P.; Shock, E. L., Energetics of overall metabolic reactions of thermophilic and hyperthermophilic archaea and bacteria. *FEMS Microbiol. Rev.* 2001, *25*, 175-243.

(22) Zehnder, A. J.; Brock, T. D., Anaerobic methane oxidation: Occurrence and ecology. *Appl. Environ. Microbiol.* 1980, *39*, 194-204.

(23) Clesceri, L. S.; Greenberg, A. E.; Eaton, A. D., *Standard Methods for the Examination of Water and Wastewater*; 20th ed.; American Public Health Association: Washington, D.C., 1998.

(24) Newman, J. *Electrochemical Systems*; 3rd ed.; John Wiley and Sons, Inc.: Hoboken, NJ, 2004.

(25) Butler, J., *Ionic Equilibrium*; John Wiley and Sons, Inc.: Cambridge, MA, 1998.

(26) Roosen, C.; Ansorge-Schumacher, M.; Mang, T.; Leitner, W.; Greiner, L., Gaining pH-control in water/carbon dioxide biphasic systems. *Green Chem.* 2007, *9*, 455- 458.

(27) Alberty, R. A., Standard apparent reduction potentials of biochemical half reactions and thermodynamic data on the species involved. *Biophys. Chem.* 2004, *111*, 115-122.

(28) Franks, A. E.; Nevin, K. P.; Jia, H. F.; Izallalen, M.; Woodard, T. L.; Lovley, D. R., Novel strategy for three-dimensional real-time imaging of microbial fuel cell communities: Monitoring the inhibitory effects of proton accumulation within the anode biofilm. *Energ. Environ. Sci.* 2009, *2*, 113-119.

(29) Feng, Y.; Wang, X.; Logan, B. E.; Lee, H., Brewery wastewater treatment using air-cathode microbial fuel cells. *Appl. Microbiol. Biotechnol.* 2008, *78*, 873-880.

(30) Liu, H.; Cheng, S.; Logan, B. E., Power generation in fed-batch microbial fuel cells as a function of ionic strength, temperature, and reactor configuration. *Environ. Sci. Technol.* 2005, *39*, 5488-5493.

Chapter 6

Conclusions and Recommendations

Abstract

Significant progress is being made with bioelectrochemical system (BES) reactor configurations, power densities, chemical production, and an increasing variety of novel engineering applications. The potential commercial application of BESs, however, remains uncertain. Order of magnitude decreases in unit costs, reductions in internal resistance (i.e., increases in ion flux), and improvements in engineered materials are required to realize the full potential of the technology. Conclusions drawn from my BES laboratory research and engineering evaluations show areas where additional scientific investigation may considerably improve BES performance.

The three most promising fields of study to advance BES technology are 1. increasing the ion flux; 2. optimizing the cathode/catholyte system design; and 3. engineering novel materials with superior characteristics. Increasing the ion flux is necessary since the ion flux often limits current and power densities. Optimizing the cathode/catholyte system design is important because it impacts many BES characteristics, including the oxygen reduction reaction (ORR) potential, catholyte conductivity (ion electromigration), anolyte conductivity, anolyte alkalinity, pH gradient, diffusion gradient, and pressure gradient. Thus, selecting a cathode/catholyte design that

positively influences these parameters toward higher ion fluxes (i.e., increased conductivity and cathode to anode gradients), increased ORR potentials, and lower pH gradient potential losses will increase BES power densities. Lastly, engineered materials, such as ion exchange membranes and electrodes, can be designed specifically for BES applications, whereas currently, these materials are borrowed from other applications. Overall, the recommendations in this chapter reflect the large number of unanswered questions regarding the science and application of BESs.

Conclusions and Recommendations

Bioelectrochemical system (BES) research is attracting increased attention from the scientific community, because the technology holds promise to produce environmentally benign and sustainable energy, replace energy intensive processes, and/or produce chemical products. And while significant progress is being made with reactor configurations, increasing power densities, chemical production, and an increasing variety of novel engineering applications, the potential commercial application of BESs remains uncertain.

Increasing the ion flux is of primary importance to increase current and power densities. According to the Nernst-Planck equation, the ion flux is a function of ion electromigration, ion diffusion, and ion convection, which are in turn functions of the potential gradient, concentration gradient, and pressure gradient. Therefore, if the potential, concentration, and hydraulic gradients of a BES are increased, the ion flux will also increase. The most direct method of increasing these gradients is by reducing the distance between the anode and cathode electrodes, which is a function of BES

architecture. The minimum electrode spacing will depend on the combined thicknesses of the cathode electrode, membrane, and anode electrode. Presuming a BES design with both electrodes in intimate contact with an ion exchange membrane, the volume requirements for the catholyte and anolyte require consideration. Since the catholyte is typically abiotic, the cathode chamber does not need to account for particulate matter in the catholyte. Therefore, a thin film of catholyte can be used to 1. ensure a fully wetted cathode, which is necessary to reduce ohmic losses and 2. maintain close contact between the catholyte and membrane, which decreases the distance ions must travel to maintain electroneutrality (chapter 5). The shorter the distance the ions need to travel, the higher the ion flux across the membrane. The biotic anolyte, however, must account for particulate matter (even with soluble organic substrates, biofilm detachment is possible), the microbial community, and the water required to transport nutrients and wastes. Thus, the anode chamber will likely be larger than the cathode chamber and the distance ions must travel from the membrane through the anolyte will be longer as well. And, since the ion flux is the rate determining step for increased BES power densities, the distance traveled by ions in the anolyte will likely be the rate determining step of the ion flux.

Besides these factors, the anode must have sufficient volume to treat large volumes of wastewater at a low cost, therefore making BES material cost a factor. Tighter anode compartment spacing will also cause higher pressure drops, which increase pumping costs and raise system pressures. Thus, the “optimum” anode architecture will likely be a compromise between the minimum electrode spacing, the space requirements to satisfy wastewater treatment requirements, and total system economics. Therefore, the

goal for BES research may eventually shift from maximizing current and power densities to lowest total cost of treatment.

Since the anode has such a strong influence on the rate limiting ion flux, the cathode/catholyte system, including an anion exchange membrane, must be designed to increase the cathode to anode anion flux as much as possible. While significant progress, particularly with pressure (chapter 4) and catholyte pH control (chapter 5), was made with the cathode/catholyte designs in my thesis, more improvements to increase the ion flux are achievable. In addition to closer electrode spacing, increasing the ion electromigration (solution conductivity), ion diffusion, and ion convection will contribute to ion flux increases. As shown in chapter 5, increasing the bicarbonate ion concentration increased the catholyte and anolyte conductivity. Pressurizing both the BES cathode and the CO_2 contactor column to increase the CO_2 partial pressure was not explored in this study. Theoretically, a higher CO_2 partial pressure will increase the catholyte bicarbonate ion concentration and decrease the pH. The higher bicarbonate ion concentration will increase the catholyte conductivity and therefore, increase the ion flux. Decreasing the cathode pH will increase the cathode ORR potential, which is favorable for the BES power density. An increased catholyte bicarbonate ion concentration will also increase the catholyte to anolyte bicarbonate ion concentration gradient, which will increases the diffusion flux. Moreover, a pressurized catholyte will can create a cathode to anode pressure gradient, which will create a convective flow of water from the cathode to anode. Increasing the convection of water will further increase the ion flux because bicarbonate ions are included in the moving water (convection plus diffusion). Lastly, pressurizing the cathode, increased the dissolved oxygen concentration (due to higher

oxygen partial pressure), and therefore reduced the cathode ORR overpotential (chapter 4), which increases the BES cell potential, and thus increase BES power and current densities.

Potentially offsetting improvements from a higher cathode partial pressure is an increase in the cathode to anode oxygen diffusion with an oxygen reduction cathode (when an air/CO_2 mixture is used in the cathode). Oxygen diffusion to the anolyte can have a negative impact on BES performance because oxygen has a more positive standard potential than the anode electrode and, in its presence, is used as the preferred electron acceptor rather than the electrode, which results in a reduced current production. In very recent studies however, stimulating effects of oxygen to the anodic performance of a pure culture of *Shewanella oneidensis* have been shown (Rosenbaum et al, submitted; Biffinger et al. 2008, Biosensors & Bioelectronics, 24 (4) 900-905 Dec. 1, 2008). If this concept could be exploited to select for a more oxygen tolerant mixed anode community, the negative impact of oxygen diffusion would be less pronounced and perhaps beneficial. In chapter 4, I had shown the negative effects of oxygen in the anode, which occurred after an immediate change in the UMFC operating configuration. If the UMFC anode was operated with some oxygen for longer periods, the operation with oxygen may select for a bacterial community that can generate an electric current in the presence of oxygen. Such an operation could have a positive effect on the current generation, but a negative impact on the coulombic efficiency.

Designing engineered materials specifically for BES applications has yet to be fully explored. Ion exchange membranes used in BESs are typically designed for non-BES applications. Nafion for instance, as often used as a BES cation exchange

membrane is designed for proton migration in proton exchange membrane fuel cells. Likewise, AEMs in the marketplace were not designed specifically for BES applications. Since BES electroneutrality is maintained by ions other than protons or hydroxide ions, membrane designs should be size selective for ions involved in BES electroneutrality maintenance. Reducing the membrane resistance would also increase the ion flux. Another research opportunity involves the anode electrode design. Key material design features would include a low electrical resistance to improve current conduction, electrical continuity between the bacteria and the current collection system to capture all of the electrons, a high surface area to support a large population of anode respiring bacteria, a thin design to minimize the distance to the membrane/cathode electrode, a surface morphology conducive to bacterial attachment, and a three dimensional shape that would enable the treatment of large water volumes.

Appendix A

Summary of how a microbial fuel cell (MFC) works

1) MFCs convert chemical energy stored in organic substrates into electrical energy by using bacteria. The bacteria oxidize the substrates and produce electrons that are collected on an electrode and then pass thru an external electric circuit. The ability to transfer electrons through a circuit depends on the electrochemical potential difference between the anode and cathode electrodes. Each has a unique electrochemical potential, which can be determined with the Nernst equation.

$$E = E^{o} + \frac{RT}{nF} \ln\left[\frac{\{C\}^{\gamma}\{D\}^{\delta}}{\{A\}^{\alpha}\{B\}^{\beta}}\right]$$

2) The difference in the electrochemical potential between the (higher electron energy) anode and (lower electron energy) cathode motivates the electron transfer from the anode to the cathode, because electrons are attracted to a lower energy state. The transfer of electrons as current is described by Ohm's law.

$$I = \frac{\Delta E}{R}$$

where, $\Delta E = E_{cell} = E_{Cathode} - E_{Anode}$

3) The transfer of electrons from the anode to cathode creates a temporary charge imbalance, with the anode becoming positively charged and cathode becoming negatively charged. Because the charge balance ($\sum_i z_i c_i = 0$) must be maintained within each MFC cell, cathode anions migrate to the anode or anode cations migrate to the cathode depending on ion exchange membrane selection. The ion migration flux is described by the Nernst Plank equation, which has three terms; i) ion migration resulting from an electric field, ii) ion diffusion, and iii) ion convection.

$$N_i = -z_i u_i F c_i \nabla \Phi - D_i \nabla c_i + c_i v$$

where, N_i = Flux of species i (mol/s-cm^2)

z_i = Charge of ion i (charge number)

u_i = ion mobility (cm^2-mol/J-s)

F = Faradays Constant 96,485 C/equiv

c_i = Concentration of species i (mol/cm^3)

$\nabla\Phi$ = Potential gradient (V)

D_i = Diffusivity of species i (cm^2/s)

v = bulk fluid velocity (cm/s)

To illustrate ion migration with different membranes, the Nernst Planck ion migration term will be considered (neglecting diffusion and convection). A positive potential gradient ($+\nabla\Phi$) will be defined as going from the electron "rich" cathode ($\Phi_{R,}\, \Phi_{C,}\, \Phi_{Cathode}$) to electron "lean" anode ($\Phi_{L,}\, \Phi_A, \Phi_{Anode}$) MFC chamber. A net positive sign will indicate ion movement from the anode to cathode.

With an AEM, anions migrate from the cathode to anode in response to the charge imbalance created by the anode to cathode electron transfer. Thus,

$$N_i = -(-1)u_i Fc_i(\Phi_L - \Phi_R) = -(-1)u_i Fc_i(\Phi_A - \Phi_C)$$

$$N_i = -u_i Fc_i(\nabla\Phi)$$

The negative sign indicates anion movement from the cathode to anode. With a CEM, cations migrate from the anode to cathode in response to the charge imbalance created by the anode to cathode electron transfer. Thus,

$$N_i = -(+1)u_i Fc_i(\Phi_L - \Phi_R) = -(+1)u_i Fc_i(\Phi_A - \Phi_C)$$

$$N_i = u_i Fc_i(\nabla\Phi)$$

The positive sign indicates cation movement from the anode to cathode. To satisfy electroneutrality, the rate of the ion flux must equal the rate of the electron flux in the MFC (equal charge equivalents).

Electroneutrality Force

Electroneutrality is related to the charge balance maintenance and can be represented by Poisson's equation (charge density) and the Laplacian of the electrical potential.[1]

$$\nabla^2\Phi = \frac{F}{\varepsilon}\sum z_i c_i \qquad (2)$$

Where, Φ = Electrical potential (V)

F = Faraday's constant (96,485 C/mol)

ε = Dielectric constant (permittivity)

Water permittivity = 6.93×10^{-12} C/V-cm

(Permittivity is the ability of a material to polarize in response to an electric field and reduce the total electric field inside the material)

z_i = Ion charge of species i

c_i = Ion concentration of species i

The key to the above equation is the proportionality constant F/ε. Because the dielectric constant of water is very small, the proportionality constant becomes very large.

$$\frac{F}{\varepsilon} = \frac{96{,}485\ C/mol}{6.93 \times 10^{-12}\ C/V\text{-}m} = 1.39 \times 10^{16}\ V\text{-}cm/mol$$

The practical implication of the large proportionality constant is that negligible deviations from electroneutrality result in large deviations from LaPlace's equation for the potential. Or, given that F/ε is so large, a significant separation of charge away from electroneutrality would require extremely large electrical forces to maintain the separation. Thus, given the large driving force to maintain the charge balance, electroneutrality can be assumed in the bulk solution.

Electroneutrality is evidenced in the microbial fuel cell by electrons (nearly instantaneously) moving from the anode to cathode in response to the potential difference, which creates an anolyte charge imbalance because of the relatively slow (as compared to the electrons) movement of anions from the cathode to anode (with an AEM). However, because the charge balance is related to the electrical potential by a large proportionality constant (2), the anolyte charge balance is rapidly reestablished by cathode to anode anion transport. Therefore, because of the deviation in the electrical potential ($\nabla^2\Phi$), it is reasonable to expect that MFC electroneutrality maintenance is a stronger force than diffusion.

References:

(1) Newman, J., *Electrochemical Systems*; Prentice Hall, Inc.: Englewood Cliffs, NJ, 1973.

(2) Prentice, G., *Electrochemical Engineering Principles*; Prentice Hall, Inc.: Englewood Cliffs, NJ, 1991.

Appendix B

Microbial fuel cell performance with a pressurized cathode chamber - Supporting Information

Fornero J. J., Rosenbaum M., Cotta M. A., and Angenent L. T. (2008). Microbial fuel cell performance with a pressurized cathode. *Environmental Science and Technology*, Vol. 42, No. 22, pp. 8578–8584.

Summary

This supporting material provides additional information on the materials and methods for the oxygen diffusion experiment and the discussion for the anolyte effluent as catholyte and membrane-less UMFC experiments. It also shows five figures: 1. the UMFC cathode electrode assembly (Fig. B1); 2. the UMFC process flow with and without the ion exchange membrane (Fig. B2); 3. the cathode potential (Fig. B3); 4. the membrane oxygen diffusion at different pressures (Fig. B4); and 5. the colored UMFC polarization and power curves with ±1 SD error bars (Fig. B5). Finally, Table B1 contains UMFC catholyte dissolved oxygen concentration data.

Oxygen Diffusion Experiment - Experimental Setup

Oxygen diffusion measurements for the ion exchange membranes were made with a 1.9 cm threaded PVC pipe union (Lowes, Moorseville, NC) secured by a lab stand with the open ends facing upward and downward. After the membrane was secured within the pipe union (4.91 cm^2 surface area), anaerobic water (i.e., water sparged with N_2 gas) was added on top of the membrane. A dissolved oxygen meter probe (Model 50B, YSI Incorporated, Yellow Springs, OH) was placed in the water to monitor the dissolved oxygen concentration. To prevent air intrusion from the open end of the pipe union, a rubber gasket was installed. Pressurized air controlled by an air regulator (Lowes Kobalt Mini Regulator, Moorseville, NC) was added beneath the membrane. The change in the dissolved oxygen concentration of the water above the membrane was then measured versus time to determine the rate of dissolved oxygen migration through the membrane. Oxygen diffusion rates through the membrane were calculated in terms of ng O_2/s-cm^2.

Anolyte Effluent as Catholyte and Membraneless UMFC – Supporting Discussion

We observed a 26.5% decrease in the power density with the change from the phosphate buffered catholyte (experiment I) to the anode effluent catholyte (experiment J) because of immediate and longer term effects. There was an immediate 40.2% decrease in the cathode potential from 0.3304 to 0.1976 V (versus Ag/AgCl), resulting from the change of the phosphate buffered catholyte to anode effluent catholyte (data not shown). This change in catholyte affected three important factors: 1. a decrease in the solution conductivity from 124.5 mS/cm to 9.3 mS/cm with the change from the phosphate buffer to the anolyte effluent, respectively. The decrease in the solution conductivity correlates

to the decrease in the catholyte monovalent equivalent ionic concentrations (catholyte = 1.19 M; anolyte = 0.08 M), which would decrease the cathode potential and the power density according to Harnisch et al.[1]; 2. a decrease in the catholyte pH from 7.6 to 7.1, which based on the Nernst equation would increase the cathode potential (and increase the power density if all other variables are held constant[2]); and 3. a removal of the nonfavorable, nonproton cation gradient for the CEM, which would increase the power density (Fig. 4-2 – and discussed in the main text). The actual lower power density by changing the catholyte suggests that changes in the catholyte ionic concentration were more important than the pH decrease and the cation gradient over the CEM. There was also the longer-term effect of a steady deterioration of the cathode potential with each successive trial of the triplicate experiment (0.1976, 0.1737, and 0.1690V at a 100-Ω external resistance). This steady cathode potential deterioration is likely due to a visible biofilm development on the cathode electrode (i.e., cathode insulation) and/or a slow poisoning of the Pt catalyst by sulfur and organic compounds in the anolyte (even though we had coated and protected Pt)[3]. While biofilm development on the cathode may be indicative of biocathode activity[4], others have found that a thickening biofilm impedes oxygen transport to catalyst sites and reduces fuel cell power.[5,6]

A similar sequential anode-cathode configuration study was performed by Freguia et al.[4], who used a noncatalyzed cathode that after several days developed an oxygen reducing biofilm (biocathode). Whereas our study with a catalyzed cathode showed a 14% decrease in the current density (from 8.57 to 7.35 mA/m^3) with the conversion to the anolyte effluent as catholyte, the Freguia et al.[4] study with the noncatalyzed cathode

showed a ~four-fold increase in the current density (from 86.1 to 328.9 mA/m^3). The COD removal efficiency with anolyte aeration in the cathode was 97.7% and 85.4% for our study and the Freguia et al.[4] study, respectively. Thus, when anode effluent was used as the catholyte (with or without the membrane), the VFAs in the cathode effluent were lower compared to the baseline performance (experiment I) due to removal of this substrate by aerobic bacteria growing in the oxygenated cathode.

The operation without a membrane (experiment K) resulted in a 99.5% decrease in the power density compared to experiment J with CEM and anolyte effluent as catholyte (0.01 versus 3.09 W/m^3) and 99.6% to the baseline experiment I. In the absence of a membrane, dissolved oxygen became available as a terminal electron acceptor for the anode bacteria at the expense of anode electron deposition. This was evidenced by the small overall cell potential (0.023 V) measured (Table 4-1). The low power densities without an ion exchange membrane are comparable with the findings of Jang et al.[7], who also found low MFC power densities associated with the absence of an ion exchange membrane.

FIGURES

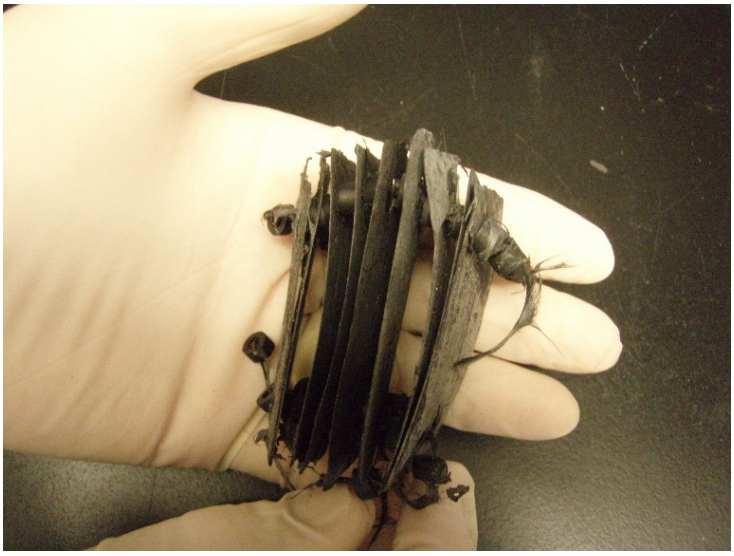

Figure B1. UMFC Cathode Electrode Assembly

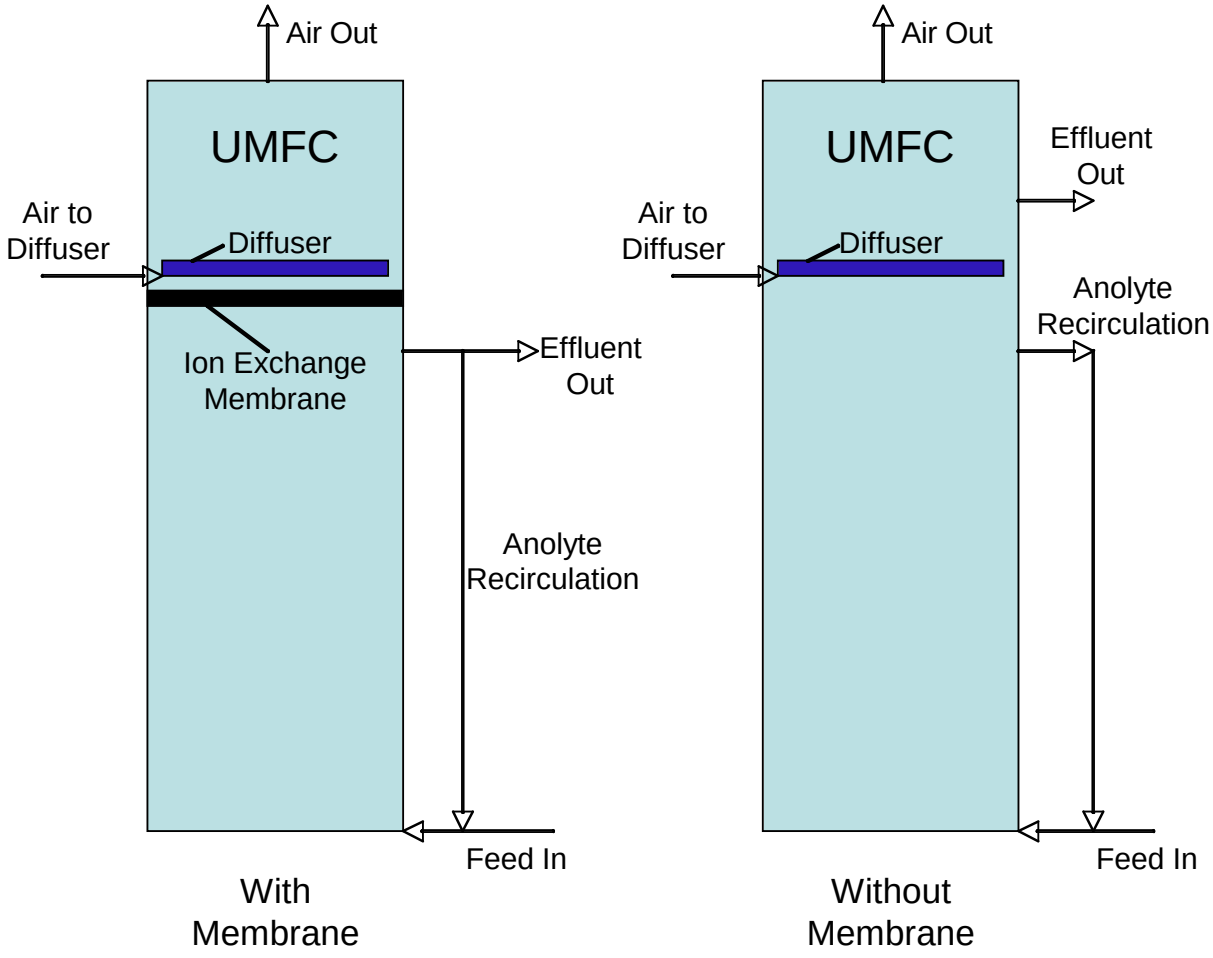

Figure B2. UMFC Process Flow With and Without Ion Exchange Membrane

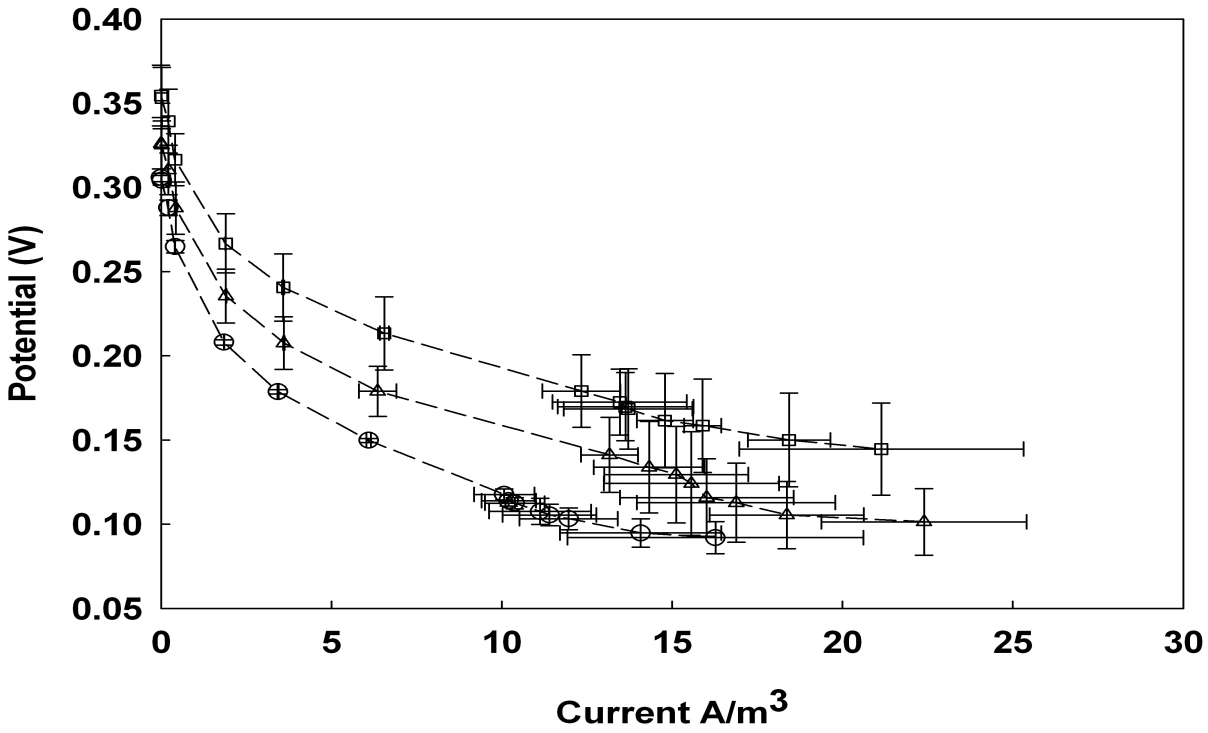

Figure B3. Cathode Potential Versus Current Density. Data taken during the AEM experiment at (□) 34.48 kPa; (△) 17.24 kPa; and (○) atmospheric pressure shows increasing cathode potentials with increasing air pressure. Data error bars reflect ±1 standard deviation.

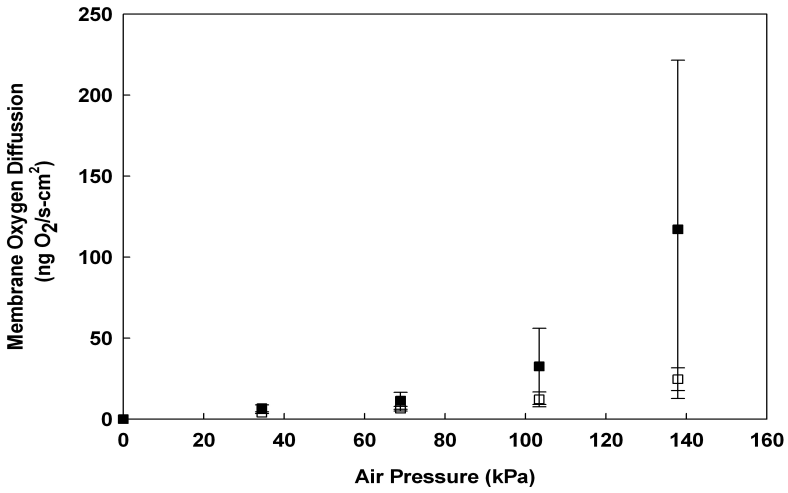

Figure B4. UMFC Membrane Oxygen Diffussion. AEM (■) and CEM (□) diffusion rates versus pressure. A higher oxygen diffusion rate was found with the AEM compared with the CEM. Data error bars reflect ±1 standard deviation.

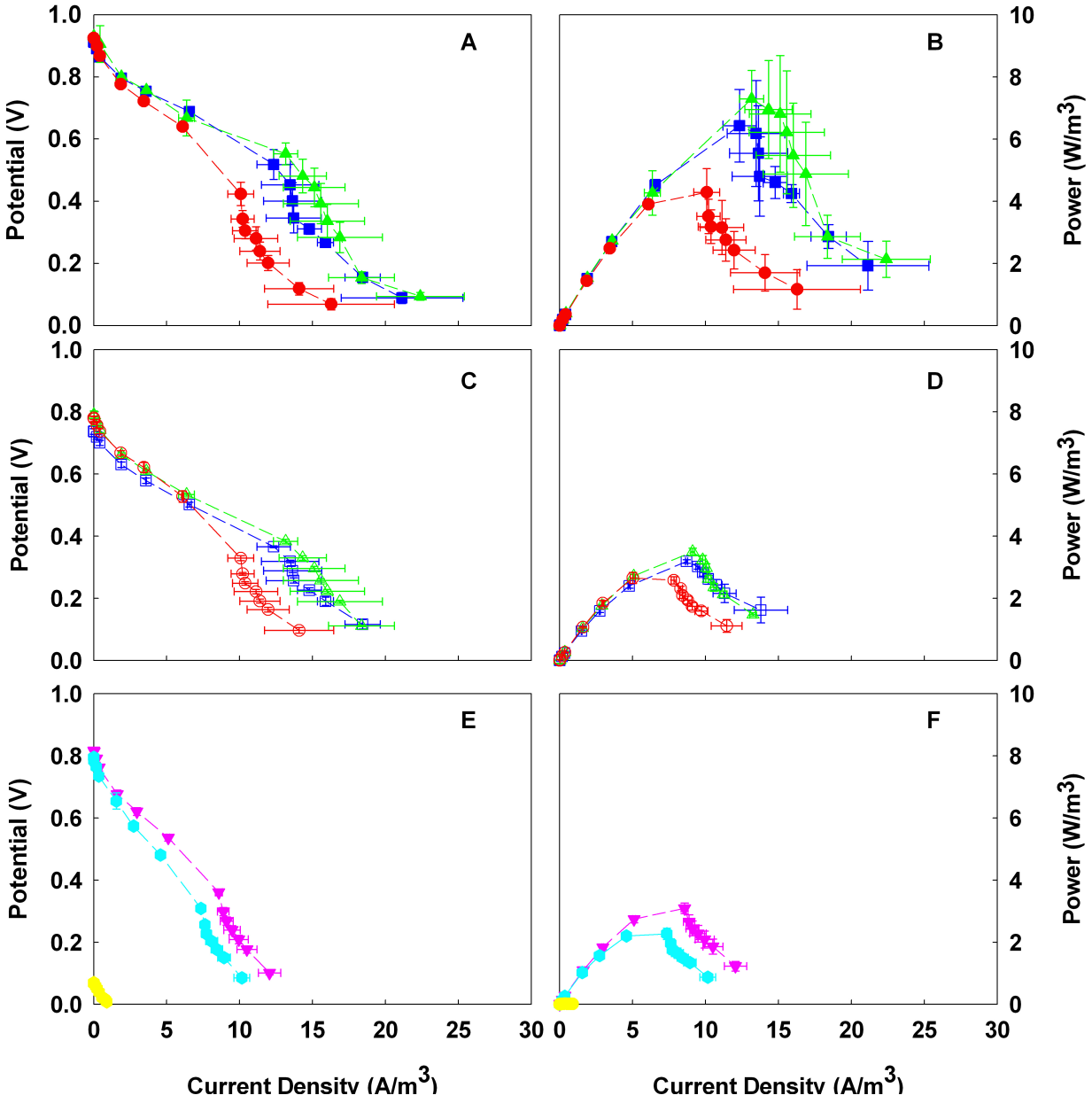

Figure B5. UMFC Polarization and Power Curves with ±1 Standard Deviation Error Bars. (A) Polarization curve with AEM; (B) power curve with AEM. AEM data

represented as solid symbols: (■) 34.48 kPa; (▲) 17.24 kPa; and (●) atmospheric pressure; **(**C) polarization curve with CEM; (D) power curve with CEM. CEM data is shown as hollow symbols: (□) 34.48 kPa; (△) 17.24 kPa; and (○) atmospheric pressure; (E) polarization curve with atmospheric pressure cathode: (▼) Nafion coated cathode electrode with phosphate buffered catholyte; (⬣) Nafion coated cathode with anolyte effluent catholyte; and (●) Membrane removed; (F) power curve with atmospheric pressure cathode: (▼) Nafion coated cathode electrode with phosphate buffered catholyte; (⬣) Nafion coated cathode with anolyte effluent catholyte; and (●) membrane removed. Data error bars reflect ±1 standard deviation.

Pressure (kPa)	Estimated Dissolved O_2[1] (pure water)	Measured Dissolved O_2[1] (catholyte)[2]
Atmospheric	8.42	8.35
17.24	9.96	9.15
34.48	11.45	10.13

[1] mg O_2/l at 24^0C

[2] 0.7 M Phosphate Buffer, pH = 7.6

Table B1. UMFC Dissolved Oxygen Concentration Data

References:

(1) Harnisch, F.; Schröder, U.; Scholz, F., The suitability of monopolar and bipolar ion exchange membranes as separators for biological fuel cells. *Environ. Sci. Technol.* 2008, *42*, 1740-1746.

(2) Zhao, F.; Harnisch, F.; Schröder, U.; Scholz, F.; Bogdanoff, P.; Hermann, I., Challenges and constraints of using oxygen cathodes in microbial fuel cells. *Environ. Sci. Technol.* 2006, *40*, 5193-5199.

(3) Shi, W. Y.; Yi, B. L.; Hou, M.; Jing, F. N.; Ming, P. W., Hydrogen sulfide poisoning and recovery of PEMFC Pt-anodes. *J. Power Sources* 2007, *165*, 814-818.

(4) Freguia, S.; Rabaey, K.; Yuan, Z.; Keller, J., Sequential anode-cathode configuration improves cathodic oxygen reduction and effluent quality of microbial fuel cells. *Water Res.* 2008, *42*, 1387-1396.

(5) Marcus, A. K.; Torres, C. I.; Rittmann, B. E., Conduction-based modeling of the biofilm anode of a microbial fuel cell. *Biotechnol. Bioeng.* 2007, *98*, 1171-1182.

(6) Rabaey, K.; Rodriguez, J.; Blackall, L. L.; Keller, J.; Gross, P.; Batstone, D.; Verstraete, W.; Nealson, K. H., Microbial ecology meets electrochemistry: Electricity-driven and driving communities. *ISME J.* 2007, *1*, 9-18.

(7) Jang, J. K.; Pham, T. H.; Chang, I. S.; Kang, K. H.; Moon, H.; Cho, K. S.; Kim, B. H., Construction and operation of a novel mediator- and membrane-less microbial fuel cell. *Process Biochem.* 2004, *39*, 1007-1012.

Appendix C

Carbon dioxide addition to microbial fuel cell cathode maintains stable catholyte pH and improves anolyte pH, total alkalinity, and conductivity – Supplemental Information

Fornero J. J., Rosenbaum M., Cotta M. A., and Angenent L. T., Carbon Dioxide Addition to Microbial Fuel Cell Cathodes Maintains Sustainable Catholyte pH and Improves Anolyte pH, Alkalinity, and Conductivity. In preparation for *Environmental Science and Technology.*

Summary

The supplemental information contains MFC fabrication photos and experimental data.

Figures

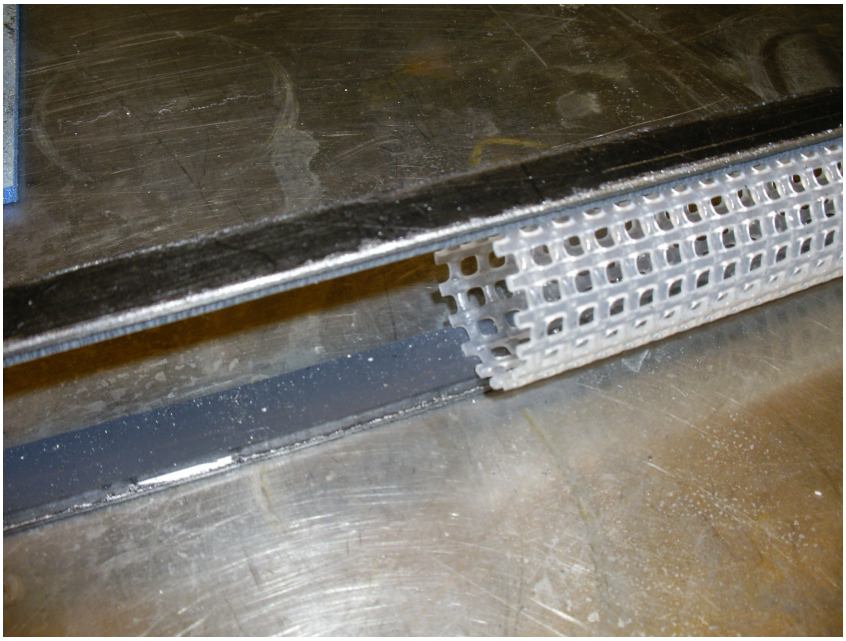

Fig. C1A) Cathode graphite electrodes glued to filtration tube

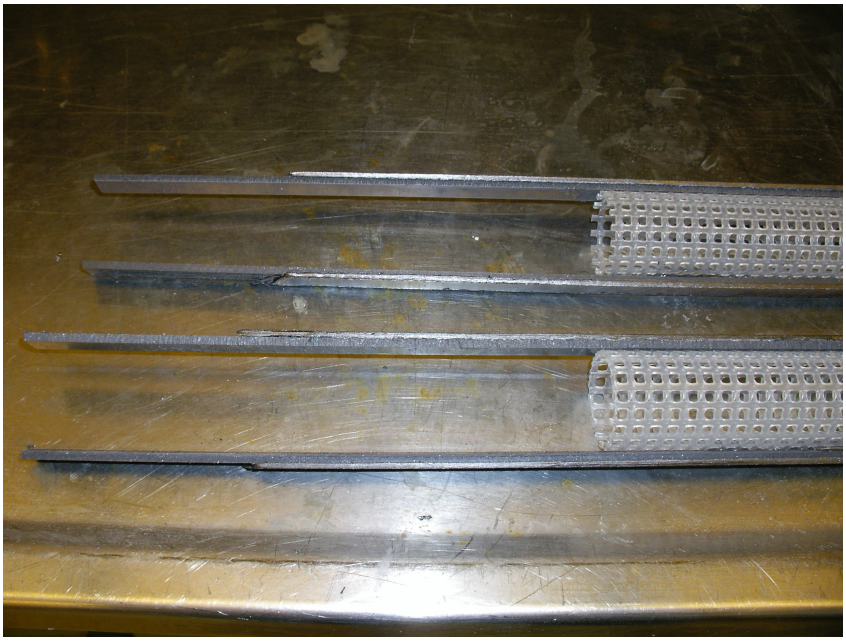

Fig. C1B) Graphite strip electrode extension

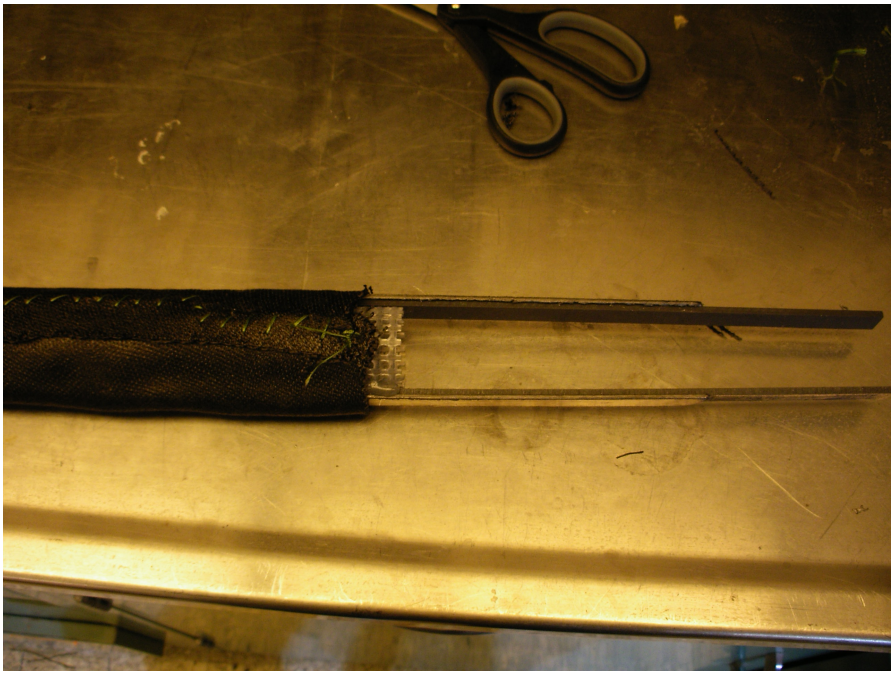

Fig. C1C) Cathode electrode carbon cloth wrapped around filtration tube and electrode post

Fig. C1D) Cathode electrode assemblies after platinum/Nafion application

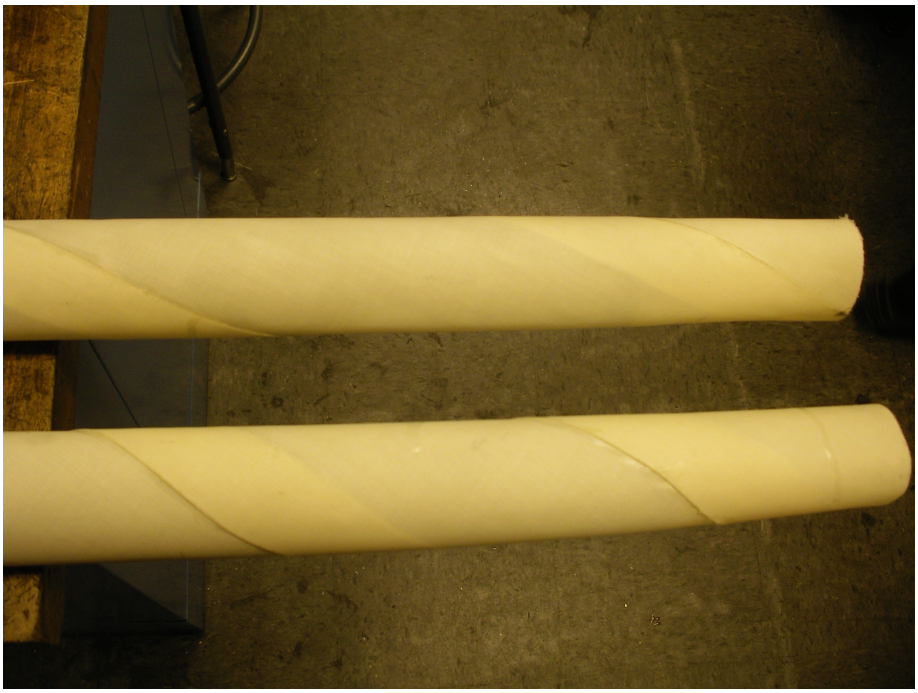

Fig. C1E) Anion exchange membrane (AEM) tubes

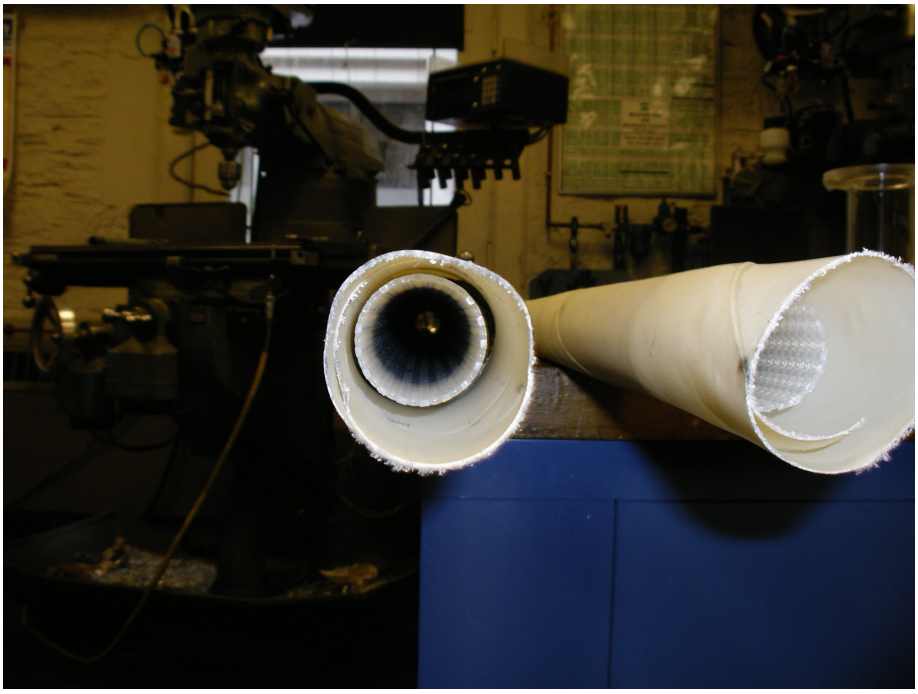

Fig. C1F) Cathode electrode assembly in AEM tube

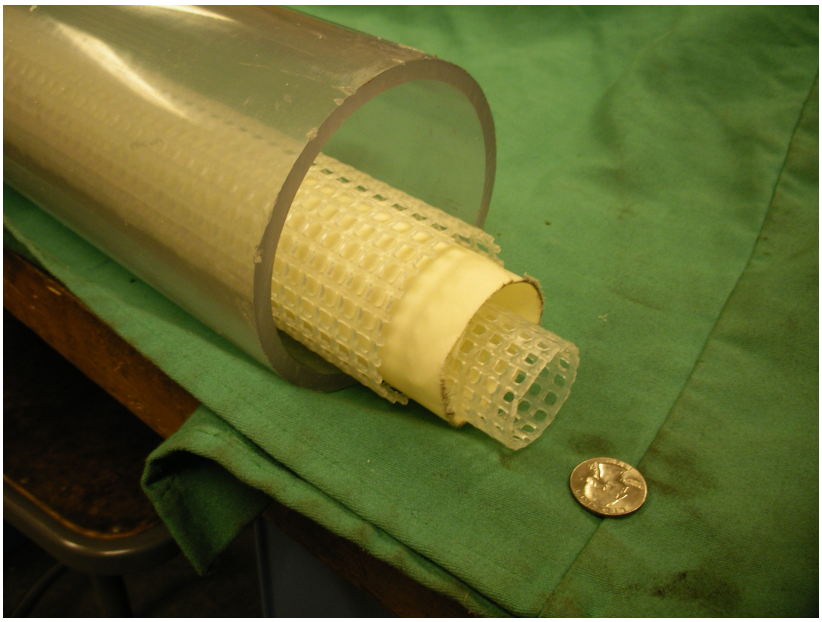

Fig. C1G) From the inside working out, cathode filtration tube, AEM, anode filtration tube, MFC enclosure pipe.

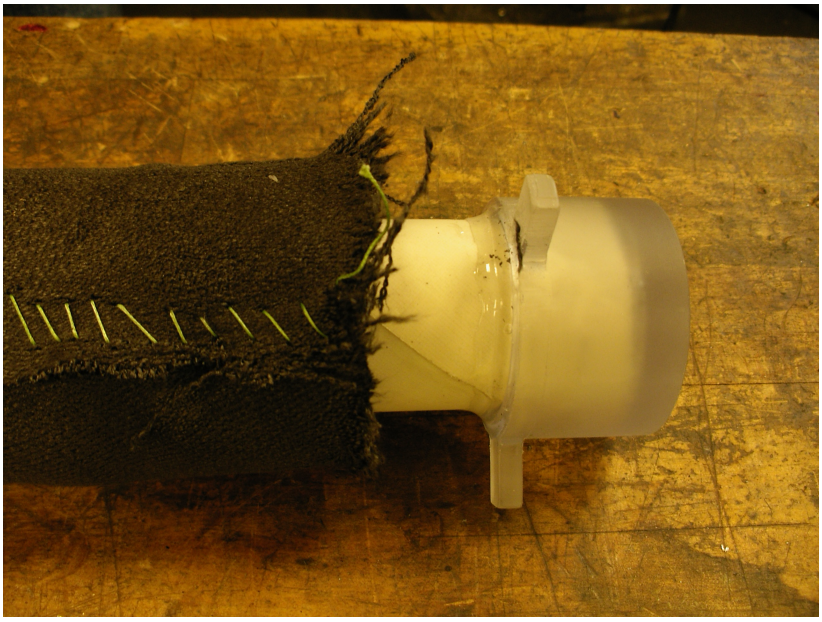

Fig. C1H) Anode electrode surrounding the AEM. The “floating head” on the AEM allowed the AEM to expand and contract. A nozzle and tube from the head connected the cathode to an external nozzle on the MFC.

Fig. C2) MFC photo following fabrication illustrating nozzles positions

Fig. C3) Carbon dioxide column with high surface area packing

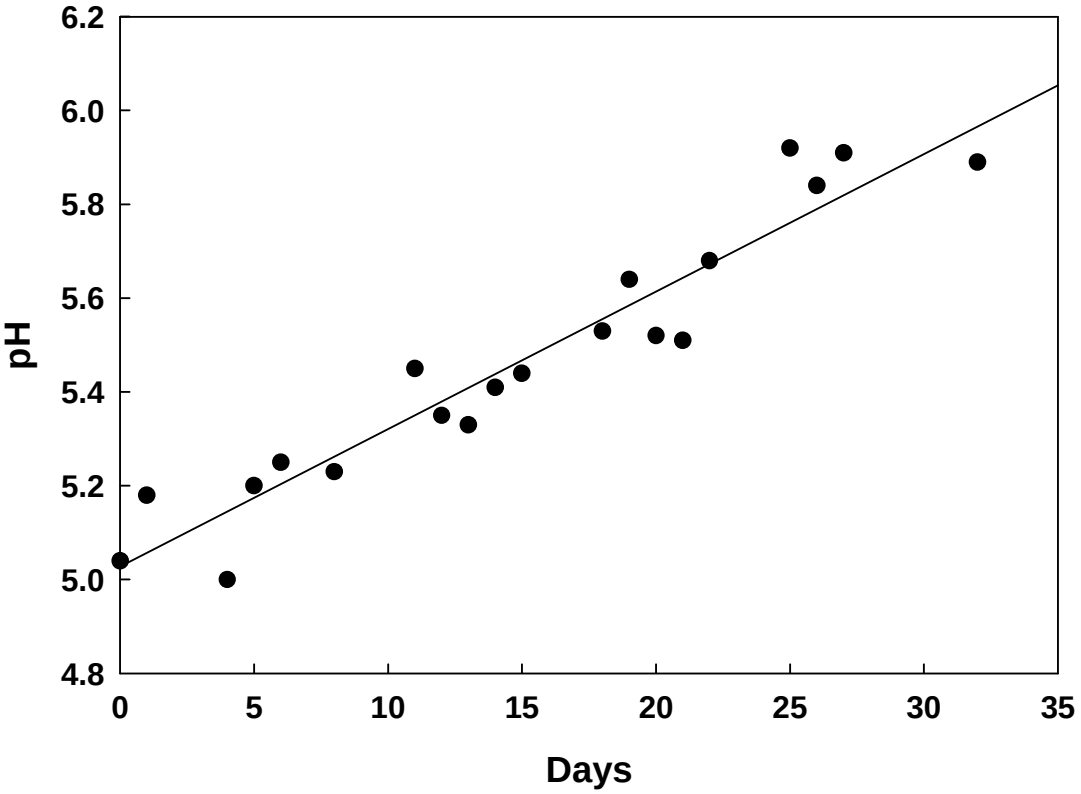

Fig C4) pH increase versus time during MFC-CC start-up resulting from anolyte cation diffusion.

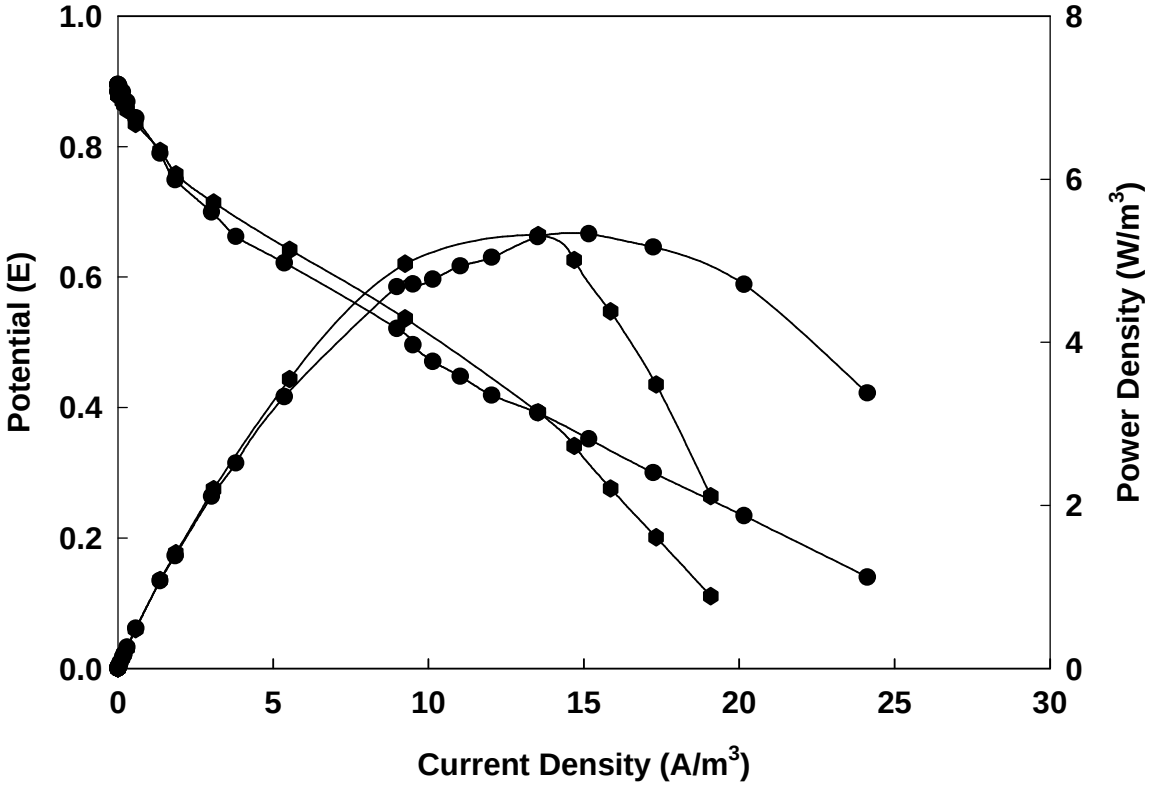

Fig. C5) MFC-CC polarization curves at pH = 5.24 (⬣) and pH = 5.94 (●)

Appendix D

Brewery MFC Feed Composition

MFC Reaction Stoichiometry:

Acetate oxidation:

$$CH_3COO^- + 4H_2O \rightarrow 2HCO_3^- + 9H^+ + 8e^-$$

Oxygen Reduction:

$$2O_2 + 4H_2O + 8e^- \rightarrow 8OH^-$$

Net reaction:

$$CH_3COO^- + 4H_2O \rightarrow 2HCO_3^- + 9H^+ + 8e^-$$

$$+ \quad 2O_2 + 4H_2O + 8e^- \rightarrow 8OH^-$$

$$CH_3COO^- + 2O_2 + 4H_2O \rightarrow 2HCO_3^- + H^+$$

Soluble chemical oxygen demand (sCOD) target of 300 mg/l:

$$300 \text{ mg } O_2/l \times \frac{1 \text{ mole O2}}{32{,}000 \text{ mg O2}} \times \frac{1 \text{ mole acetate}}{2 \text{ moles O2}} \times \frac{1 \text{ mole acetic acid}}{1 \text{ mole acetate}} \times \frac{60 \text{ g acetic acid}}{1 \text{ mole acetic acid}}$$

= 0.281 g acetic acid/l x 1.0 ml/1.049 g (density conversion)

= 0.268 ml acetic acid/l

Feed solution composition (per liter):

Acetic acid	0.268 ml
4M NaOH	0.265 ml
Yeast extract	0.025 g
NH_4Cl	0.03 g
K_2SO_4	0.006 g
$FeCl_2 – 4H_2O$	0.033 g
K_2HPO_4	0.033 g
$NaHCO_3$	1.0g
Iron Citrate	0.11g
Mineral solution (10ml)	
NaCl (25 g/l)	0.25 g
KCl (10 g/l)	0.10 g
$CaCl_2$ (10 g/l)	0.10 g
$MgCl_2$-$6H_2O$ (10 g/l)	0.10 g
Trace elements (1.0 ml)	
$FeCl_3$ (6,926 mg/l)	0.0069 g
$CoCL_2$-$6H_2O$ (2,000 mg/l)	0.002 g
EDTA (1,000 mg/l)	0.001 g
$MnCl_2$-$4H_2O$ (500 mg/l)	0.0005 g
$NiCl_2$-$6H_2O$ (142 mg/l)	0.000142 g
Na_2SeO_3 (123 mg/l)	0.000123 g
$AlCl_3$-$6H_2O$ (90 mg/l)	0.00009 g

H_3BO_3 (50 mg/l)	0.00005g
$ZnCl_2$ (50 mg/l)	0.00005 g
Na_2MoO_4-$2H_2O$ (66mg/l)	0.000066 g
Na_2WO_4-$2H_2O$ (50mg/l)	0.00005 g
CuCl2-2H2O	0.000038 g
HCl (1.0 ml/L)	

C:N:P Ration (per liter):

Carbon:

$$0.281 \text{ g acetic acid} \times \frac{1 \text{ mole acetic acid}}{60 \text{ g acetic acid}} \times \frac{2 \text{ moles carbon}}{1 \text{ mole acetic acid}}$$

= 0.0094 moles carbon

Nitrogen:

$$0.03 \text{ g } NH_4Cl \times \frac{1 \text{ mole } NH_4Cl}{53.49 \text{ g } NH_4Cl} \times \frac{1 \text{ mole nitrogen}}{1 \text{ mole } NH_4Cl}$$

= 0.00056 moles nitrogen

Phosphorous:

$$0.033 \text{ g } K_2HPO_4 \times \frac{1 \text{ mole } K_2HPO_4}{174.2 \text{ g } K_2HPO_4} \times \frac{1 \text{ mole phosphorous}}{1 \text{ mole } K_2HPO_4}$$

= 0.00019 moles phosphorous

Mole ratios:

	Actual	Target
C: 0.0094	100	100
N: 0.00056	6	5
P: 0.00019	2	1

MFC Feed Pump Calculations;

Size 16 pump head 0.8 ml/rev

Size 14 pump head 0.21 ml/rev

Revs (0.8 ml/rev + 0.21 ml/rev) = 1000 ml = 1.0 L

Revs/L = 990

Size 16 pump head 0.8 ml/rev x 990 revs = 792 ml (79.2%)

Size 14 pump head 0.21 ml/rev x 990 revs = 208 ml (20.8%)

1,000 ml

Feed concentrate composition:

1.0 L of feed concentrate makes 1.0 L/0.208 = 4.807 L of total feed

Therefore, the feed concentrate composition (per liter) needs to be 4.807X the diluted feed composition. For instance, if $NaHCO_3$ = 1.0g/L in the diluted feed, the $NaHCO_3$ = 4.807 g/L in the feed concentrate.

Feed Concentrate Composition (per liter):

Acetic acid	1.29 ml
4M NaOH	1.27 ml
Yeast extract	0.12 g
NH_4Cl	0.144 g
K_2SO_4	0.029 g
K_2HPO_4	0.159 g
$NaHCO_3$	4.807 g
Iron Citrate	0.529 g
Mineral solution (48 ml)	
NaCl (25 g/l)	0.25 g
KCl (10 g/l)	0.1 g
$CaCl_2$ (10 g/l)	0.1 g
$MgCl_2$-$6H_2O$ (10 g/l)	0.1 g
Trace elements (4.8 ml)	
$FeCl_2 – 4H_2O$	0.042 g added per liter of dilution water

Feed concentrate composition and preparation sequence:

	One liter	**20 liters**
DI water	900 ml	18,000 ml
4M NaOH	1.27 ml	25.4 ml
Acetic acid	1.29 ml	25.8 ml
K_2HPO_4	0.159 g	3.18 g
$NaHCO_3$	4.807 g	96.14 g
NH_4Cl	0.144 g	2.88 g
K_2SO_4	0.029 g	0.580 g
Iron Citrate	0.529 g	10.58 g
Yeast extract	0.12 g	2.4 g
Mineral solution	48 ml	960 ml
Trace elements	4.8 ml	96 ml
DI water	44.5 ml	890 ml
$FeCl_2 – 4H_2O$	0.042 g added per liter of dilution water	

Appendix E

Catholyte pH Prediction Calculation*

$$pH = 2\,pH_{unbuffered} + \log[HCO_{3\,\text{added}}^{-}] - \frac{\sqrt{I}}{(1+\sqrt{I})\,(\text{A}+0.5)} + \frac{I}{10}$$

Where,

I = ionic strength = $0.5\sum c_i z_i^2$

A = Debye-Huckel parameter

If 0.01 M $NaHCO_3$ is added to the MFC catholyte, the predicted pH is as follows,

$$I = 0.05[(0.01)(+1)^2 + (0.01)(-1)^2] = 0.01$$

$$A = 0.5$$

$$pH = 2\,pH_{unbuffered} + \log[HCO_{3\,\text{added}}^{-}] - \frac{\sqrt{I}}{(1+\sqrt{I})\,(\text{A}+0.5)} + \frac{I}{10}$$

$$pH = 2(3.94) + \log[0.01] - \frac{\sqrt{0.01}}{(1+\sqrt{0.01})\,(0.5+0.5)} + \frac{0.01}{10}$$

$$pH = 7.88 - 2 - 0.091 + 0.001$$

$$pH = 5.79$$

* Gaining pH-control in water/carbon dioxide biphasic systems. Roosen. C., et al, Green Chemistry, 2007

Appendix F

Preliminary investigation of whether homoacetogenic bacteria can utilize a cathode electrode as the sole electron donor to support autotrophic growth and the production of acetate

Abstract

Increases in the CO_2 concentrations of the Earth's atmosphere have raised concerns regarding the potential environmental and societal impact if the rate of increase of the CO_2 concentration remains unchecked. In this chapter, we investigated the possibility of using microbial processes in microbial electrolysis cells (MECs) to transform CO_2 to acetate, which is a usable chemical. By treating wastewater with a mixed community of microbes in the MEC anode (as it was studied for MFCs in chapters 4 and 5) and reducing CO_2 to acetate with homoacetogens in the MEC cathode, wastewater treatment plants may be used to simultaneously treat wastewater and transform CO_2 gas into usable chemicals.

The aim of this study was to determine whether acetogens can directly accept electrons from a cathode electrode to reduce CO_2 to acetate, thus, eliminating the need for an intermediate electron carrier (hydrogen, platinum to react with hydrogen, or an electron mediator). In seeking bacteria that are potentially able to directly accept

electrons from a cathode electrode to reduce CO_2 to acetate, *Moorella thermoacetica* was selected. Pure culture studies were performed in two electrochemical half cells, one of which included a three electrode system to apply a potential to an anode and measure the responding current. The other cell, without an applied potential, was used as a control. Bacterial activity was measured by the acetate concentration in the medium, electrical current and optical density. Although, 18 separate experiments were performed to induce *M. thermoacetica* to directly accept electrons to reduce CO_2 to acetate, the exploration was unsuccessful in the lab: while bacterial growth was measured, no acetate production could be shown.

Summary

The intent of this study was to explore whether acetogens could directly accept electrons from a cathode electrode to reduce CO_2 to acetate, thus, eliminating the need for an intermediate electron carrier (hydrogen, platinum to react with hydrogen, or an electron mediator). By treating wastewater with a mixed community of microbes in the MEC anode and reducing CO_2 to acetate with homoacetogens in the MEC cathode, wastewater treatment plants may be used to simultaneously treat wastewater and transform CO_2 gas into usable chemicals

The bacterium *Moorella thermoacetica,* provided by the United States Department of Agriculture laboratory in Peoria, that was selected as a candidate homoacetogen for the study. Experiments were conducted with pure cultures to eliminate the possibility of acetate utilization by other microbes. Active bacteria were sustained by reviving bacteria once every two weeks from the original culture, which was stored in a -

80 freezer. Upon revival the bacteria were successively transferred to new rich medium (ATCC 1190) vials three times per week. All bacteria work was performed under sterile working conditions and anaerobic atmosphere.

Experiments were performed with two single chamber cells, one of which included a three electrode system to apply a potential and measure the current response with the help of a potentiostat. The other cell, without an applied potential, was used as a control**.** ATCC 1190 medium was used for the single chamber cell experiments, which was devoid of glucose (an electron donor) or resazurin (an electron mediator) to ensure the electrode was the sole electron donor in the experiment and that the bacteria could independently obtain electrons from the electrode. In the amperometric-i(t) tests, a constant potential (-0.5 to -0.6 V vs. Ag/AgCl sat. KCL) was applied and the corresponding current was recorded over time. If there was increasing bioelectrochemical activity, this test would indicate an increase in the current that corresponded with an increase in the bacteria density. Besides this, the potentiostat was used to perform cyclic voltammetry analysis. The cyclic voltammetry test applies a reversible potential scan (0 to -0.7 V and -0.7 to 0 V) to the three electrode cell and measures the current produced versus the applied potential. This test shows if there is an electrochemical response (higher current) at a specific potential and is thus use useful for identifying electrochemical activity. The acetate concentration in the ATCC medium was measured with a gas chromatograph. Bacterial activity was measured by comparing the acetate concentration in the medium before and after the application of an applied potential, the electrical current measured with the amperometric – i(t) test, and (in some experiments) changes in the optical density of the medium.

Eighteen experiments were performed (Table F-1) of which fourteen were an attempt to create conditions suitable to *M. thermoacetica* for the direct acceptance of electrons to reduce CO_2 to acetate. The remaining four experiments tested the possibility of an abiotic acetate reduction, the electrochemical impact of nutrient additions, ATCC 1190 medium evaporation rates, and a mixed culture of pulverized Anheuser Busch anaerobic digester feed (Table F-1, experiments 10, 11, 13, and 14, respectively). While several experiments (Table F-1, experiments 7, 9c, 12, 14, 15, and 17) showed positive evidence of bacterial growth, only one experiment (7) showed a small net increase in the medium acetate concentration relative to the control. Thus, based on my work it seems unlikely that *M. thermoacetica* can use electrons directly from an electrode for the reduction of CO_2 to acetate. However, my experiments did not reach the depth necessary to be conclusive and the data is merely shown here as preliminary data.

Experiment #	Date	Potential	Gas*	Growth**	Acetate	Experiment Modifications
1	25-Sep-08	-0.60 V	B	N	N	
2	3-Oct-08	-0.50 V	A	N	N	Used -0.5V potential to avoid potential H_2 production
3	9-Oct-08	-0.60 V	A	N	N	Added 100% CO_2 to MFC head space
4	13-Oct-08	-0.60 V	A	N	N	
5	22-Oct-08	-0.50 V	B	N	N	Fabricated and used two identical three electrode MFCs (MFC + Control)
6	27-Oct-08	-0.50 V	B	N	N	Ran experiment with multiple controls + OD600 measurements
7	30-Oct-08	-0.55 V	C	Y	~Y	Initiated continuous N2/CO2 gas sparge
8a	9-Dec-08	-0.55 V	C	N	N	Filter sterilized fermented yeast extract in ATCC 1190 medium
8b	17-Dec-08	-0.57 V	C	N	N	
8c	23-Dec-08	-0.57 V	C	N	N	Added methylene blue electron mediator
8d	30-Dec-08	-0.57 V	C	N	N	Extended run with methylene blue
9a	8-Jan-09	-0.57 V	C	N	N	Added Ni, W, and iron citrate to ATCC mineral solution Added filter sterilized yeast extract after autoclaving Added 2 mg/L nicotinic acid to final medium
9b	14-Jan-09	-0.57 V	C	N	N	
9c	16-Jan-09	-0.57 V	C	Y	N	Injected glucose near end of run and noted a significant current decrease

* A = Batch 100% CO2 head space gas
B = Batch 80% N2 / 20% CO2 head space gas
C = Continuous 80% N2 / 20% CO2 gas purge
** Visual or OD600 indication of bacterial growth

Table F-1 *Moorella thermoacetica* experimental history

Experiment #	Date	Potential	Gas*	Growth**	Acetate	Experiment Modifications
10	29-Jan-09	-0.57 V	C	NA	N	Abiotic test to determined there was abiotic acetate reduction
11	6-Feb-09	-0.57 V	C	NA	N	Tested FS yeast extract and nicotinic acid addition to medium
12	9-Feb-09	-0.57 V	C	Y	N	Measured acetate concentration, pH, and OD_{600} 2x/day for 15 days
13	9-Mar-09	-0.57 V	C	NA	N	Measured medium evaporation rate versus time
14	13-Mar-09	-0.57 V	C	Y	N	Inoculated with Anheuser Busch Reactor Feed (mixed culture)
15	18-Mar-09	-0.57 V	C	Y	N	Injected 250 μM BES to inhibit methanogens
16	7-Apr-09	-0.57 V	C	N	N	Changes to carbon fabric electrode Used high density cell culture grown in glucose and rinsed in PBS
17	4-May-09	-0.57 V	C	Y	N	Repeated high density cell culture inoculation
18	21-May-09	-0.57 V	C	N	N	Used 1mM Methyl Viologen as electron mediator

* A = Batch 100% CO2 head space gas
B = Batch 80% N2 / 20% CO2 head space gas
C = Continuous 80% N2 / 20% CO2 gas purge
** Visual or OD600 indication of bacterial growth

Table F-1 *Moorella thermoacetica* experimental history

Appendix G

AATC 1190 Rich Medium

	AATC 1190
KH_2PO_4	1.5 g/L
Na_2HPO_4-$12H_2O$	4.2 g/L
NH_4Cl	0.5 g/L
$MgCl_2$-$6H_20$	0.18 g/L
Yeast Extract	2.0 g/L
Glucose	8.0 g/L
Rezasurin (0.1%)	1.0 ml/L
Wolfe's Modified Mineral Elixer	5.0 ml/L
Nitrilotriacetic acid	1.5 g/L
$MgSO_4$-$7H_2O$	3.0 g/L
$MnSO_4$-H_2O	0.5 g/L
NaCl	1.0 g/L
$FeSO_4$-$7H_2O$	0.1 g/L
$Co(NO_3)_2$-$6H_2O$	0.1 g/L
$CaCl_2$	0.1 g/L
$ZnSO_4$-$7H_2O$	0.1 g/L
$CuSO_4$-$5H_2O$	10.0 mg/L

$ALK(SO_4)_2$	10.0 mg/L
Boric Acid	10.0 mg/L
Na_2MoO_4-$2H_2O$	10.0 mg/L
Na_2SeO_3	1.0 mg/L
Vitamin Solution	0.5 ml/L
Biotin	40.0 mg/L
p-Aminobenzoic acid	100.0 mg/L
Folic acid	40.0 mg/L
Pantothenic acid calcium salt	100.0 mg/L
Nicotinic acid	100.0 mg/L
Vitamin B12	2.0 mg/L
Thiamine HCl	10.0 mg/L
Pyridoxine hydrochloride	200 mg/L
Thioctic acid	100 mg/L
Riboflavin	10.0 mg/L
Reducing Solution	40.0 ml/L
0.2N NaOH	200 ml
Na_2S-$9H_2O$	2.5 g
L-Cysteine-HCl	2.5 g

Notes:

- Began using filter sterilized fermented yeast extract in experiment 8a and onward.
- Began using 2.0 mg/L nicotinic acid added to final lean medium after experiment 9a.
- Added 20 mg Na_2WO_4-$2H_2O$ and 20 mg, $NiCl_2$-$6H_2O$ to the Wolfe's Modified Mineral Elixer after experiment 9a.

.

Appendix H

Filter Sterilized Fermented Yeast Extract Protocol

1. Used 250 ml glass serum bottles (x5) with a pressure seal.
2. Added 0.05 M NaHCO3 to 1.0 L of deionized water
3. Added 20 ml of anaerobic digester granules
4. Added 50 g of yeast extract (5% weight/liquid volume)
5. Flushed with 96% N_2/4% H_2 gas
6. Sealed and placed in incubator at 37.5°C for 4 days
7. Placed syringe needles in rubber seals to keep the caps from blowing off the bottles because of the gas production.
8. Placed the fermented yeast extract in centrifuge tubes and spun down the solids.
9. Filter sterilized with 0.22 micron filter paper
10. Purged with 96% N_2/4% H_2 gas for 15 minutes and then placed in anaerobic hood overnight to eliminate oxygen.
11. Stored in refrigerator (4°C) and in the dark (aluminum foil)

Note: The solution has a foul odor, so work was performed in a chemical hood where possible.